Ministry of Higher Education
and Scientific Research
University of Diyala
College of Science
Department of Chemistry

Characterization and applications of zeolite prepared from naturally available materials (Iraqi Kaolin and rice husk)

A Thesis Submitted to Council of the College of Science,
University of Diyala in Partial Fulfillment of the Requirements
for the Degree of Master of

Science in Chemistry

by

ELAFF HUSSEIN ALI

B.Sc. in Chemistry Science 2008

College of Science – University of Diyala

Supervised by

Prof. Dr. Karim Henikish Hassan **Prof. Dr. Ahmed Najem Abd**

2021 AD **1442AH**

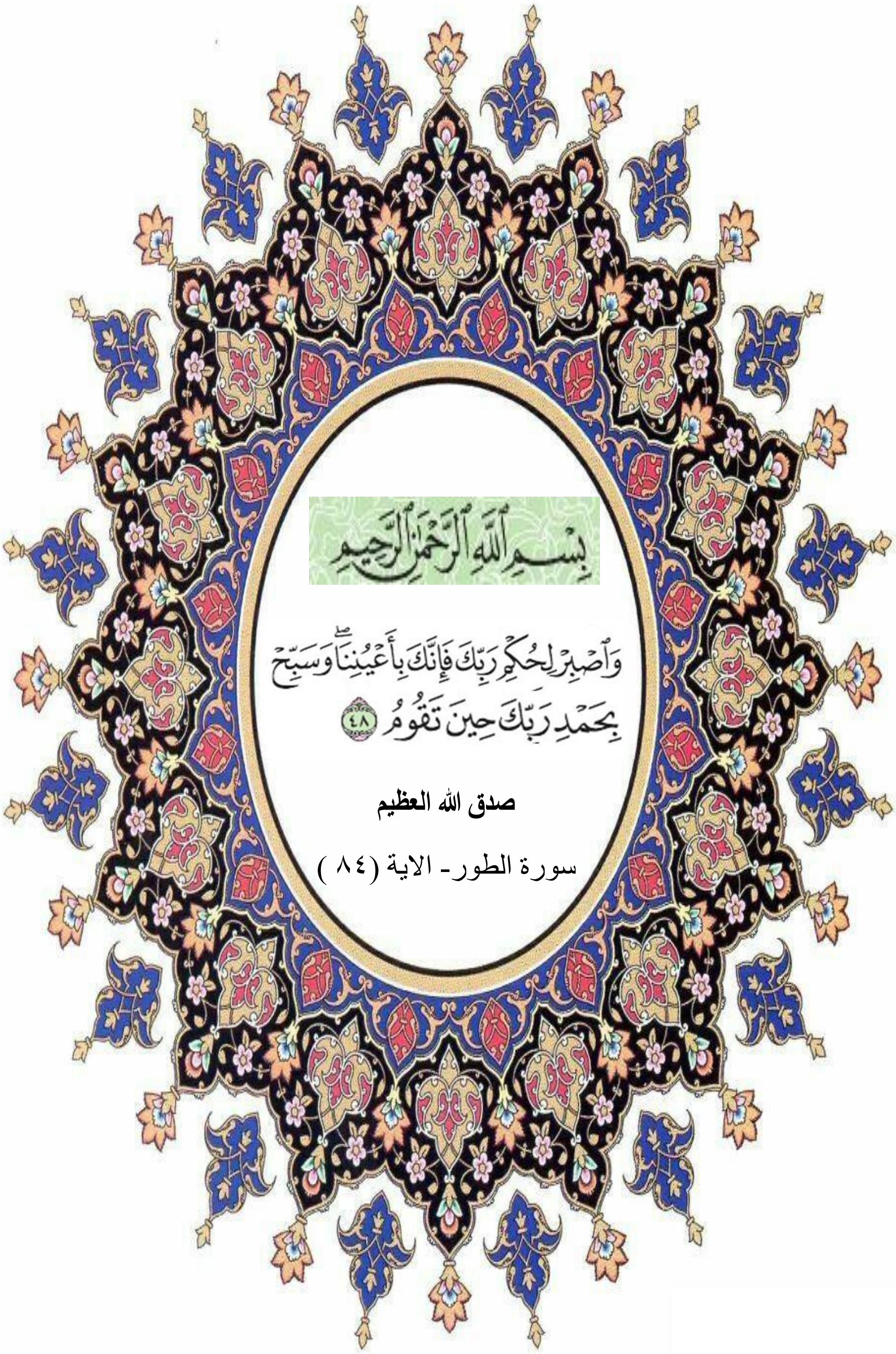

بِسۡمِ ٱللَّهِ ٱلرَّحۡمَٰنِ ٱلرَّحِيمِ

وَٱصۡبِرۡ لِحُكۡمِ رَبِّكَ فَإِنَّكَ بِأَعۡيُنِنَاۖ وَسَبِّحۡ
بِحَمۡدِ رَبِّكَ حِينَ تَقُومُ ٤٨

صدق الله العظيم

سورة الطور- الاية (٨٤)

Dedication

To the beacon of knowledge, to the master of creation, to ***our noble Messenger Muhammad, may God's prayers and peace be upon him and his family***

To whom God has entrusted with prestige and dignity .. To who taught me to give without waiting .. To whom I bear his name with pride .. I hope that God will extend in Your life to see fruits whose harvest has come after a long wait, and your words will remain stars for me to guide today, tomorrow and forever .. ***My dear father***

To my angel in life .. To the meaning of love and to the meaning of tenderness and dedication .. To the smile of life and the secret of existence To whom her prayer was the secret of my success and her tenderness A surgical balm to the most precious of my beloved .. ***My beloved mother***

*To whom their love runs in my veins and delights in their memory so my heart goes to****.. my brothers***

To those who walked together as we worked the way together towards success and creativity.. To my colleagues and colleagues

To those who taught us golden letters, words from pearls, and phrases from the highest and most clear phrases in science, to those who crafted their knowledge for us as letters, and from their thought a beacon that illuminates us in the history of science and success ***to the honorable professors*** *.*

For all of you, I dedicate my work.

The researcher…Elaf

Acknowledgment

First of all, I thank Allah for inspiring me with strength, patience and willingness to perform this work. I deeply thank my supervisor, ***Prof. Dr. Karim Henikish Hassan*** *and* ***Dr. Ahmed Nagem Abd*** *, who were guiding my thoughts my works on this thesis. I ask God to reward them with all good things in their lives.*

Special thanks are extended to the Dean, Chairman, and the staff of the Chemistry Department, College of Scienec, Diyala University. Thanks also to all postgraduate unit staff, dean assistant for scientific affairs staff.

Many thanks to my family ***(Father, Mother, Sisters and Brothers)*** *who sustained and encouraged me throughout the work.*

The researcher.. Elaf

ABSTRACT

It is known that the molecular sieve is a material with pores (very small holes) of uniform size. These pore diameters are similar in size to small molecules, and thus large particles cannot enter or absorb, while smaller particles can. Molecular sieves or zeolite are as a widespread industrial dressing with a unique chemical structure, which is used in most industrial facilities as an absorbent for gases or even As triggers. The 4A° zeolite was prepared from Iraqi kaolin and rice husk using the process of converting rice husk to silica and kaolin to sodium aluminate where the zeolite was prepared. Then, it was characterized by X-ray diffraction, FTIR spectroscopy and AFM (atomic force microscopy), scanning electron microscopy (SEM) and energy dispersive X-ray microscopy (EDX) where measurements were taken for samples (kaolin, meta-choline, alumina, silica and zeolite) respectively. The results of the measurements proved the formation of zeolite in addition to the possibility of using kaolin / rice husk as a raw material for the production of zeolite.

Water pollution is a major concern because water is a basic necessity for the life and survival of all living things. All over the world, but its quality is constantly changing through different human activities, so amounts of money are spent annually to ensure water purification (minerals are removed) to avoid its negative effects such as deteriorating soap and accelerated sedimentation on taps changes the physical and chemical properties of the water. Water hardness is determined by measuring the total concentration of magnesium and calcium in the water source. Hardness of water affects environmental cultures as well as many other species that depend on a constant concentration of calcium carbonate. Contamination of water with many minerals is very harmful to the environment. Therefore, use 4 zeolite to remove calcium and magnesium ions from aqueous solutions. In this field, a number of factors that affect the removal of calcium and magnesium removal rate on the adsorbent materials (nanoparticles) were studied. It was found that the time required to remove calcium and magnesium ions and to reach the equilibrium state is 50 minutes on zeolite, as well as removing calcium ions and removing magnesium ions Decrease with increase

The concentration of adsorbent material increases with the weight of the

adsorbent surface. As for the effect of temperature on the adsorption of calcium and magnesium, it has been shown that the removal rate decreases with increasing the temperature, which indicates that the process is a heat emitter.

When calculating the values of the thermodynamic functions of the adsorption process (Δ S, ΔH, ΔG), it was found that the adsorption process is automatic, heat emitting and less random when calcium and magnesium ions overlap. The results were matched by using four kinetic equations, which are: the pseudo-first degree equation and the equation The pseudo-second-degree equation, the internal diffusion equation of particles, and the Elovich equation from the above results show that the adsorption process is subject to the pseudo-second-degree equation because the correlation coefficient, which is (R2), showed the best result with other existing models The Lancemire isotherm was found to be the best for describing the behavior of the adsorption process compared to theisothermate Freundlich and Temkin

LIST OF CONTENTS

Chapter Three (Experimental Part)

Chapter Four (Results & Discussion)

LIST OF TABLES

LIST OF FIGURES

LIST OF SYMBOLS AND ABBREVIATIONS

Symbol or Abbreviation	Definition
AAS	Atomic absorption spectrophotometer
AFM	Atomic force microsope
Avg	Average
A	Langmuir constant related with adsorption capacity
B	Langmuir constant relatedwith energyof adsorption
AT, BT	Temkin adsorption constant
C0	Initial concentration of the adsorbent
Ct	Concentration of adsorbate after any time
Ce	Equilibrium concentration of adsorbate
C	Constant of the van der Hoff equation
D	Crystallite Size
EDX	Energy dispersive spectroscopy
FTIR	Fourier transform infrared spectroscopy
FWHM	Full width at half maximum
k_f , n	Frendelsh experimental constants
K	Equilibrium Constant
K1	Pseudo-First Order Constant
K2	Pseudo-Second Order Constant
KD	Diffusion Constant
Kelovich	Elovich model constant
M	The weight of the adsorbent
Min	Minute
Qe	Adsorption capacity of the adsorbent at equilibrium
q_e	Quantity of adsorbate at equilibrium
Qt	Quantity of adsorbate at any time
R	Gas constant
R2	Correlation coefficient
R%	Percentage removal of adsorbate
RMS	Root mean square
Rpm	Revolution per minute
SEM	Scanning electron microscopy
T	absolute temperature
XRD	X-ray diffraction
ΔG	Change in free Gibbs energy
ΔH	Enthalpy
ΔS	Entropy
ϴ	Braggs angle
L.O.I	Loss on ignition
PBU	Primary Building Unit
SBU	Secondaru Building Unit

Chapter One

Introduction

1.1. General introduction

Zeolite, also known as molecular sieve, is a crystalline microporous material mainly formed by tetrahedral building units shared by SiO4 and AlO4 corners. These units form a three-dimensional (3D) framework with clear channels and molecular size cavities. The voids in the crystals allow the zeolite to distinguish molecules based on their size or geometry. With variable chemical composition and unique pore topology, zeolite has been widely used in industrial applications such as adsorption/separation, ion exchange processes, and as a catalyst in oil refining and fine chemical synthesis processes[1].

Zeolites are members of the family of microporous solid aluminosilicates called "molecular sieves". The term molecular sieve refers to the special properties of these materials, that is, the ability to selectively sort molecules based mainly on the size exclusion process. Molecules confine the molecule in a small space, which may cause changes in molecular structure and reactivity. Zeolite is widely used as a petrochemical catalyst due to its many pores, active sites, thermal stability and shape selectivity (for example, in fluid catalytic cracking and hydrocracking) [2].

Most natural zeolites are formed due to volcanic activity. When a volcano erupts, magma (the molten rock inside the earth) penetrates the earth's crust and flows out in the form of lava, accompanied by gas, dust and dense ash. Volcanoes usually occur where tectonic plates diverge or converge. In such locations on the island or near the ocean, the lava and ash that are ejected usually flow into the ocean. After reaching the ocean, the hot lava, water and salt from the ocean react. These reactions have led to the production of crystalline solids called zeolites over thousands of years[3].

Zeolite synthesis is an active research area, because zeolites with uniform micropores are important in many industrial processes of catalysis, adsorption and separation, and are finding new applications in the fields of electronics, magnetism, chemical sensors, and medicine. Zeolite is a highly crystalline, microporous and hydrated aluminosilicate mineral containing a balanced alkali metal or alkali metal cation. In other words, the zeolite framework consists of SiO2 and AlO2 units connected on all sides. The micropores in zeolite are intracrystalline channels whose size is precisely determined by the crystal structure. zeolite A is one of the most extensive synthetic zeolites and has found its place in various industrial applications. It is well known that Zeolite A is used in the gas separation industry. Zeolite A has a strong affinity for carbon dioxide and a weak affinity for methane, making it an effective CO2 adsorbent, that is, in pressure swing adsorption (PSA) applications[4].

Zeolite is widely used due to its outstanding physical and chemical properties and can be used in many fields of human activities: industrial technology, medicine, pharmacy, water and wastewater treatment, ecology, agriculture, and soil environmental protectio [5]. The application of zeolite in detoxification of soil contaminated by heavy metals is particularly important. According to Maicaneanu et al. (2013) zeolite has catalytic properties and can realize adsorption and desorption and ion exchange processes. There are two types of zeolites: natural and synthetic zeolites.

According to literature review, water hardness problems exist all over the world. Among several known forms of pollution, water pollution has caused great concern. In this regard, synthetic zeolite is of great interest as a packing material for underground reaction bed reactors designed to remove hard water minerals from the ground and ground for industrial purposes.

As stated by reports, there are water hardness problems all over the world due to the following reasons:

1. Water is the main necessity of life, and the well-known forms of pollution attach great importance to water pollution
2. It is extremely important for the survival of all living organisms[6].
3. Various human activities are constantly changing its quality, and these activities cost a lot of money
4. Determine the hardness of water by measuring the total concentration of magnesium and calcium in the water source. The hardness of water affects ecology, fish farming and many other species depend on a stable calcium carbonate concentration[7].

1.2 Previous studies

In the past decades, impressive accomplishments dealing with the synthesis and applications of metal particles confined in zeolites have been achieved. Most recently, several elegant review papers dealing with different aspects of this important topic have been disclosed (Chai et.al,2019)

Chandrasekhar & Pramada(1999), investigated the effect of calcination temperature on the synthesis of zeolite 4A° from kaolin. The clay used was gotten from Thiruvananthapuram district of Kerala, India with a fairly good crystallinity, having a Hinckley Index = 0.79. It was concluded that, the optimum temperature of dehydroxylation was 900 °C for a period of 1 hour, also zeolite 4A° with 80% crystallinity and good brightness was formed at a metakaolin temperature of 900 °C and a holding time of 4 to 5 hours. Zeolite with similar crystallinity has been successfully synthesized using other metakaolinzation temperature when the reaction is carried out for a longer period of 8 hours[8].

Ahmed (2000), studied the preparation and agglomeration of zeolite 5A and 3A by ion exchange of powder zeolite 4A° with 1M solution concentration of chloride salts at 94 °C for 8 hours. The binders studied were kaolin clay, bentonite clay, aluminum hydroxide and calcium carbonate with 10, 20, 25, and 30 wt. %. The most suitable binders for 5A were kaolin and bentonite clays with 20-25 weight[9] % .

Keka O. (2001), studied the synthesis and characterization of zeolite from fly ash. They concluded that X type zeolite can be synthesized from fly ash by alkali fusion followed by hydrothermal treatment and that the fly ash, could be converted to pure X-type zeolite using suitable treatment conditions, the properties of the zeolite formed strongly depend upon these treatment conditions and concentrations of the raw materials. Zeolites having varying surface area, silica/alumina ratio, and crystallinity were obtained when the reaction parameters are altered, the crystallinity of the synthesized zeolite was also found to change with fusion temperature and have a maximum value of 823 K, for best quality, in terms of surface area and crystallinity, X type zeolite can be obtained at the following conditions, NaOH/fly ash ratio of 1:3, fusion temperature, 823 K, aging time of 24 hour and 6 hours for the hydrothermal treatment[10]**.**

Yaşyerli (2002), experimented removal of hydrogen sulfide by natural clinoptilolite zeolite in a fixed bed adsorber at 100 and 600°C. The adsorbent contains 80-85% clinoptilolite, and 5-10% clay binder. The adsorption capacity was decreased from 0.087 to 0.03 gram sulfur/gram clinoptilolite by temperature increasing from 100 to 600 °C [11].

Al-Khattaf (2002), focused on the catalytic cracking of hydrotreated Arabian light vacuum gas oil using micro activity test unit using ultra stable Y zeolite. The process variable were reactor temperature 520oC, catalyst to oil ratio 0.5-3, and atmospheric pressure .These conditions give a conversion between 75-88%wt and a gasoline between (42-44%) wt[12] .

Chantawong & Harvey (2003), synthesize of zeolite A from kaolin by hydrothermal treatment with various concentrations of NaOH solutions (0.5-4N) crystallized at 100 C° from 1 to 5 hours. Solid to liquid ratio was 1 gram metakaolin to 20 milliliter NaOH solution. The best crystallinity of zeolite obtained at 2N NaOH solution with 4 hours[13] .

Shams & Mirmohammadi (2007), prepared zeolite 4A° extrudates with different contents of kaolin clay and carboxymethyl cellulose. The extrudate was calcined at 600°C, and kaolin content was converted to 4A° zeolite by immersing the extrudate in NaOH solution. The 4A° zeolite extrudate was converted to 5A zeolite by ion exchange process using calcium chloride solution. The best results obtained when 30% of binder kaolin is used, and use of small amount of carboxymethyl cellulose with inorganic binder increased the adsorption capacity of 5A with 16% compared to 5A without carboxymethyl cellulose[14] .

Wu (2005), hydrocracked process for converting fuel oil to BTX using beta zeolite catalyst promoted with ruthenium metal. The cracking reaction conditions were: temperature 400 ◦C, pressure 800 psig in a stainless steel reactor tube of 5 ml Alundum alumina. They concluded that the modified catalyst produced higher BTX over that not modified catalyst[15].

Dalai et al.(2005), synthesized and characterized NaX and Cu- exchanged NaX zeolite from silica obtained using rice husk ash. Rice husk ash, sodium hydroxide, aluminium hydroxide and silica gel were used as the starting materials. The silica solution was first prepared by treating the rice husk ash with 2.5 molar aqueous sodium hydroxide solution at a temperature of 800° C for a period of 5 hour with continues shaking. They concluded that a number of zeolite types were synthesized using silica obtained from rice husk ash. A series of NaCuX zeolite were also prepared by exchanging Na of the synthesized NaX with copper[16].

Shawabkeh & Harahsheh (2007), used oil shale ash to adsorb hydrogen sulfide from liquefied petroleum gas. The maximum uptake 30 mg H2S per liter of LPG was achieved by treating 150 ml LPG with one gram of ash of particle size 500-710 micron. This value decreased with increasing particle size of the ash, and increasing adsorption temperature [17].

Atta et al.(2007), used Kankara kaolin and rice husk ash mixture to produce zeolite P and analcime with the conventional hydrothermal method of zeolite synthesis in the presence of sodium hydroxide solution. The aging process lasted 72 hour and the subsequent crystallization of the mixture was done at a temperature of 80°C at 24 hour [18].

Christidis & Papantoni (2008), synthesized faujasite type zeolite from silica and pearlite ‘Perlite is an amorphous volcanic glass that has a relatively high water content, typically formed by the hydration of obsidian. It occurs naturally and has the unusual property of greatly expanding when heated sufficiently. It is an industrial mineral and a commercial product useful for its low density after processing. '. Both the silica and the pearlite were mixed in sodium hydroxide solution and commercial form of aluminium hydroxide was dissolved in the sodium hydroxide to produce the synthesized gel. Crystallization of the gel to produce zeolite was done at a temperature of 90°C for 120 hour and mixed phases of zeolite Y, zeolite P were produced [19].

Htay & Oo(2008), produced zeolite Y from kaolin by fusing kaolin with sodium hydroxide at 850°C for 3 hours. The fused mixture was hydrothermally crystallized at 100°C for 16 hour and the product was mixed phases of zeolite Y[20].

Kovo et al.(2009), investigated the synthesis and characterization of zeolite Y from Nigerian Ahoko Kaolin using a novel, at low temperature, metakaolinization technique., 30 kg of raw representative sample of kaolin clay was used along with sodium hydroxide. From the study it was concluded that reactive metakaolin can be produced at very short exposure times, of the order of 10 minutes, to a temperature of 600 °C. This is a significant reduction in both time and temperature compared with previous studies and represents both a reduced energy requirement and the potential for a continuous production process[21].

Rahman et al.(2009), synthesize Faujasite zeolite with rice husk ash as the precusor material. The synthetic gel was produce by mixing the rice husk ash and sodium hydroxide solution with commercial sodium aluminate and the synthetic gel produced was aged for 24 h and then crystallized at 90°C for 22 hour. studied the synthesis of zeolite NaA from Brazilian chrysotile and rice husk. Chrysotile was used in its natural form and after leaching in a typical acid leaching treatment, 30 g of chrysotile were refluxed with a HC1 solution (5 M L-1) for 2 days at 800 °C, according to procedure described in the literature. The resulting chrysotile was thoroughly washed with distilled water and then dried in an oven at a temperature of 100 °C. It was concluded that Zeolite Na A can be synthesized by a direct hydrothermal route, using silica from Chrysotile and rice husk as a silica source. Brazilian Chrysotile and rice husk seems to be good alternative silica sources for zeolite NaA synthesis. In the case of Chrysotile, in its natural form, no zeolitic material could be obtained, demanding a leaching procedure before its use. Even then, traces of non- reacted Chrysotile could be detected in the resulting zeolites. Except in the use of natural Chrysotile, all the other investigated possibilities afford highly crystalline zeolite NaA [22].

Reyes, *et al.* (2010), examined the synthesis of zeolite A from metakaolin by two methods. The first method is the classic hydrothermal transformation of the starting material while the second method is the alkaline fusion at 600C° for 1 hour. For both methods crystallization was carried out by hydrothermal treatment under static conditions at 100°C and in autoclave at 200°C for 22 to 96 hour. XRD analysis, scanning electron microscopy, and Fourier transform infrared spectroscopy showed that the fusion method gave pure crystalline zeolite[23].

Ugal, *et al.*, (2010) studied the preparation of zeolite 4A° from Iraqi kaolin. Metakaolinite was treated with 8M sodium hydroxide solution with a solid: liquid ratio of 1: 5 at 90 °C for 4 hour. the obtained zeolite powder was mixed with 15 % raw metakaolinite, and calcined for 4 hour at 500° C[24].

Rawa Ch. Yousif (2010), studied the catalytic activity of two different types of y zeolite catalyst using cumene cracking as a model for catalytic cracking process .The two catalysts were prepared from local clay (kaolin) with different Si/Al ratio. The prepared catalyst was modified by exchanging sodium ion with ammonium ion using ammonium nitrate and converted ammonium ion to hydrogen ion.The process variable were: temperature range (450 to 525) oC, weight hourly space velocity (WHSV) range (5 to 20) h-1 and atmospheric pressure. The prepared catalysts had Si/Al ratio 3.542 and 5.758.

The results show that the catalyst of 5.758 Si/Al ratio gave the higher cumene activity than the catalyst with 3.542 Si/Al ratio. It was also found that the cumene conversion increases with increasing temperature and decreasing WHSV[25].

Mostafa, et al., (2011), studied the preparation of zeolite A from kaolin calcined at 800-850 °C for 4-12 hours. Solid metakaolin to NaOH solution ratio was 0.5-5.0: 5, concentration of NaOH solution was 3-6 M and processing time of zeolitization 1-5 hours. The best conditions were kaolin calcined at 800C° for 12h, the zeolite produced at 100C° for 3h, solid: liquid ratio 0.5-1.5:5, and 3M NaOH solution. Using lower alkalinity and solid: liquid ratio 1.5: 5 for 3 hours contributes to the enhancement of the chromium adsorption capacity from 10.6mg/g to 11.06 mg/g[26].

Mezni et al(2011), used Tunisian illite clay to produce a mixed phases of zeolite X and RHA. This was made possible by the fusion of the Tunisian illite clay with sodium hydroxide solutions and heating the mixture hydrothermally at 110°C for 96 hours[27] .

Farag and Zhang(2012), simulated the synthesis of zeolite 4A° and 5A by calcining kaolin at temperatures between 500 and 6000 °C to form metakaolin. The metakaolin is then mixed with caustic soda and water in a gel make-up tank to produce zeolite 4A° gel. To obtain zeolite 5A, zeolite 4A° gel is fed to anion exchanger, where it is mixed with calcium chloride and water. In this process some of Na+ ions in zeolite 4A° gel are replaced by calcium ions, Ca+2 The wet zeolite 5A was then allowed to pass through a dryer to remove part of the water and form the dry zeolite at 1000 F. It was observed that, in the kaolin conversion process to produce zeolites 5A, hydrogen and oxygen utilization efficiency can be improved via water and steam recycling while Oxygen and Sodium utilization efficiency can be improved through Na2O recycling. Also, in the hydrogel process that produces Zeolite 4A° water recycling can improve Hydrogen and Oxygen utilization efficiency [28].

Saceda et al.(2012), synthesized zeolite Y by partially substituting rice husk ash with chemicals of high purity and crystallization of the zeolite was done at 100°C [29].

Georgiev et al.(2013), studied the most important stage during the synthesis of zeolite NaX from Bulgarian clay as the basic raw material. The use of additives such as sodium hydroxide and lithium hydroxide helps the crystallization optimization to achieve a high pure phase of the synthesized zeolite which took place after 36 hour at 950 °C [30].

Ma et al.(2014), synthesized zeolite type X using kaolin as the precusor material and the conventional method by the fusion of the kaolin with sodium hydroxide at a temperature of 90°C for 8 hours [31].

Cheng et.al. (2017), describe the structure of zeolites starting from atomic level to the complex networks of channels and voids that permeate the material. The chemistry within the material is outlined relating it to its crystal structure. The resulting properties are described relating them to the crystal structure and the chemistry. Finally, the applications of the material are summarised relating them to the material crystal structure, chemistry and properties [32].

Chai et.al. (2019), illustrated the synthesis of metal zeolites, various strategies, such as direct synthesis from inorganic or ligand-assisted noble metal precursors, multistep postsynthesis encapsulation and ion-exchange followed by reduction, are introduced and compared. For the characterization of metal zeolites, several most useful techniques, such as electron microscopy, X-ray based spectroscopy, infrared and fluorescence emission spectroscopy, are recommended to check the successful confinement of noble metal particles in zeolite matrix and their unique physiochemical properties [33].

Ramamurthy (2019), obtained to establish the value of chirally-modified, commercial zeolites as media for achieving chiral induction in photochemical reactions. A recent report of the synthesis of a chiral zeolite is likely to stimulate zeolite-based chiral photochemistry in synthesizing enantiomerically-pure organic molecules. The availability of chiral zeolites in future is likely to energize research in this area [34].

Vegere et.al., (2020), described four different methods for zeolite A (Linde Type A; LTA) synthesis were investigated and compared. The four investigated synthesis methods were the microspheres the metakaolin-based, the NaOH accelerated metakaolin-based and the aluminosilicate gel-based methods, respectively. The impact of the hydrothermal synthesis temperature was studied at 60, 80 and 100 °C was studied for each of the methods resulting in the purest product was determined to be an aluminosilicate gel-based method (fourth) followed by a microspheres method (first), both being most efficient at 80 °C [35].

Schulman et. al. (2020), summarized the structural properties of 2D layered precursors and 2D zeolite derivatives, as well as the acidity properties of 2D zeolite derivative structures, especially in connection to their 3D conventional zeolite analogues' structural and compositional properties. The timeline of the synthesis and recognition of 2D zeolites, as well as the structure and composition properties of each 2D zeolite, are discussed initially [36].

Gackowski & Datka(2020), reviewed different strategies towards obtaining mesoporous zeolites Y:desilication; surfactant templating and assembly of zeolite crystals. The impact of those methods on physicochemical properties is covered, with a special focus on the acidity of the samples measured with infrared (IR) spectroscopy. The methods of characterization of acidity are presented. Quaternary ammonium cations used for desilication lead to obtaining crystalline; mesoporous and highly acidic zeolites. Si-OH-Al groups of extremely high acidity can be produced by calcination in a humid atmosphere [37].

Derakhshankhah et.al.(2020), shed light on interactions of zeolite nanoparticles with fibrinogen and amyloid beta which had been comprehensively investigated in our recent reports. Given the significance of zeolite nanoparticles' interactions with serum or interstitial proteins conferring them new biological identity, the preliminary approaches for deeper understanding of administration, distribution, metabolism and excretion of zeolite nanoparticles are elucidated [38].

1.3 Aim of study

1. The aim of the present study is to : preparation of nano silica from rice husk and characterize it
2. Preparation nano alumina using kaoline and characterize it.
3. preparation of zeolite and characterize it.
4. Determining the ideal condition for the adsorption of Mg(II) and Ca(II) ions such as (contact time, quantity of adsorbent , temperature and initial metal ions concentration).
5. Thermodynamic studies of adsorption processes of Mg(II) and Ca(II) ions on this adsorbent.
6. Investigate the kinetic studies of the adsorption processes.
7. Determing an adequate adsorption isotherm and the related constants.

Chapter Two

Theoretical Part

2.1 Zeolite

2.1.1 Definition

Zeolites are microporous crystalline solids with well-defined structures. Commonly they comprise silicon, aluminum and oxygen in their framework water and or other molecules within their pores. Many occur naturally as minerals, and others are synthetic, and are made commercially for specific uses [39].

The term zeolite was formerly invented at 18th century by the Swedish mineralogist Cronstedt who observed that the Greek word means "boiling stone" and he called this substance zeolite[40].

Natural zeolite is formed from volcanic glass, clay with poor crystallinity, feldspar or silica under humid conditions at a temperature below 200°C[41]. Faujasite is a mineral in the zeolite group of silicate minerals. This group consists of faujasite-Na, faujasite-Mg and faujasite-Ca. Like other zeolites, faujasite is synthesized from alumina sources such as sodium aluminate and silica sources such as sodium silicate and other aluminosilicates such as kaolin which are also used[42].

2.1.2. Structure

Zeolite is a three-dimensional crystalline compound constructed from AlO_4 and SiO_4 tetrahedra [43]. The main feature of zeolite is that its framework consists of a network of 4 connected atoms. One way to think about this is to use tetrahedrons, with a silicon atom in the middle and oxygen atoms at the corners, and then these tetrahedrons can be connected by their corners [39]. Figure (2.1) illustrates the structure of zeolite.

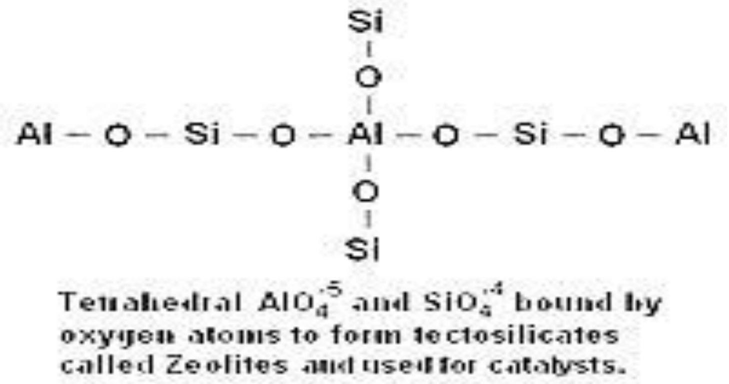

Figure (2.1): Zeolite structure[43]

Zeolite structural formula based on crystallographic unit cell, the smallest structure unit is represented by :

$M_{x/n}[(AlO_2)_x(SiO_2)_y]\cdot WH_2O$

Where n is valence of cation M, W is the number of water molecules in each unit cell, and x and y are the total number of tetrahedral atoms in each unit cell. The y/x ratio (Si/Al ratio) is usually 1 to 5 or 10: Tetrahedral Si: (Si + Al) ratio is one of the main composition variables. Some zeolites (such as mordent) are rich in silica State is over, others are more aluminum[41].

The frame structure contains channels or interconnected voids occupied by cations and water molecules. Cations are mobile and usually undergo ion exchange, and water can usually be removed reversibly by heating[44].

2.1.3 Zeolite utility as catalyst

Zeolite has the capableness to catalyze analytical reactions in the inward cavity and it has dual of characteristics that force it particularly consistent for use as a raw material for preparing catalysts [45]:

1. They are cation exchangers; hence, numerous cations with dissimilar catalytic characteristics can be presented by their crystal pore system, in which turn delivers prospects to generate diverse catalytic characteristics.

2. Zeolite is a crystalline porous material whose pore size is the same as that of simple molecules; therefore, when the shape and size of a specific pore system have a strict effect on the reaction, they will have molecular sieve characteristics. In the case of zeolites used for shape selective catalysis, they control the entry of reactants and products and control the selectivity of the catalytic reaction.

Zeolite usage as a catalyst has several compensations for its effortlessness reconversion and recirculation at a lower charge, thus reducing waste and decreasing by-products (regularly with higher activity). Multiple catalytic steps can be joint and substituted by homogeneous catalysts in order to decrease environmental contamination in the traditional chemical industry (inorganic acids, salts, heavy metals). Hydrogen-exchanged zeolites, whose framework-bonded protons produce high acidity, are used in many organic reactions, including crude oil cracking, isomerization, and fuel synthesis.

For the high selectivity of zeolites, they are frequently the greatest effectual and cost-effective technique for a number of refinery adaptations[45].

Precisely, the strong bonding of the “mercapto” group to the metal species and the copolymerization of the “alkoxysilane” group with the zeolite “organosilane” precursor ensure that the highly dispersed metal centers are effectively encapsulated in the zeolite matrix. A step forward, this ligand is widely used to synthesize other precious metal particles encapsulated in zeolite. For instance, Iglesia and colleagues stated the usage of bifunctional (3-mercaptopropyl) trimethoxysilane ligands to encapsulate precious metal clusters throughout the hydrothermal crystallization of LTA zeolite[33] (Figure 2.2).

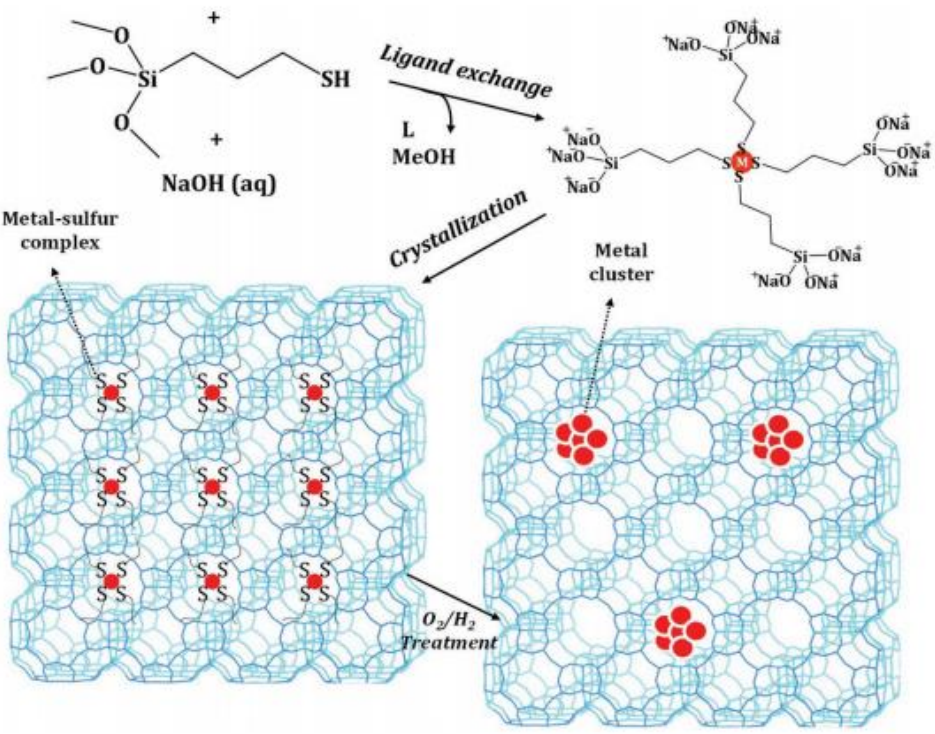

Figure (2.2): Shows diagram process of mercaptosilane-assisted metal encapsulation during zeolite crystallization. [33]

2.1.4 Zeolite types and properties

In theory, the potential of different framework structures is immeasurable- approximately 40 species can be identified in nature, and more than 150 synthetic zeolites have been designed. The most commercially important synthetic zeolites are zeolites A, X, Y and ZSM-5. Zeolite is a white crystal with many unique properties essential for profitable use, including:

1. High degree of hydration, dehydrated easily.
2. Density considered low as well as huge void volume throughout dehydration.
3. The constancy of the crystal framework structure throughout dehydration.
4. Conversation of cation presentation.
5. Unchanging size of molecular channels in dehydrated crystals.
6. Capability of absorbation gas and vapor.
7. Catalytic presentation of H + exchange procedure.
8. Singular electrical properties [41].

Accordingly, the silica-aluminum ratio of the zeolite framework, synthetic faujasite is distributed into X and Y zeolite, and the ratio is 2 to 3 in X zeolite, and the ratio is 3 or higher in Y zeolite. The negative charge of the framework is balanced with the positive charge of the cation in the non-framework position. This zeolite has ion exchange, catalytic and adsorption properties.

The constancy of the zeolite increases with the silica/alumina of framework ratio. In which also affected by the type and amount of cations located in non-framework positions. For catalytic cracking, Y zeolite is usually used in the form of rare earth-hydrogen exchange. By using heating, hydrothermal or chemical method, some alumina can be removed from the Y zeolite framework, thereby obtaining high silica Y zeolite. The zeolite is used for cracking and hydrocracking catalysts. The implementation dealumination in faujasite silica Faujasite result was first usage as a catalyst for fluid catalytic cracking to convert high-boiling petroleum crude oil fractions into more valuable gasoline, diesel and other products. Zeolite Y replaces zeolite X in this application because it is both more active and stable at high temperatures due to the higher Si/Al ratio.

Similarly, it is used as a platinum/palladium base material in hydrocracking units to increase the aromatics content of reformulated plant products[42].

For the metal substances supported by zeolite, three types can be identified: metal substances supported on the outer surface of zeolite crystals (a), metal species encapsulated within the channels or cavities of zeolites (b), and metal species incorporated into zeolite framework (c) this is shown in (Figure 2.3)[33].

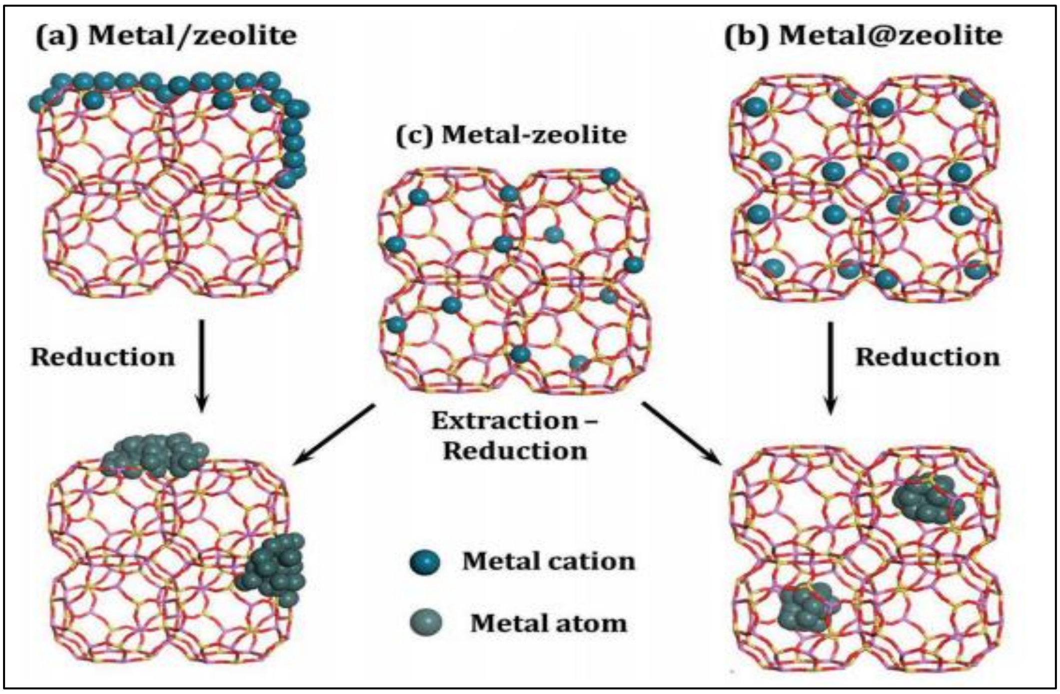

Figure(2.3): Shows three typical of metal-containing zeolites

Usually a simple impregnation method is used to prepare a sample of type (a) from the zeolite support and the metal precursor, called metal/zeolite. During the calcination and reduction process, the migration of metal substances and their aggregation into larger particles always occurs in contrast, for the samples of (b) signified as metal zeolites, the metal classes are professionally protected by the frameworks of zeolite. The composite system of channels and micropores can supply robust captivity effects and considerably inhibit the particle growth to a particular size region. At the same time, the interconnecting channels of the zeolite allow free entry of guest molecules into the metal species confined in the zeolite. In addition, with the powerful restriction and close proximity in a very limited space, synergistic dual-functional samples can be generated from the metal zeolite in the metal particles and the intrinsic functional sites in the zeolite, and it is expected to find a wider range of uses. Although the sample in (c) is called Me zeolite, the metal species are incorporated into the zeolite framework in the form of cations, and further extraction and reduction processes are required to obtain zeolite-supported metal particles. In this case, according to the detailed steps of extraction and reduction the sample of (c) can be converted to (a) or (b)[33] .

Zeolites (3A, 4A°, 5A,& 13X) have three properties that make them unique and deserving of a separate category:

1-They are extremely crystalline, have a well-defined structure, and surround the aluminum silicate framework cavity occupied by large ions and water molecules. The opening diameter of the cavity is between 0.8 and 1 nm, which is approximately the size of the molecule. The size and shape of these pores determine which molecules enter the cavity and which are excluded, so they are called molecular sieves

2- The cations in the cavity are easily replaced by a large number of cations of different valences, and these cations exert a large amount of electrostatic or polarizing force on the small size of the cavity.

3-Introduce cations into the cavity by ion exchange carry out activities on; this promotes opportunities for bifunctional catalysts involving acidity and other activities. Zeolite A is synthesized in the form of sodium and has the general chemical formula (2. 1) [46].

$Na12[AlO2.SiO2]12.27H2O$ ……. (2. 1)

2.2 Tests of zeolite

2.2.1 X-ray diffraction

The diffraction phenomenon is caused by the interference caused by objects in the wave pool, and the pattern of intensity change is called the diffraction pattern. Diffraction occurs when the size of the diffracting object is equivalent to the wavelength of the radiation. The wavelength of X-rays is comparable to the bond length in molecules and the distance between atoms in crystals. By analyzing X-ray diffraction patterns, even in complex crystal structures, detailed pictures of atomic positions can be drawn the relationship between X-ray diffraction drawing intensity and diffraction angle[47].

The sharp changes in the intensity of each peak in the XRD patterns of Y and X may be caused by changes in the electron density distribution in the zeolite unit cell. The electron density distribution depends on the extent to which the pores in the zeolite are filled with guest molecules and the properties of the guest molecules. In this XRD method, the guest molecule H2O completely fills the pores. If some or all of the cations in Y and X are exchanged by other cations, the intensity will also change. Figure (2.4) shows the X-ray diffraction pattern[48].

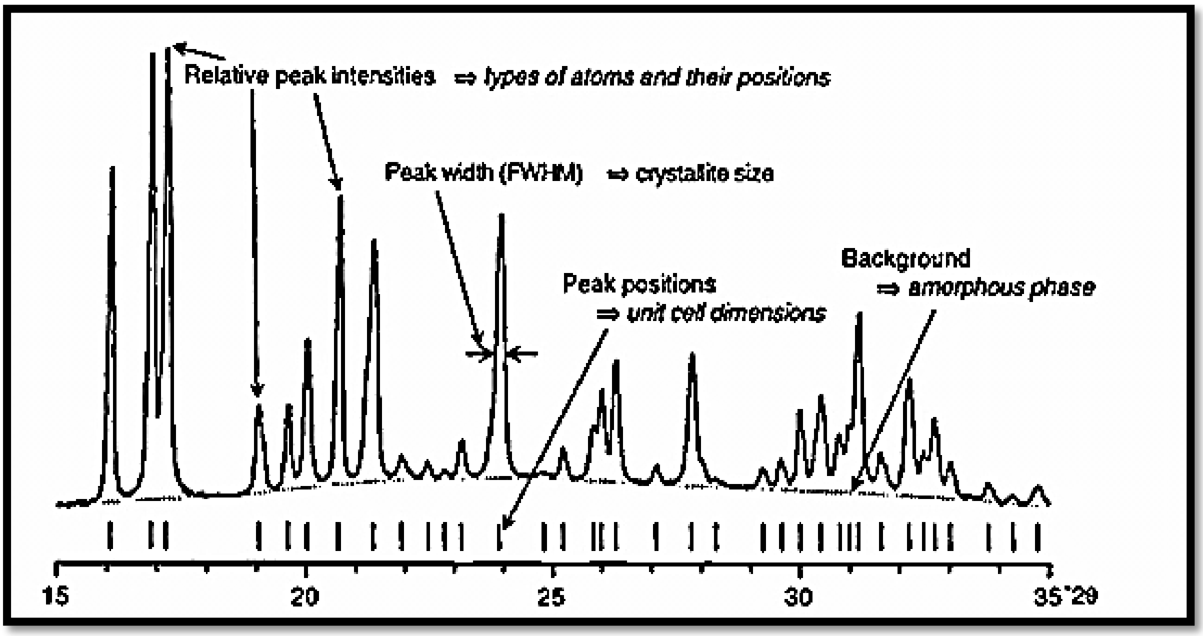

Figure (2.4): Shows X-ray diffraction pattern[48]

2.3 Zeolite Structure

In 1937, Hey defined zeolite as a group of crystalline solids, namely monovalent and divalent alkali hydrated aluminosilicates, in which the ratio of (R̈, R2) O: Al2O3 is 1, where R̈ is a divalent additional framework cation, R2 is a monovalent extra skeleton cation framework cation. Zeolite can lose part or all of its water without changing the crystal structure, and can adsorb other compounds to replace the removed water, and can perform alkali exchange [49]. Zeolite structures can be constructed from SiO4 and AlO4 tetrahedral units.Figure (2.5) illustrates how these tetrahedral units are assembled to give the structure of Zeolite A.

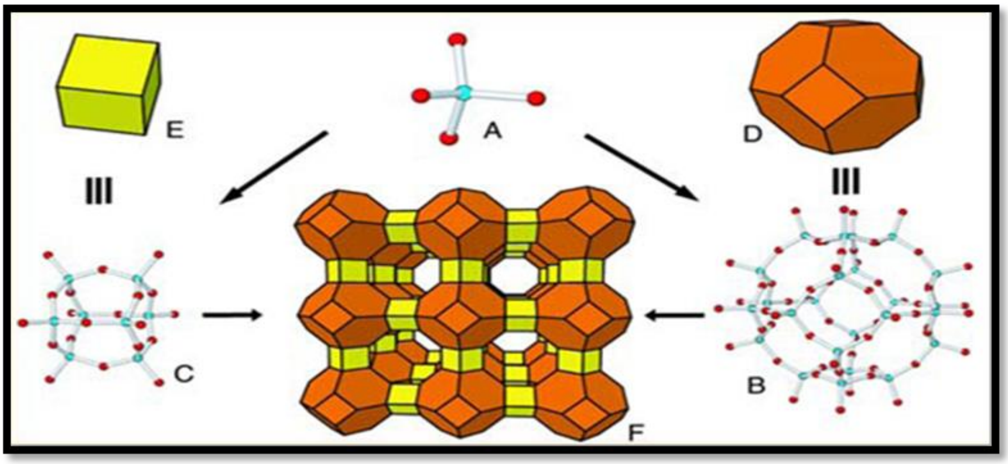

Figure (2.5) : Shows Zeolite structure [50]

Consider connecting SiO4 and AlO4 tetrahedra (A) to obtain secondary building units, such as sodalite cages (B) and double tetracyclic units (C), as shown in Figure (2.5). (D) and (E) are schematic diagrams of sodalite cages and double tetracyclic units, they do not show the oxygen position. The final framework structure of zeolite A (F) can be constructed by connecting sodalite cages together. The pore diameter of the A-type zeolite framework is about 4Å, which can be connected to a larger cavity inside the material. For each AlO4 tetrahedron doped with this material, the framework will acquire a charge of –1, which must be balanced by the presence of extra cations (so-called extra framework) in the pores of the zeolite. These substances are usually small enough to pass through the pore system of the zeolite for ion exchange, so Na+, K+, NH+4, H+, Zn+2, Mg+2, and Ca+2 are all instances of ion-exchangeable further framework cations[50].

Zeolite has a microporous network composed of AlO4 and SiO4 tetrahedra connected by shared oxygen atoms (Figure 2.6).

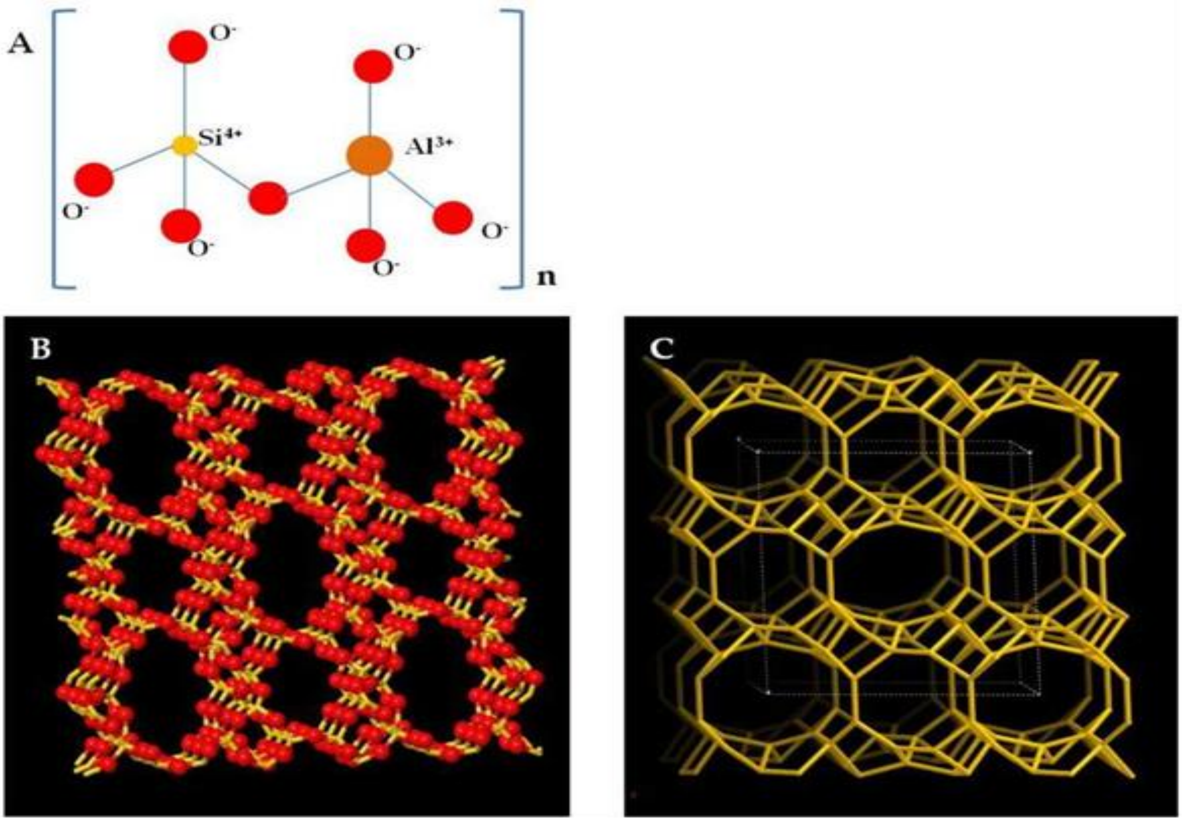

Figure (2.6)Shows (A) AIO4 and SiO4 tetrahedrons joined by oxygen atoms that constitute the reticular structure of the zeolite. (B) and (C) Clinoptilolite [51]

The structure committee of the International Zeolite Association (IZA) finally produced a zeolite structure atlas, in which a three-letter code is assigned to each zeolite framework type, which is used to describe and define a network of shared tetrahedrons at the corners of atoms, regardless of its composition how is it[52] These three-letter codes usually come from the name of the source material. As of July 2010, there are approximately 194 different zeolite frameworks, each with its own code [53]. Examples of some of the most important zeolite frameworks and their codes include zeolite A with LTA code A representing Linde type A, while the codes assigned to zeolites X and Y, FAU, mean zeolite with faujasite topology, and finally The sample codes of ZSM-5 and silicalite are used as MFI. Today, the name of zeolite follows three main conventions and all are accepted. For example, the polyhedron commonly called a cage present in zeolite LTA is actually a cavity. Cages extant in certain zeolite frameworks are displayed in Figure[54] (2.7)

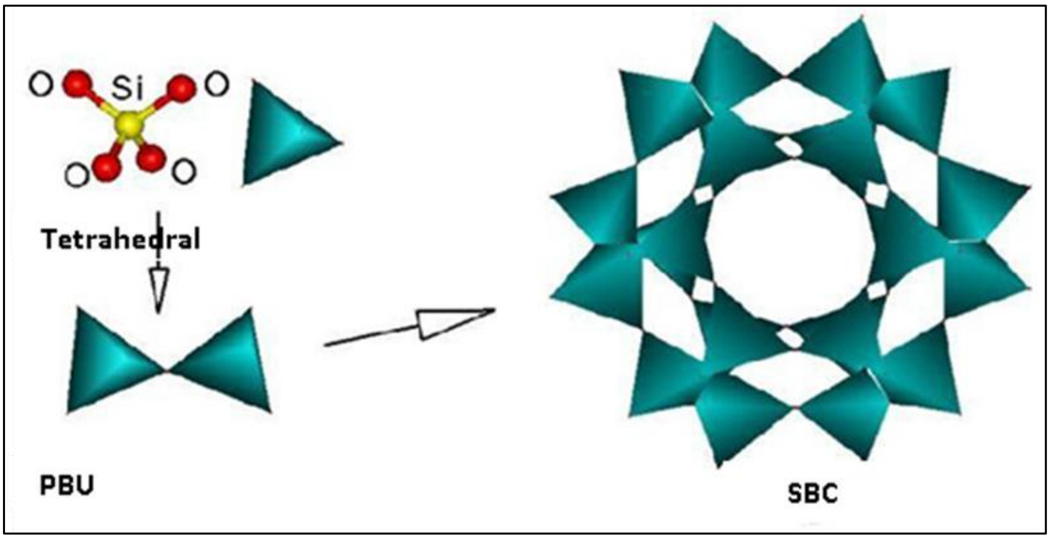

Figure(2.7): Shows diagram showing the relationship between the Tetrahedral, the PBU and the SBU [46]

Zeolites have several altered structures and there basic unit is the SiO4 and AlO4 tetrahedral, and they are bound together by sharing an oxygen atom. Zeolites A, zeolites X and zeolite Y contain a cubo-octahedral (i.e. p-cages) having the SiO4 and AlO4 tetrahedral at each corners of the framework. Often zeolite A structures are a result of the bonding between P-cages through squared surfaces that have a cube shape. The bonding between the six-angled surfaces and the hexagonal prisms results in the formation of the X-zeolite and the Y zeolite corresponding to the fogasite zeolite. The ZSM 5 zeolite system has a complex structure, which is due to the existence of a system with two cross channels, one linear and one zigzag[46].

In order to better understand the zeolite structure, we first need to understand the pore structure. The pore structure of zeolite is characterized by the presence of cavities or channels in the crystal lattice of each zeolite, and the volume and diameter of the pores are usually connected to each other through pores, and these pores also have a specific diameter of each zeolite. Among these channeled zeolites, those with channels extending parallel to each other exhibit a multi-dimensional and/or non-multidimensional cross-channel system as demonstrated in Table (2.1)

Table(2.1) shows the diameters in (m) of the pores for zeolite A, X and Y as well as the pore volumes (in%).

Zeolites	A	X	Y
poreDiameter (10^{-10}m)	4.1	7.4	7.4
Pore Volume (%)	47	50	48

Table(2.1), Illustrates the value of a zeolite composed of sodium cations, which are mobile and can be exchanged in the zeolite lattice. When these sodium cations present in the zeolite lattice are exchanged by potassium cations, the pore size is reduced to 0.3 nm. The correct cation exchange will affect the adsorption and catalytic performance of the zeolite[55].

The pore size and shape existing in the zeolite framework affect the adsorption performance of the zeolite and its ability to act as a molecular sieve. Zeolite classification can be based on the pore size present in the zeolite framework, and can be defined by the number of T atoms present in the framework, where T = silicon or aluminum ion. It is known that the type of open pore system existing in the zeolite framework will affect its catalytic and adsorption processes. Currently we have:

i. 8 member rings (usually called small pore zeolites). An example is zeolite A.
ii. 10 member rings (usually called medium pore zeolites). Instance is ZSM-5 zeolite.
iii. 12 member ring (often referred to as the large pore size zeolite) with zeolites X and Y as examples as shows in Figure (2.8 A,B)

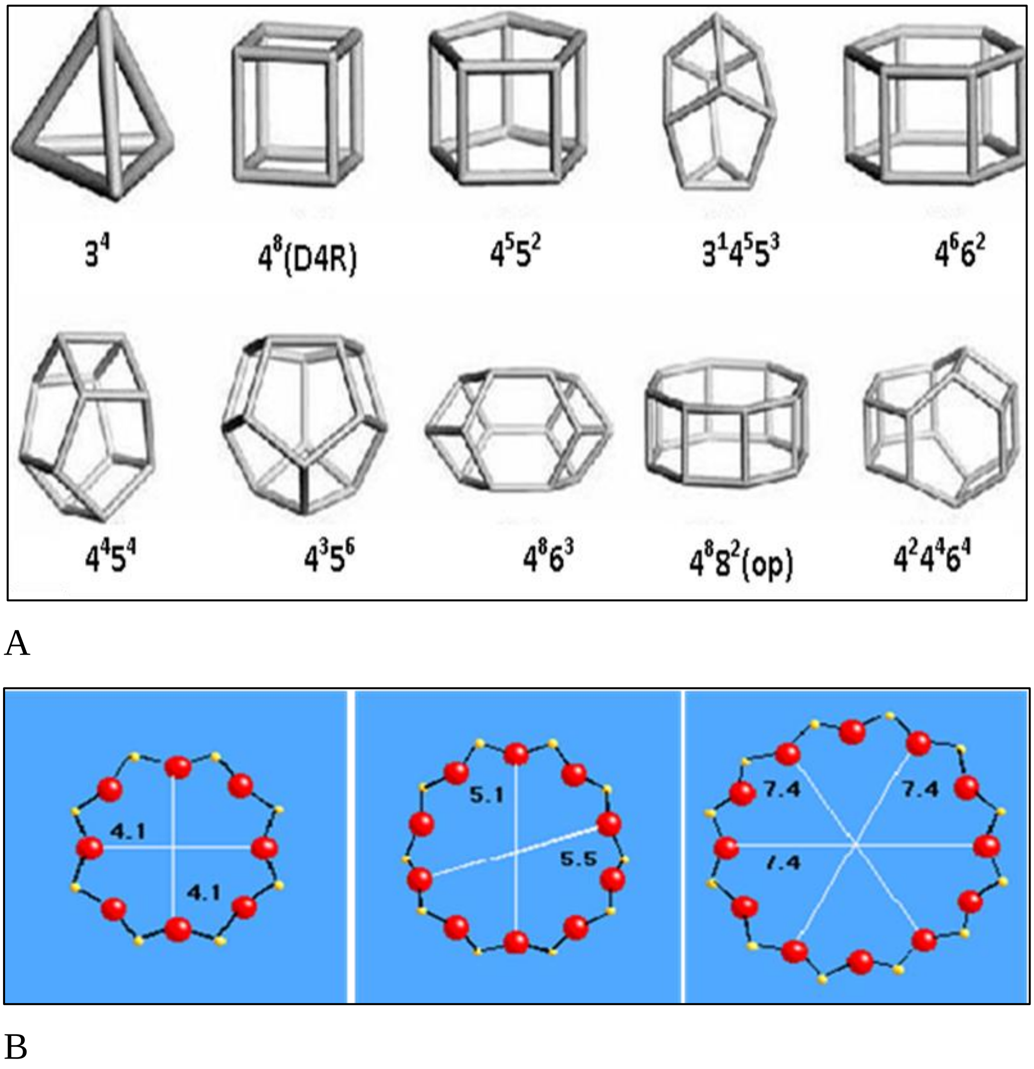

Figure(2.8 A,B): Shows structure of the pores in some zeolites showing (1) an 8-ring, zeolite A (2) a 10-ring, ZSM-5 (3) a 12-ring, zeolite Y11 [46]

There are two main types of zeolites: natural and synthetic zeolites. There are more than 200 zeolites to choose from, 50 of which are natural zeolites, and the remaining 150 are synthetic zeolites. Natural zeolite is the result of indirect volcanic activity. The most common natural zeolite is clinoptilolite, while synthetic zeolite is made from natural materials (such as kaolin) or synthetic materials such as sodium aluminate and silica. Natural zeolite was first found in pores and cavities in basalt, and later in sedimentary rocks closer to the earth's crust. Natural zeolite was originally used as an adsorbent in agriculture [56], the annual output of natural zeolite is expected to exceed 50,000 tons, and sales are expected to reach 40,000 tons within a few years [57], but the nature of these natural zeolites is inconsistent, because the chemical composition of zeolites obtained from different areas of the same mine will change, This is also a bad deposit. The zeolite content may be as low as 15-20%, so the cost of mining from this site is high. Finally, inhalation of fibrous Erionite and Mordenite from these natural zeolite sites may be harmful to human health adsorbent[58].

It has been observed that natural zeolite has better resistance to acidic environments and higher thermal stability than many common commercial synthetic adsorbents. And their thermal stability tends to increase with the increase of Si/Al ratio and the presence of alkaline cations in the zeolite framework[59].

2.4 Adsorption and separation of compounds by zeolite

The consequence of type A zeolite in the adsorption process may be caused by two diverse values. First, it is possible to separate molecules with different cross-sections from each other by allowing only smaller molecules to pass through uniform zeolite pores, so that they can enter the actual adsorption cavity (molecular sieve effect). Secondly, due to the polar nature of the inner surface of the zeolite crystals, more polar molecules are adsorbed in preference to fewer polar molecules (polar effect). Some of the adsorption characteristics of Zeolite A are based on the sieve effect, while others are based on the polarity effect. In some cases, both principles are effective[60].

The key physical property of each adsorbent is surface hydrophobicity. In zeolite adsorbents, the hydrophobicity can be changed by changing the ratio of silicon to aluminum. Depending on the degree of dealumination, the zeolite surface usually exhibits polar and non-polar adsorption behavior. The highly dealuminated zeolite preferably adsorbs non-polar compounds from a mixture of adsorbents with different polarities[61].

The adsorption strength and selectivity of the gas on the zeolite depend on the size, shape and structure of the zeolite cavity, the cation charge density and the polarizability of the guest adsorbed molecules. Generally, large or more polar polar gas molecules will be more strongly and selectively adsorbed on the zeolite with smaller pores and larger cationic charge density. Generally, divalent cations have a greater charge density than monovalent cations of similar size[56].

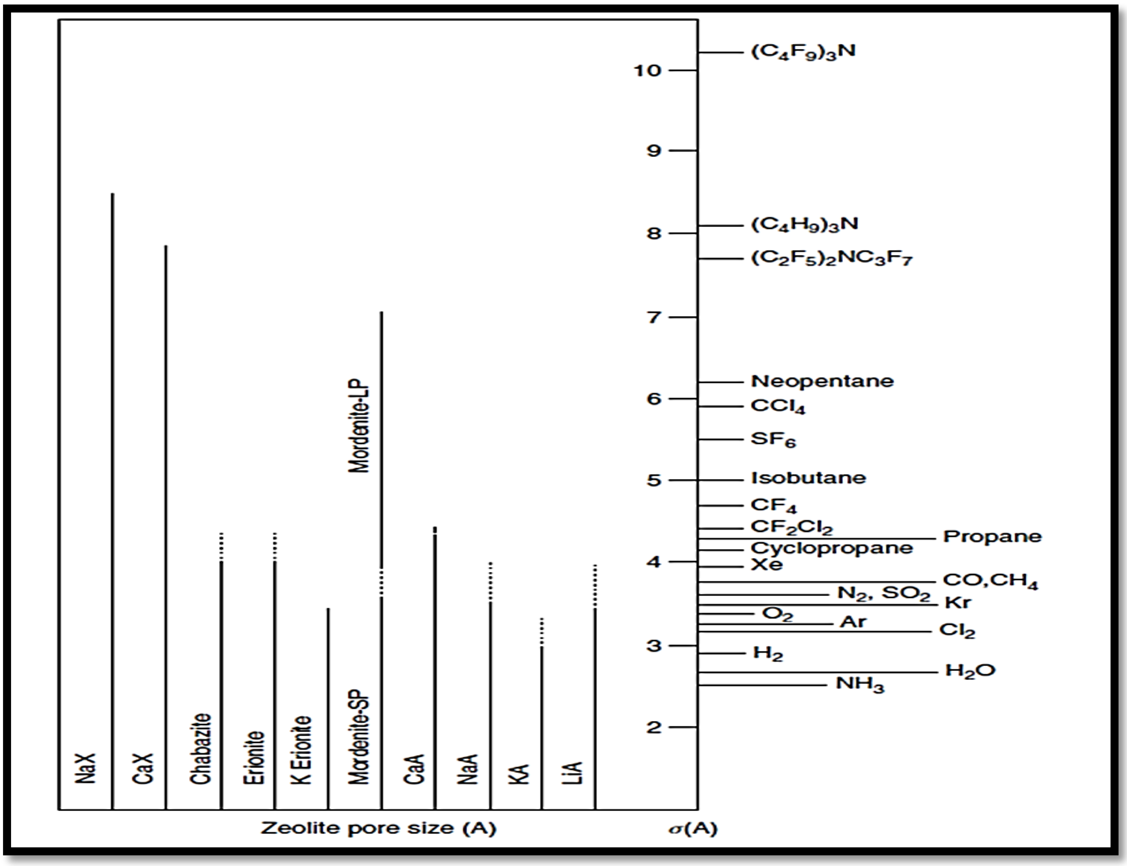

Figure (2.9): shows correlation for molecular sieving of molecules with kinetic diameter σ in various zeolites with different effective pore sizes [62]

Typical cations are alkali metals, alkaline earth metals and proton H+. Figure (2.10) illustrates an example of a common cage structure called sodalite and how it is composed of silicon, aluminum and oxygen atoms. Each row in Figure (2.10) represents a bridged oxygen atom, and the intersection is located on the silicon or aluminum atom. Some of the characteristics of Y-type zeolite are high thermal stability, large internal surface area, and easy-to-reach active sites[63]

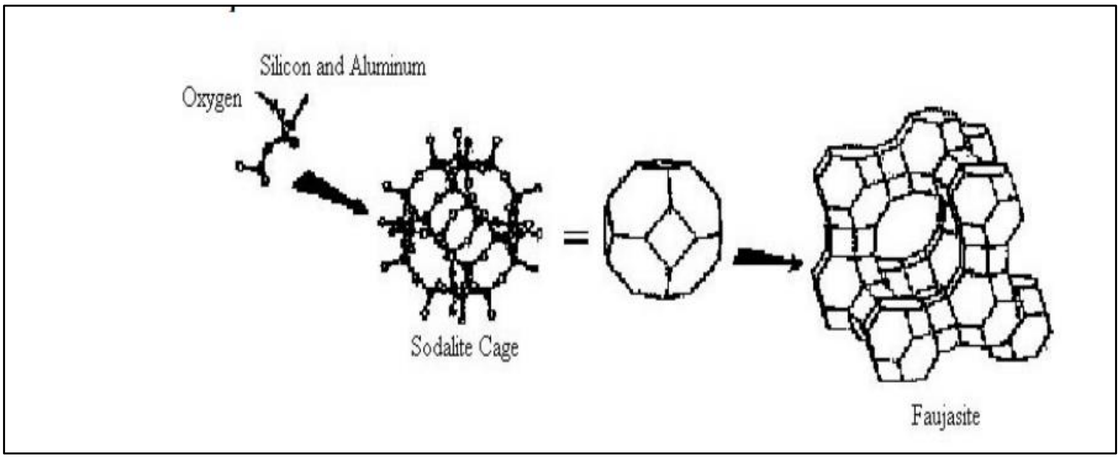

Figure (2.10): Shows schematic of zeolite frameworks [63]

2.5 Methods used in zeolites synthesis

The production of crystalline solid materials can be divided into two categories. Some reactions occur in the solid state, while others occur in the liquid state. This solid-state reaction usually occurs at a temperature higher than 300°C to overcome the difficulties caused by the transportation of reactants to the site where the reaction occurs. In the other group, the reaction is in the liquid phase, the solvent [64], since molecular transportation in the liquid phase is much easier than that in the solid phase, these syntheses are carried out at relatively low temperatures well below 300°C. Hereafter, the syntheses of zeolites are carried out in the liquid phase and there are three methods used in the synthesis of zeolites and they include:

2.5.1 Hydrothermal method

The hydrothermal method is the earliest method of synthesizing zeolite, in which the synthesis is carried out under the conditions of water as the solvent, alkali solution as the mineralizer, and temperature of 90-180°C. The reactants are usually placed in an autoclave lined with Teflon, which has a hydrothermal synthesis pressure up to 15 bar to optimize the production of zeolite. Since the temperature required for hydrothermal synthesis of zeolite is much lower, this method is easier and cheaper than other methods[64]. The nucleation and crystallization of crystals does not necessarily occur in solution, but can occur at gels present in the mixture.

2.5.2 Solvothermal method

The method of solvothermal synthesis of zeolite involves the use of solvents to produce zeolite. Based on this broad description, since water is by far the most common solvent, hydrothermal method can also be said to be a member of this category. However, there are other solvents, such as alcohols, hydrocarbons, pyridine, etc., which have been successfully used in zeolite synthesis. The solvents used in the solvothermal method of molecular sieve synthesis range from non-polar , hydrophobic to polar and hydrophilic[64] .

2.5.3 Ionothermal method

Ionothermal is additional special class of solvent thermal synthesis technology where in the solvent used are mostly ionic compounds and not molecular in nature as in the case of thermo-solvent solvents. The solvents used in the thermo-ionic method of zeolite synthesis are called ionic liquids and their ionic nature has an effect on some specific properties such as low vapor pressure[64].

2.5.4 Materials for zeolite synthesis

Zeolite is usually synthesized using the hydrothermal synthesis method using commercial chemicals as the primary source of SiO2 and Al2O3[65] .The process of producing these chemicals is costly which leads to complications and a higher cost of zeolite synthesis, which leads to a limitation of the commercialization and uses of this zeolite in many industrial applications, from the disadvantages mentioned above, the use of cheap and relatively abundant raw materials which act as sources Combined silica and alumina for the synthesis of zeolite is highly desirable[66].

For example, a comparison of the cost of obtaining the source of silica and alumina from chemical feedstocks and kaolin / metacoline [67] was performed. The result showed that the clay as a precursor to zeolite A has a 15% cost advantage over a commercial chemical such as sodium silicate.

Compared with natural zeolite, synthetic zeolite made from natural or synthetic raw materials has a wide range of chemical properties, pore sizes and better thermal stability. Compared to natural zeolite, they are widely used commercially because they have higher purity and more uniform particle size[55].

Preparation of synthetic zeolite from chemical sources of silica and alumina is very expensive, however cheaper raw materials such as clay minerals, natural zeolite, municipal solid waste, coal ash, industrial slag, incineration ash, etc., are used as raw materials for zeolite synthesis. At present, there is a lot of research underway regarding the use of clays and other raw materials in zeolite synthesis, which have the advantage of being relatively cheaper, readily available and more abundant. As displayed in Table (2.2) [68].

Table(2.2): Shows A tabular representation of cheap, abundant and readily available raw materials that has been used to synthesize zeolite and the type of zeolite synthesized [68]

Name of Raw Material
Kaolin
Rich husk ash
Fly ash
Waste perlite
Sio2 sinter and perlite glass.
Template –free batches of macroporous alumina disks
Halloysite mineral
Lithium slag
Brazilian chrysotile and rice husk
Coal fly ash
Silicic acid and sodium aluminate

The characteristics that enable zeolite aluminosilicate crystals to perform all of these functions in several industrial applications are their uniform pore size and shape, their cation mobility as a catalyst, and their hydrophilic and/or hydrophobic properties to coal solutes. Composed of [SiO4] and [AlO4] tetrahedrons, they extend infinitely in a three-dimensional network connected by shared oxygen atoms. This kind of [SiO4] and [AlO4] tetrahedrons can be represented by TO4, usually called the main structural unit (PBU), where T represents silicon (Si4 +) or aluminum (Al3 +) ions, and O4 represents each oxygen atom shared by two T atoms. [46]. This is shown in Figures (2.11)& (2.12)

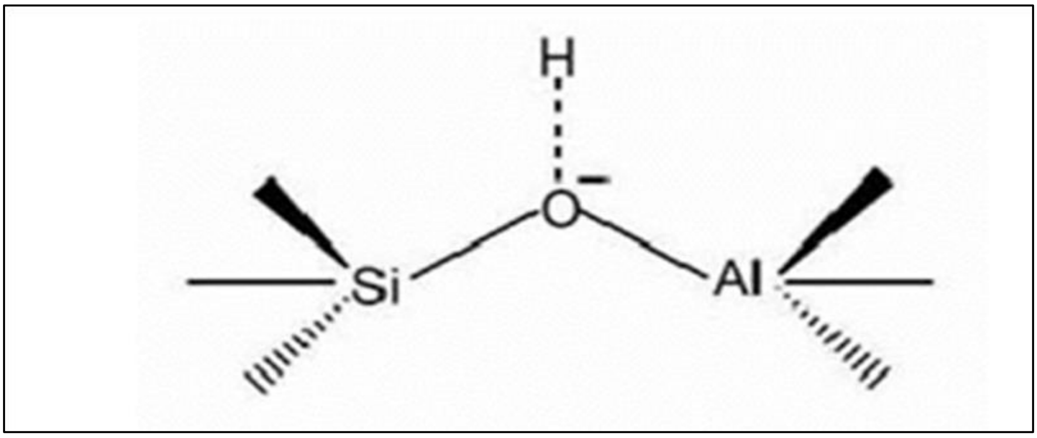

Figure (2.11) : Shows description of the chemical Structure of Zeolite [46]

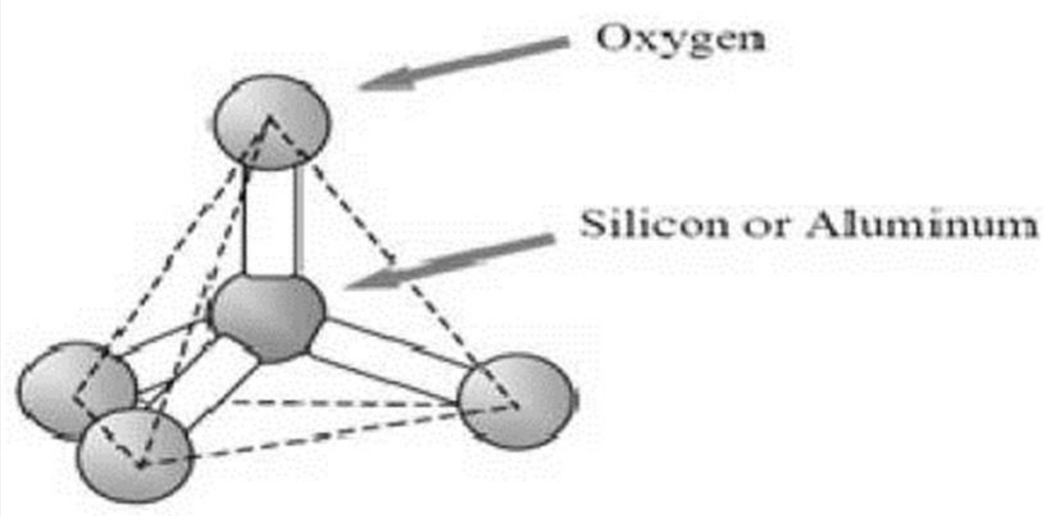

Figure(2.12): Shows schematic of the building unit of zeolite structure [30]

Zeolites are represented based on their crystallographic unit cell by the general formula in equation(2.3) [30].

$$M_{a/b}[(AlO_2)_a(SiO_2)_y]CH_2O \quad \text{………(2.3)}$$

Where M represents alkali metal or alkaline earth metal cations, b represents the valence of alkali metal or alkaline earth metal cations, c is the amount of crystallization water per unit cell of zeolite, a and y represent the [SiO4] and [AlO4] four sides in the unit cell of zeolite body. The ratio of y/a is usually 1-5, but in the case of silica-based zeolites, the value of y/a can be 10-100.

2.6 The Hardness of water

Water is one of the most important natural resources, as the planet is largely covered by water. However, approximately 98% of this water is sea water and is therefore undrinkable due to the salt. Only about 0.036 percent of the planet's total water supply is found in lakes and rivers. A WHO / UNICEF survey indicates that 45 developing countries show that women and children have main accountability for collecting water in the enormous majority of households around (76%). This is the period not devoted working in an income-generating job, caring for family members, or going to school [69].

The massive increase in world population and rapid advances in industrialization are causing an increase in the demand for water, making it valuable in more and more countries in some parts of the world an essential commodity. A recent research paper published in Nature indicated that 80% of the world's population is exposed to high levels of threat to water security [70].

The problem of water hardness has been reported in various places around the world. Among the many known forms of pollution, water pollution is a major concern because water is a fundamental necessity of life and absolutely necessary for the survival of all living things. All over the world, but its quality is constantly being changed through various human activities in which an amount of money is spent annually to ensure water purification (minerals are removed) to avoid its negative effects such as deteriorating soap and accelerated sedimentation on taps changes the physical and chemical properties of the water [6].

Water hardness is determined by measuring the total concentration of magnesium and calcium in the water source. It influences environmental cultures as well as many other species dependent on a fixed concentration of calcium carbonate. The World Health Organization states that hard water may lead to cardiovascular disease [71]. Various industrial trials use water as the main source of operations and to generate steam in the boiler. The textile industry, the paper industry, the sugar industry, the dying industry and the beer industry are the main sectors that use water to generate steam.

Nevertheless, direct use of hard water boiler feed reduces the boiler efficiency to produce high capacity steam due to the presence of water hardness in the water by scale formation, sludge, prepping, foaming and corrosive boilers [71].

Insufficient calcium intake has been associated with an increased risk of osteoporosis, (kidney stones), colorectal cancer, high blood pressure, stroke, coronary artery disease, insulin resistance, and obesity

Nowadays, synthetic zeolite is used commercially more often than natural zeolites due to the purity of crystalline products and uniformity of particle sizes. However, the preparation of synthetic zeolite from chemical sources of silica and alumina is very expensive. These costs can be reduced by using clay minerals, obsidian (perlite and pumice), rice husks, diatoms, and ash, ash or paper sludge ash as feedstock [72].

2.7 Theories of adsorption

Various types of adsorption isotherms exist, the main ones presence the following:

2.7.1 Langmuir isotherm

The American chemist Iraving Langmuire, who won the Nobel Prize in Chemistry in 1932 for his "discoveries and investigates in the field of superficial chemistry", developed the relationship between the amount of gas absorbed on the surface and the pressure of that gas in 1916[73].

A model is prepared based on the presence of adsorption fixed number of sites on the surface of the adsorbent, every single site capable holding a single adsorption molecule. Entire sites are corresponding in their adsorption affinity of particles, and the exterior is unchanging thus no interaction between adsorbed particles exists.

Langmuir adsorption is considered monomolecular, and does not take into account the situation in which further adsorption may occur on the adsorbent already on the surface.

The Langmuir isotherms can be expressed as follows[74].

Where**:**

$Ce/Qe=1/ab+Ce/a$ ……(2.3)

Qe: The adsorption capacity at equilibrium per unit weight of adsorbent, **(mg/g)**.

Ce: The equilibrium concentration of adsorbate after adsorption, **(mg /L)**.

a: The Langmuir constant which is a measure of adsorption maximum capacity **(mg/g)**.

b: The Langmuir constant which is a measure of energy of adsorption **(L/mg)**

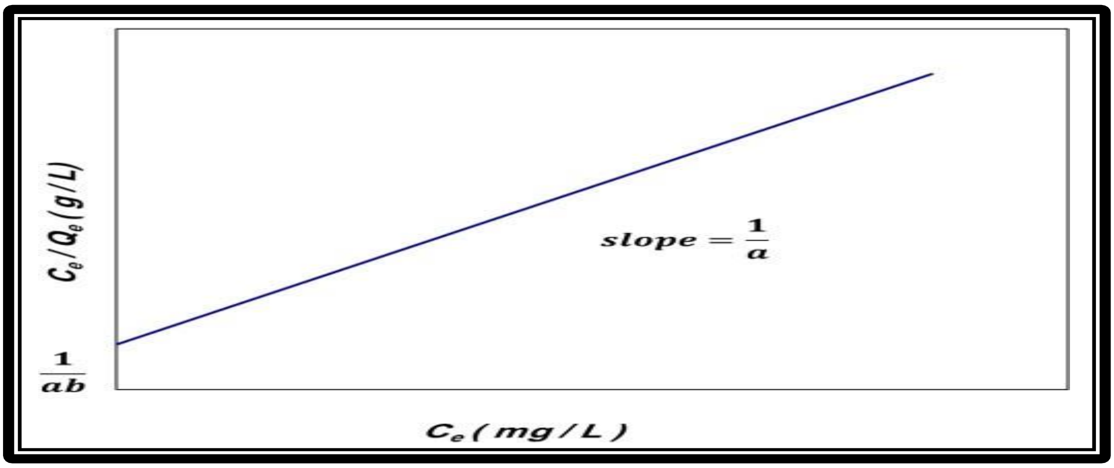

Figure (2.13): The linear form of Langmuir isotherm[74]

This model can be utilized as a linear illustration of the experimental data by plotting (Ce/Qe) aganist (Ce) as presented in Figure (2.13). The Langmuir's constants (a) and (b) can be assessed from the slope (1/a) and (1/ab) intersection in the linear equation[75].

2.7.2 Freundlich isotherm

The German physicist, Herbert Max Finley Freundlich, in 1926 presented an experimental adsorption temperature scale for an imperfect system. In deriving the Langmuir isothermal, the existence of independence and similarity in binding energy at each adsorption site was assumed. This linear relationship is obeyed by many but not all of them have low concentration[73]**.**

His suggestion was based on experimental dimensions. The isothermal equation for Freundlich absorption can be derived by assuming a heterogeneous surface with adsorption on each class of sites subject to the Langmuir equation. Heterogeneous adsorption sites contain diverse latent energies and various superficial geometric figures, thus site to site affinity towards similar molecule differs as shown in the equation of Freundlich: [74]

Qe = Kf Ce 1/n …… (2.4)

Where:

Qe: quantity of adsorbate adsorbed per unit weight of adsorbent at equilibrium, **(mg/g)**.

Ce: equilibrium concentration of adsorbate in solution after adsorption, **(mg/L)**.

n: adsorption process extent.

Kf: Freundlich constant, **(mg/g)**.

The Freundlich constants can be obtained from the slope and intercept of the plot between the **(log Qe)** versus (**log Ce)** after taking logarithms both side of equation **(2.4)** we get:

log Qe = log Kf + 1/n log Ce **………**(2.5)

If **(log Qe)** is strategized in contradiction of **(log Ce)** a straight line should be obtained as displayed in Figure **(2. 14)**. The slope of the line will provide the rate of **(1/n)** and the stop on the Y-axis provides the rate of **(log Kf) .[75]**

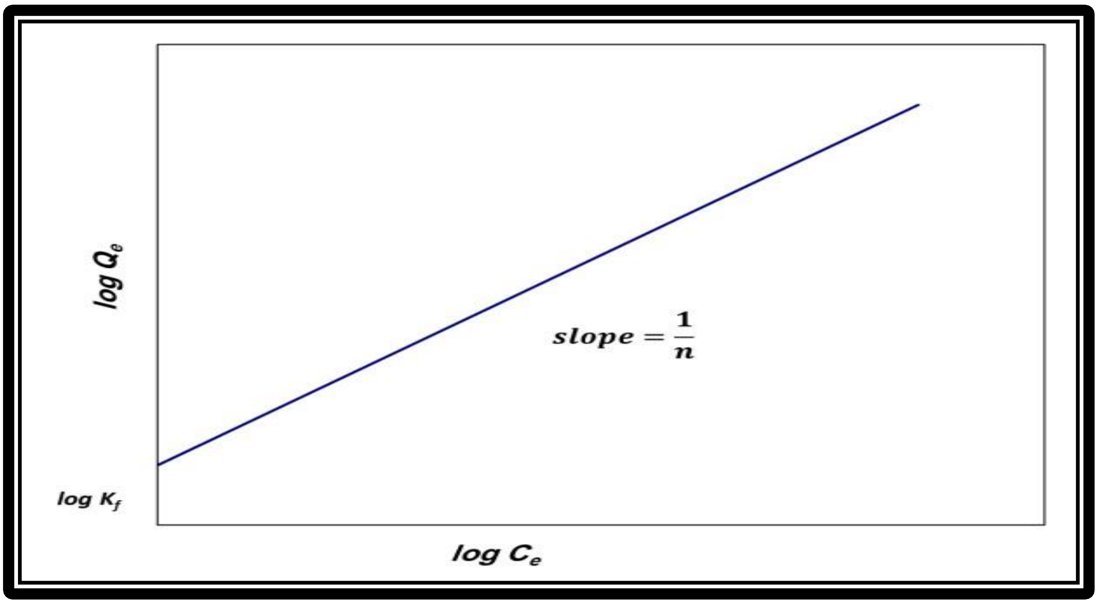

Figure (2.14): The Linear relationship Freundlich isotherm [75]

2.7.3 Temkin isotherm

Isotherm of Temkin includes an agent that obviously takes into explanation condensation of species - reaction of adsorbents This isotherm assumes that

1. The adsorption temperature of all particles in the layer decreases linearly with coverage by reason of the adsorption interactions with the absorber.
2. The absorption is categorized by constant dissemination, and with this energy, even some maximum binding energy.

The Temkin isotherm is given by the following equation: [73]

Qe = BT ln (AT. Ce) ……….(2.6)

Where:

AT: is the equilibrium binding constant, **(L/g)**.

BT: the Temkin isotherm constant which can be obtained as follow:

BT = RT / bT ………(2.7)

Where:

bT: is related to heat of adsorption, **(J/mol)**.

R: is the universal gas constant, **(8.315 J/mol.K)**.

T: is the absolute temperature, **(K)**.

A linear form of Temkin isotherm was acquired by reorganizing equation:

$$\mathbf{Qe = BT\ ln\ AT + BT\ ln\ Ce} \qquad \ldots\ldots\ldots.(2.8)$$

The Temkin coefficients **(AT)** and **(BT)** were obtained from the slope and interrupt of the plot between the **Qe** and **ln Ce**.

2.8 Thermodynamic study of adsorption of zeolite

A change in temperature can affect the adsorption from solutions straightly if the constituents of the solution are completely miscible, or in concentration with nature and variation the solubility if they are not entirely miscible[76].

The constant of adsorption equilibrium, K is clarifies thermodynamically through utilizing "Van't Hoff equation" as [77]

$$\text{Lnk}=-\frac{\Delta H}{R}\cdot\frac{1}{T}+\frac{\Delta S}{R} \qquad \ldots\ldots\ldots.(2.9)$$

Where :

k : The thermodynamic equilibrium constant

ΔH : The enthalpy change ($kJ.mol^{-1}$.)
ΔS : The change in entropy ($kJ.mol^{-1}.K^{-1}$)

R : The gas constant (8.314 $J.mol^{-1}.K^{-1}$)

T : The absolute temperature (K).

If ***ΔH*** does not depend on the temperature within a known temperature interval, then lnk is a linear function of the reciprocal of the absolute temperature. The slope of the line lnk pair (1/T) is equal to ***–(ΔH/R),*** and the cross section on the ordinate axis is equal to ***(ΔS/R).*** Therefore, the temperature depends on the equilibrium constant of the reaction and ΔH. Temperature also depends on solubility. The effect of temperature on adsorption depends on the enthalpy change. The reaction that absorbs heat (ΔH>0) is called endothermic reaction, and the reaction that releases heat

(ΔH<0) is called exothermic reaction. The entropy of the system is a function of the state of the system. Its change is equal to the sum of the reduced heat absorbed by the system during equilibrium. Entropy is a single valued, continuous and finite function of the state [76].

2.9 Adsorption kinetics

Kinetics is the science of studying chemical processes to describe the rate of absorption and the factors that can influence rates. This rate helps control the absorption time at the liquid and solid interface through using main kinetic models :

1. A pseudo-first-class model.
2. A pseudo-quadratic model.
3. The diffusion model within particles.
4. Elovich model.

2.9.1.Pseudo-first order model

The first-order adsorption rate equation for solvents from a liquid solution on coal was the first kinetic equation for the adsorption of a liquid / solid system based on solid capacitance, and it has been used extensively to describe the adsorption kinetics. In order to distinguish the kinetic equation on the basis of the absorption capacity of a solid from that based on the concentration of the solution.

The Lagergren equation is represented, first degree and also called pseudo first degree equation [78]:

$$dq/dt = k1\ (qe - qt) \qquad \ldots..(2.10)$$

In which :

qt is the amount adsorbed at any time, (mg/g)

qe is the amount adsorbed at equilibrium(mg/g)

k1 is the pseudo- first order rate constant (min-1)

The integrated form of the equation (2.11) for the boundary conditions ***of t=0, qt = 0 and t = t, qt = qt .***

$$\ln(qe - qt) = \ln qe - k1\ t \qquad \ldots\ldots(2.11)$$

The pseudo-first order constants can be obtained from the slope and intercept of plot between ln(q_e-q_t) and time (min).

2.9.2.Pseudo-second order model

Class II model, rate determination step is surface absorption which includes chemical absorption, so the physical and chemical reactions between the two phases lead to removal from solution. Equation of this form is given by[79]:

$$dq_t / dt = k_2 (q_e - q_t) \qquad \text{.....(2.12)}$$

Where k_2 is the pseudo-second order rate constant (g/mg.min) . When t = 0 to t = t and $q_t = 0$ to $q_t = q_t$, the Equation becomes**: -**:

$$1/ (q_e - q_t) = 1/q_e + k_2 t \qquad \text{......(2.13)}$$

Equation (2.13) can be rearranged to obtain the following linear form:

$$t/q_t = 1/(k_2 q_e^2) + 1/(q_e)t \qquad \text{......(2.14)}$$

The pseudo-second order constants can be obtained from the slope and intercept of the plot between the t/q_t against t.

2.9.3.Intra-particle diffusion model

The intra-particle diffusion model describes the adsorption processes, where the rate of adsorption depends on the speed at which the adsorption propagates towards the adsorbent (i.e. the process is controlled by diffusion),which is gives by[80]:

$$q_t = k_D t^{1/2} + C \qquad \text{.....(2.15)}$$

In which :

q_t : the amount of adsorbed at any time (mg/g)
k_D : the diffusion constant (mg/g $min^{1/2}$)
$t^{1/2}$: the sequare root of the time ($min^{1/2}$)
C : the thickness of boundary layer.

The diffusion constant was determined from the slope of the plot between q_t and $t^{1/2}$.

2.9.4 Elovich Model

The Elovich or Roginky –Zeldovich equation is generally expressed as follows[81]:

$dqt/dt=\alpha \exp(-\beta qt)$ ….(2.16)

Where

qt:the amount of adsorbed at any time (mg/g)

α:the initial adsorption rate (mg.g-1.s-1),

β:adsorption constant (g/mg-1) during any one experiment.

To simplify Elovich's equation, [82] suppose $\alpha\beta t >> 1$, and when applying the boundary conditions qt = 0 at t = 0 and qt = qt at t = t, equation (2.17) becomes [83] .

$qt=\beta \ln(\alpha\beta)+ \beta \ln t$ ……. (2.17)

Thus the constant can be obtained from the slope and intersection of the linear graph of qt versus ln t. Equation (2.17) will be used to test the applicability of Elovich's equation to adsorption kinetics.

Chapter Three

Experimental Part

3.1 Instruments

3.1.1. Tools and Instruments utilized in practice

The instruments and tools that are utilized in current study have itemized below with their specifics, origin, and places where obtainable.

Table (3.1): The instruments used in this study.

NO.	Instrument name	Specifics & Origin	Place Where available
1	**Electric Balance**	KERN & Shone GmbH, Type ACS 120-40, NO. WB12AE0308,CAPACITY 120g READBILITY, d= 0.1 mg (Germany)	The Laboratories of Chemistry Department, College of Science, University of Diyala, Iraq
2	**Oven**	BINDER , Hotline International (20-360° C) (Germany)	
3	**Hot Plate Magnetic Stirrer**	MS-H280-pro ISO LAB Laboratory, GmbH (Germany)	
4	**Water Bath with Shaker**	BS – 11,230 VAC-50 HZ, (Korea)	
5	**Electrical Furnace**	Type – Nabertherm, , Max Temperature 1300 ° C , 400V, 15.0 A, 50/60 HZ (Japan)	The Laboratories of Physics Department, Collage of Science, University of Diyala, Iraq

3.1.2 Devices utilized in categorization

The devices utilized are displayed in Table (3.2) with their specifics, origin, and place where obtainable.

Table (3.2): Apparatus used in characterization.

	Devices names	Specifics & Origin	Place Where obtainable
	X-ray Diffraction Spectroscopy (XRD)	XRD-6000 Cuka (X=1.5406 A°), 220/50, HZ, ،SHIMADZU (Japan)	Lab. of X-Ray Diffraction in Central Service laboratory, College of Education Ibn- AL-Haitham, University of Baghdad, Iraq
	Atomic Absorption Spectro photometer (AAS)	Shimadzu AA-7000, (Japan)	Lab. of Atomic Absorption Flame in Central Service laboratory, College of science Bio science department, University of ،Baghdad Iraq
	Atomic Force Microscope (AFM)	Scanning Probe Microscope, AA 3000 SPM 220 V-Angstrom Advanced Inc, AFM contact ،mode (USA)	The Special Laboratory of Dr. Abdulkareem M.A. AL-Sammarraie Iraq
	Scanning Electron Microscope (SEM)	TESCAN(Czech Republic) Origin	The Special Laboratory, Tehran, Iran College of Science, University of Sharif of Technology
	Energy Dispersive Spectroscopy (EDX)	TESCAN(Czech Republic) Origin	
	Fourier Transforms Infrared spectroscopy (FTIR).	SHIMADZU (IR PRESTIGE21) Origin	Laboratories of Chemistry Department, College of Science, University of Diyala, Iraq

3.2. Materials

3.2.1. The chemical materials .

Here are the properties of the chemicals used in this work:

Table (3.3) : chemicals used in this work

NO.	Chemicals	Formula	Purity	Molecular Mass	Source
1	**Calcium chioride dehydrate**	$CaCl_2.2H_2O$	99.9%	147.01	Espana
2	**Ethanol absolute**	C_2H_5OH	99.9%	46.069	Espana
3	**Magnesium(II) chloride hexahydrate**	$MgCl_2.6H_2O$	98.0-100:%	203.30	India
4	**Sodium hydroxide**	NaOH	99%	40	Espana
5	**Sulfuric acid**	H_2SO_4	96%	98.08	Belgium

3.2.2 Kaolin Clay

Kaolin clay was supplied from the State Corporation for Geological Survey and Mining. Kaolin clay is available at the Dwaikhla quarry in the Anbar region. Table (3.4) shows the chemical composition of kaolin clay determined by the State Corporation for Geological Survey and Mining.

Table: (3.4) The chemical composition of Dwaikhla kaolinite used in the preparation of type 4Å zeolite.

No.	Constituents	Weight, (%)
1	**SiO_2**	50.01
2	**Al_2O_3**	32.80
3	**Na_2O**	0.27
4	**TiO_2**	1.27
5	**Fe_2O_3**	1.24
6	**MgO**	0.24
7	**CaO**	0.28
8	**K_2O**	0.66
9	**L.O.I (wt%)**	12.30

3.2.3 Rice husks

Raw rice husks were collected from a small rice production unit in Baqubah, Diyala, Iraq.

3.3 Synthesies of zeolite 4°A

3.3 .1. Silica preparation via utilizing rice husk.

The rice husk was treated with 10% sulfuric acid (H2SO4) for 24 hours to remove all impurities. The treated rice husk was washed thoroughly with distilled water, dried at 100 ° C and pyrolysis in oxygen at 500 ° C for 6 hours, to produce silica [57] by steps and flow chart. displayed in figuer. (3.1) and (3.2)

A B C

Figure (3.1) : Shows steps of the preparation of SiO2.

Rice husk (a); carbonised rice husk (b); completely incinerated rice husk (c)[57].

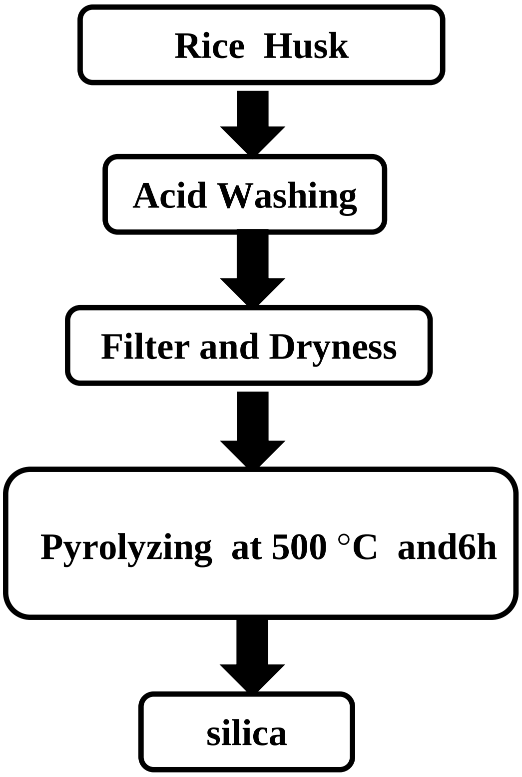

Figure (3.2) : Shows flow diagram of the procedure was used to extract silica powders from rice husk.

3.3.2. Alumina preparation via utilizing kaoline

The Iraqi kaolin extracted was from the Dwaikhla mine as a raw material. Kaolin powder calcined to 800 ° C for three hours in an electric oven. After cooling at room temperature, kaolin is ground by grinding machine and then sieving in a 75 μm sieve by a sieve grinder. Mix 8.3 g of kaolin powder and 276.6 ml of sulfuric acid at a concentration (1.5 M) in a 1000 ml inverter condenser at 500 rpm for 6 hours at 80 °C. Then allow the mixture to cool at room temperature after it is filtered to remove the residue, which is mostly silica, to obtain the filtering liquid from aluminum sulfate. 152 ml of filtered filter solution was added dropwise to 684 ml of ethanol at 5 ml / min, where it was stirred with a magnetic stirrer and then filtered. The separated precipitate was washed with ethanol, then dried at 80 ° C for 10 hour, and finally the precipitate was calcined at 500 ° C for 2 hour in an electric oven, to obtain alumina powder[85].

Figure (3.3):Shows steps of the preparation of Al_2O_3

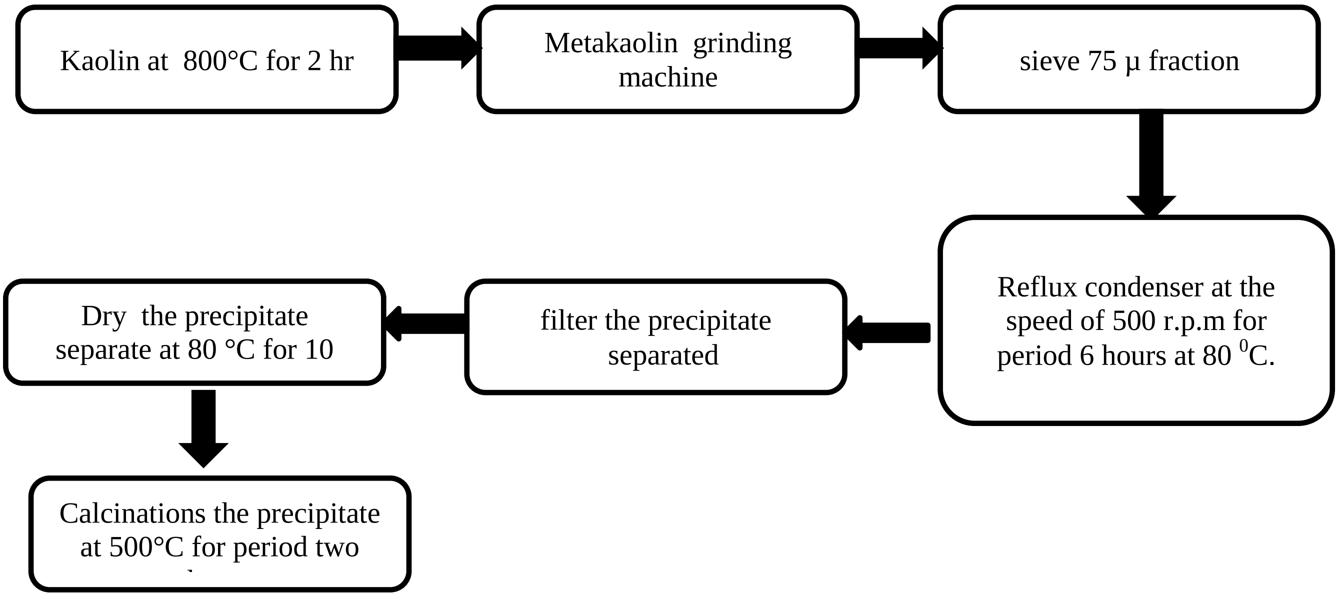

Figure (3.4): Diagram of steps for Al_2O_3 Preparation.

3.3.3 Zeolite preparation

A 500 mL Teflon beaker containing a magnetic stirrer was washed with deionized water. Sodium hydroxide (1.6616 g) was added slowly to deionized water and stirred until a clear and homogeneous solution appeared for about 5 minutes. The aqueous solution of sodium hydroxide was ready to prepare the seed gel. 2 ml of aqueous solution of sodium hydroxide was added to 0.7515 g of sodium aluminate oxide until a homogeneous mixture was formed; Silica oxide or 1.5361 g rice husk ash was added separately to 5.5 mL aqueous NaOH until homogeneously mixed. Both preparations were mixed under vigorous stirring to obtain a homogeneous mixture. The sample was time 24 hour at room temperature[86] .

3.4 Solutions preparation utilized in work:

3.4.1 sulfuric acid

In a glass beaker, 360 ml of deionized water and 40 ml of concentrated sulfuric acid are gradually added.

3.4.2 Sodium hydroxide solution

(1.6616g) of sodium hydroxide was weighed and transferred into (100) ml volumetric flask and the volume was completed to (100) ml with deionized water and stirring until clear and homogenous solution acquired.

3.4.3 Standard stock solution of Mg(II) ions

(1000) mg / liter Mg (II) stock solution with a weight of (8.3645) g of ($MgCl_2.6H_2O$) was prepared and dissolved in deionized water then diluted to the a (1000) ml volumetric flask. A series of solutions were prepared with (50, 100, 150, 200 and 250) mg / l in suitable dilute volumes from stock solution and deionized water.

3.4.4 Standard stock solution of Ca(II) ions

(1000) mg/L stock solutions of Ca(II) was prepared by weighing (3.661) g of ($CaCl_2.2H_2O$) and dissolve it in deionized water and then dilute it to the (1000) ml volumetric flask. A series of solutions with (50, 100,150,200 and 250) mg/L were prepared by adequate volumes dilution from the stock solution and deionized water.

3.5 Investigating the factors affecting adsorption method.

3.5.1 Effect of contact time on Mg (II) ions and Ca (II) adsorption

The time sufficient for the adsorption process to reach equilibrium at a temperature of 298 K was determined using five (100) ml volumetric flasks containing (50) ml of a solution of $Mg+^2$ and $Ca+^2$ ions. A concentration per ion of (100) mg / l and an adsorbent amount of (0.1) g of prepared SiO_2 / Al_2O_3 were added to each beaker and covered with a glass stopper and placed in a water bath shaker at a constant temperature of (298). K at (150) revolutions per minute at different time intervals (10, 20, 30, 40, 50) minutes. The solution was then filtered to prevent the zeolite particles from interfering the concentrations of $Mg +^2$ and $Ca+^2$ in the solution were measured to reach equilibrium using an atomic absorption meter.

3.5.2 Effect of quantity of Zeolite 4A° adsorbent.

The effect of the amount of absorbent was studied using (0.06, 0.08, 0.10, 0.12, 0.15) g of 4A ° zeolite to remove $Mg +^2$ and $Ca +^2$ ions using (50) ml constant of (100) mg / l $Mg +^2$ and $Ca +^2$ ions temperature (298) K, and a stirring speed (150) rpm. The adsorption contact time was (50) minutes in all cases.

3.5.3 Effect of temperature on adsorption

Adsorption experimentations are carried out as stated in section (3.5.1-3.5.3) at diverse temperatures (293, 303, 313,323 and 333) K to remove Mg(II) and Ca(ll) ion from aqueous solutions.

3.5.4 Effect of initial concentration of Mg (ll) and Ca(ll) ions

The effect of concentration was studied using a solution containing (50) ml of (50, 100, 150, 200 and 250) mg / l in the following cases: (0.1) gm of zeolite **4A°**degree, temperature (298)K, and stirring speed (150) revolutions per minute. The contact time for absorption of Mg (ll) ions and Ca (ll) used was (50) minute in all experiments.

3.6. Metal calculation removal

The percentage removal of metal (R%) was calculated using equation [57]

$$R\% = (C0-Ce) \quad)/C0 \times 100) \qquad \ldots\ldots\ldots\ldots\ldots\ldots\ (3.1)$$

Where

R % : The percentage metal removal.

Co : The initial concentration of metal ion (mg /l).

Ce: The equilibrium concentration of metal ion after adsorption at any time (mg /l).

3.7. kinetics of Mg(II) and Ca (II) ions Adsorption

For the purpose of studying the absorption kinetics of magnesium and calcium ions, five volumetric flasks (50 ml) of each ion were used at an initial concentration of (100) mg / l. Weight (0.1) g of prepared SiO2 / Al2O3 and placed in aqueous agitator at (150 rpm). Samples were withdrawn from the vibrator for regular periods (5,15,25,35,45) min and filtered to separate the absorbent, then atomic absorption spectroscopy was used to measure the absorbance of the solutions to determine the concentration. The reaction of the absorbent surface was studied at temperatures 308, 313,318 and 323 K.

Chapter Four

Results and Discussion

4.1 Characterization of the materials

4.1.1. X-ray diffraction

The X-Ray diffraction was employed to check and determine the crystalline phase of materials. The data of strongest three peaks for Kaolin ,metakaolin, alumina ,silica and zeolite are shown in Table (4.1) , (4.2),(4.3) (4.4) and (4.5) respectively. The X-ray diffraction pattern of are shown in Figures (4.1) , (4.2),(4.3), (4.4) and (4.5) for kaoline, metakaolin,alumina,silica and zeolite respectively as well.The particale size were calculated from Deby-sherver formula given below[87].

$$D = \frac{0.9\,\lambda}{\beta \cos\theta} \quad \text{.....................(4.1)}$$

In which :

D: is the crystallite size.

λ: is the length wave of radiation.

θ: is the Bragg's angle.

β: is the full width at half maximum (FWHM).

The estimated particle size of the Kaolin is (50.88) nm ,metakaolin is (50.88) nm, alumina (34.36)nm , Silica (33.88)nm and Zeolite (43.37)nm . The presence of sharp peaks in XRD pattern and particle size being less than (100) nm refers to the nano-crystalline nature of the prepared materials .

The XRD pattern revealed structural defects in kaolin because of variability in the peak positions and modulation of their intensities in kaolin XRD patterns. XRD identification of order/disorder is challenging because of overlapping peaks and interferences in kaolin [88] .

The XRD spectra analysis of hexagonal kaolin was very difficult because kaolin contained several mineral phases and many impurities. This led to appear of overlapping peaks due to complex structure of hexagonal kaolin. Therefore, additional treatments will be used to remove some ambiguity [89]. At low diffraction angles, there was a fairly large continuous background because of Lorentz polarization and the presence of amorphous phases and broad peaks (26.62° ,12.30° ,24.89°) were also observed. Furthermore, the low intensity and the more or less pronounced symmetry of the peaks at the smallest angles were likely because of the greater disorder of the structure of this kaolin [90] . All were shown in Table (4.1) and Figure (4.1)

Table: (4.1) The strongest three peaks in XRD spectrum of raw kaolin.

NO.	2Θ/(deg)	d/(Å)	FWHM/(deg)	Intensity/(counts)
1	26.6237	3.3454	0.1613	408
2	12.3031	7.1884	0.3933	202
3	24.8970	3.5734	0.3770	185

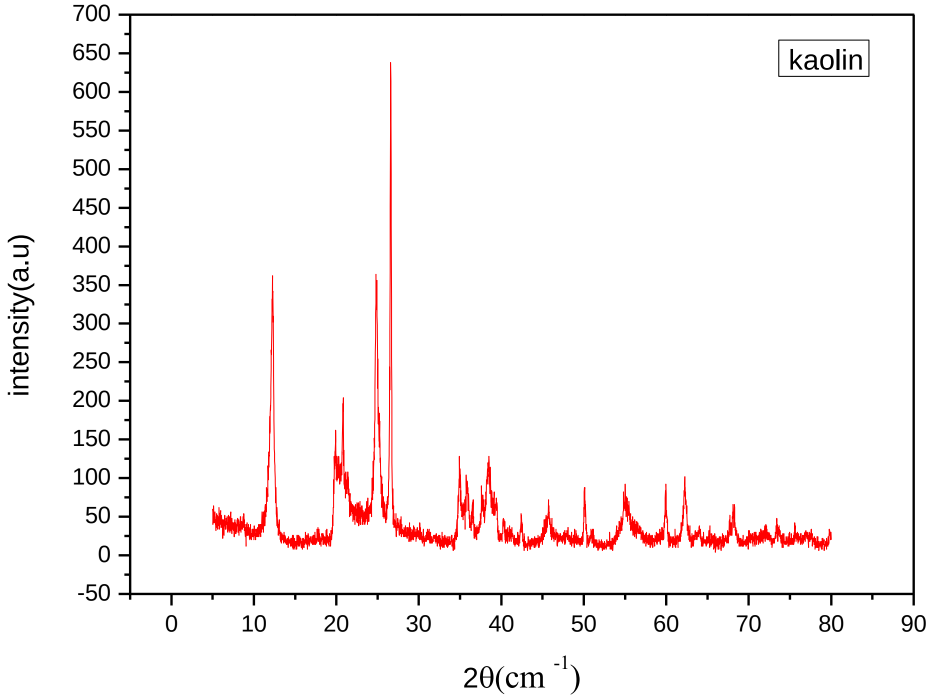

Figure.(4.1): XRD pattern of raw Kaolin.

Figure (4.2) presents the XRD pattern of complete poorly crystalline metakaolin formed by calcination of kaolin (at 800 °C for 3 hours), indicating on the formation of a new phase of dehydroxylated, hence the internal structure was destroyed with containing negative charges and shows only one characteristic diffraction peaks located at (26.63º, 20.84º,50.09º) that is attributed to kaolinite remains in the calcined kaolin. Aluminosilicate Na2(Al2Si3O) are found in the treated kaolin, in addition to disappearing of peaks related to all raw minerals [91,92]

Table :(4.2) The strongest three peaks in XRD spectrum of prepared metakaolin.

NO.	2Θ/(deg)	d/(Å)	FWHM/(deg)	Intensity/(counts)
1	26.6305	3.3446	0.1640	467
2	20.8494	4.2571	o.1780	82
3	50.0956	1.8194	0.1785	60

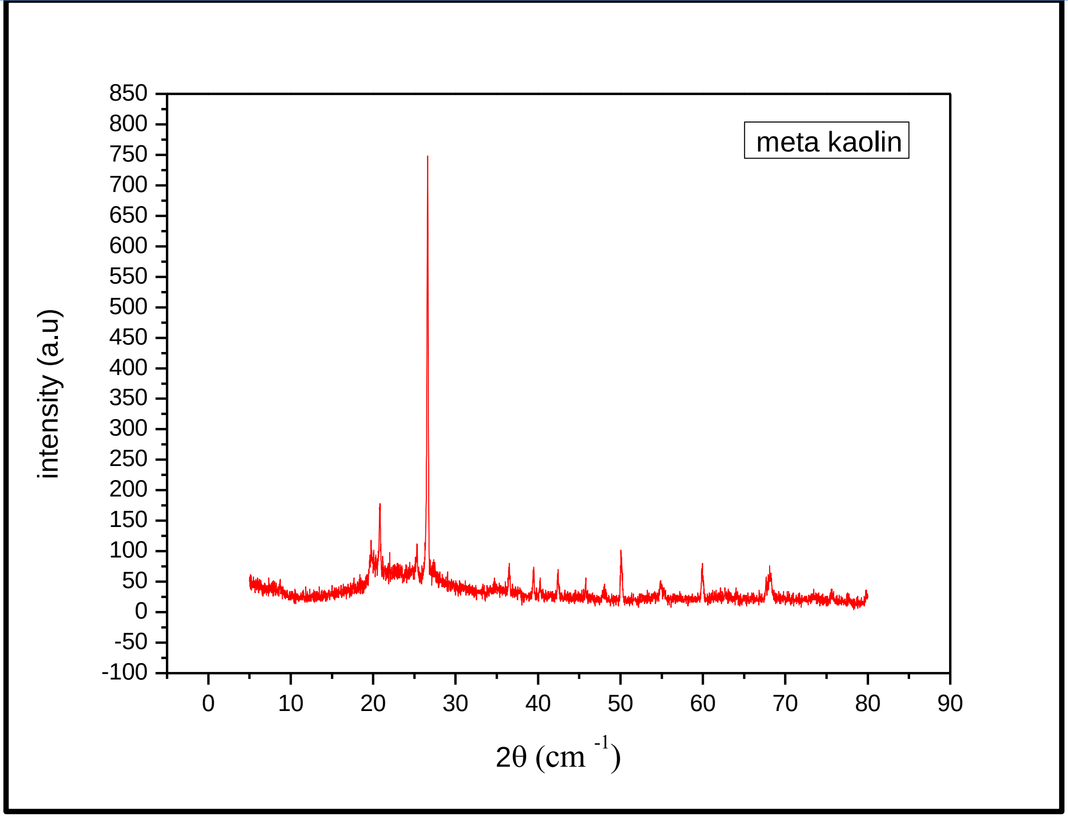

Figure.(4.2): XRD pattern of prepared metakaolin.

One significant result of the X-ray diffraction study is the asymmetry of the most of the alumina reflections in the low angle side of the peaks. The extent of this skew- ness is –alumina silicate composites compared to only alumina produced .peaks are observed at(32.26°)(33.99°)(19.19°) is thus clear that the observed asymmetry is sample-dependent

Table :(4.3) The strongest three peaks in XRD spectrum of prepared alumina.

NO.	2Θ/(deg)	d/(Å)	FWHM/(deg)	Intensity/(counts)
1	32.2681	2.77200	0.24360	216
2	33.9929	2.63519	0.22740	114
3	19.1910	4.62112	0.23480	107

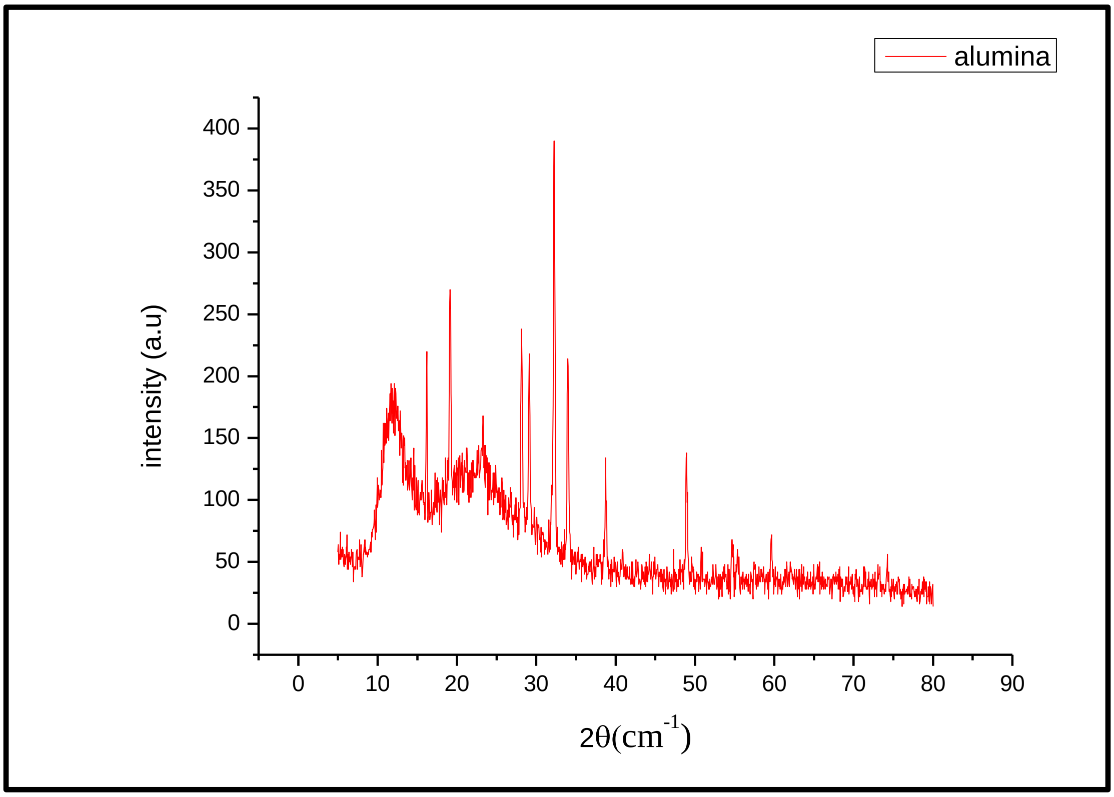

Figure (4.3): XRD pattern of prepared alumina.

Studying X-ray diffraction data of Table (4.4) presented the structural state of rice husk silica and shown that it is dependent on the processing temperature. Often the structure of the silica is investigated by X-ray diffraction (XRD) and the state is revealed by the shape of the diffractogram obtained. A study done by Hamdan et al. [93] showed that over various temperature ranges rice husk silica can exist in either crystalline or amorphous state as shown in Figure (4.4)

Figure (4.4) is a diffractogram of rice husk silica processed through burning in temperature 500 ◦C , These findings are in agreement with the work of Kapur [94] who studied the structural behaviour of silica over a temperature range of 400-1500 ◦C and reported that at combustion temperature above 900°C, the silica in rice husk ash consisted of cristobalite and a small amount of tridymite. Other researchers [95] reported similar results. Thus, to obtain amorphous silica from rice husk, the processing temperature should not exceed 700°C, as phase transition to the crystalline structure of crystobalite would soon follow, although no specific temperature has been reported for this transformation.

Table (4.4): The strongest three peaks in XRD spectrum of prepared of silica.

NO.	2Ө/(deg)	d/(Å)	FWHM/(deg)	Intensity/(counts)
1	32.2681	2.77200	0.24360	216
2	33.9929	2.63519	0.22740	114
3	19.1910	4.62112	0.23480	107

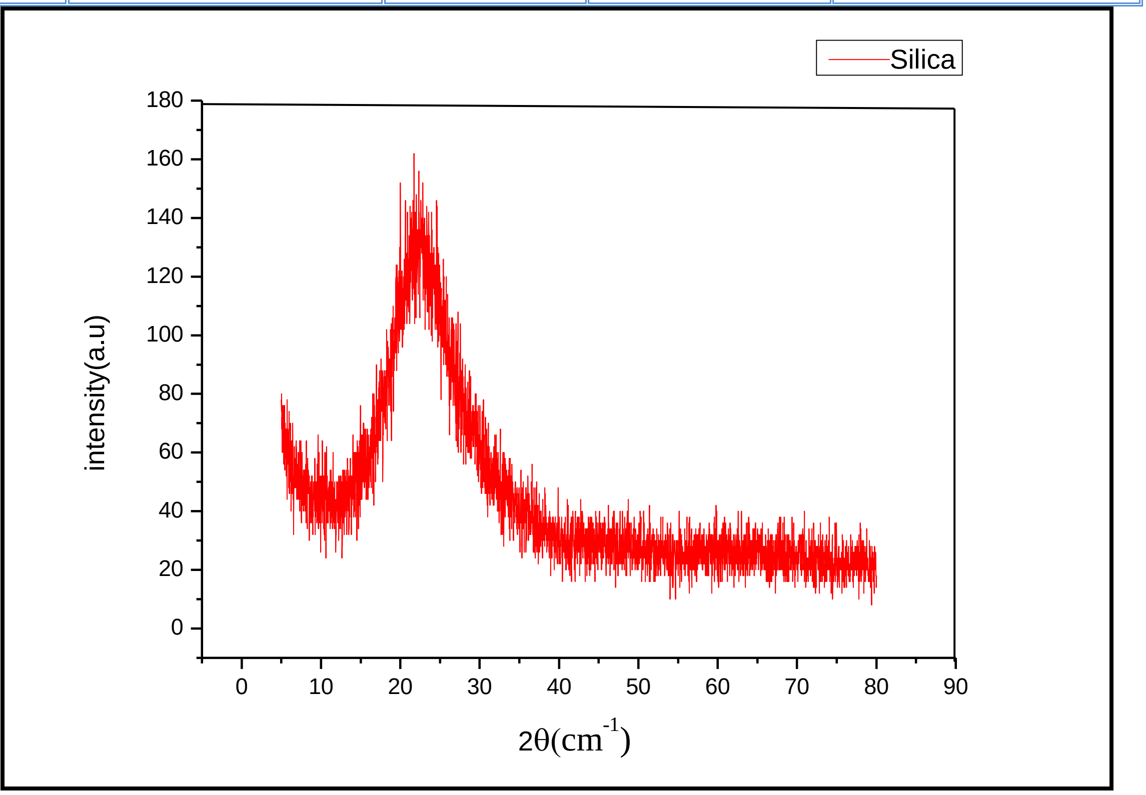

Figure (4.4): XRD pattern of prepared silica

Finally, the XRD data and pattern of prepared zeolite are given in Table (4.5) and Figure (4.5) respectively and illustrated the agglomerated cubic crystals of final synthesized zeolite 4A° after treated with NaOH solution The based (SiO_2/Al_2O_3) synthesized zeolite has three major intense diffraction peaks at 2θ value of (19.94°, 20.91°, and 22.55°)and indicates that the peak in the range of 2θ 20–35° which is an indicative of degrees of crystalline which is fundamental properties of zeolite. This indicates that most of the zeolite amorphous material was being crystallized. and found that the synthetic zeolites 4A° have more crystalline SiO2 in the form of quartz tetrahedral crystal lattices structures [96].

So from the X-ray diffraction patterns, it can be observed that the prepared zeolite has a good crystallinity.

Table (4.5): The strongest three peaks in XRD spectrum of prepared zeolite.

No.	2 θ/(deg)	d/ (Å)	FWHM/(deg)	Intensity/counts
1	19.9485	4.4473	0.1866	351
2	20.9159	4.2437	0.2104	337
3	22.5527	3.9393	0.1856	111

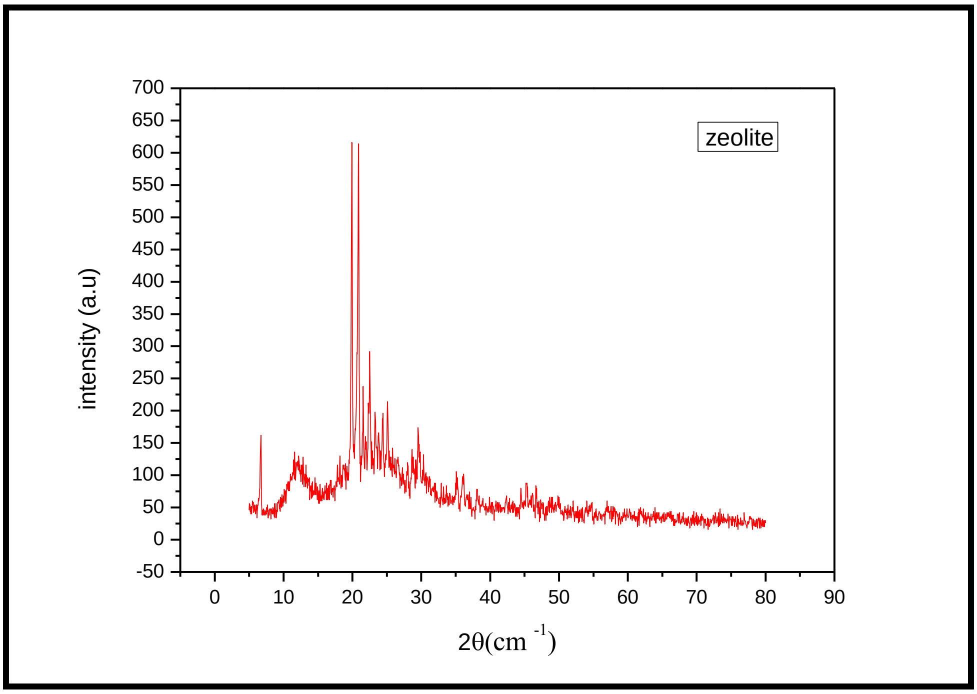

Figure (4.5): XRD pattern of prepared zeolite

4.1.2 Atomic force microscope study.

Atomic force microscopy (AFM) is an instrument used to study the shape and texture of different surfaces. This method allows for diversity control and evaluation of the exact morphological proper ties of the sample, indicating better facilities than other microscopic methods. In AFM surface scanning in 3D, the image analysis allows to select gives the mean root square roughness, the average particle height and intensity spectra of periodicity in the order of particles [97.98]. Using appropriate software, it is possible to evaluate the properties, such as roughness, porosity, med ium size, and particle size distribution which affect the optical, electrical, mechanical, magnetic properties of the sample surface.

The AFM analysis is used to provide information about the average grain size[98]. Figures (4.6), (4.7) , (4.8),(4.9) and(4.10) show typical AFM images of the (kaolin), (metakaolin) , (alumina),(Silica) and (4A° zeolite) respectively.

Figure (4.6) explains images of AFM for kaolin with (size = 2022, 2047 nm) and ability analytical (pixel = 488,490) . Figure (4.6-A) is AFM images in three dimensions (3D), it explain structure shape for grain, and Figure (4.6-B) is AFM images in two dimensions (2D), it found that average roughness is (6.22) nm and the root mean square (RMS) is (7.37) nm .

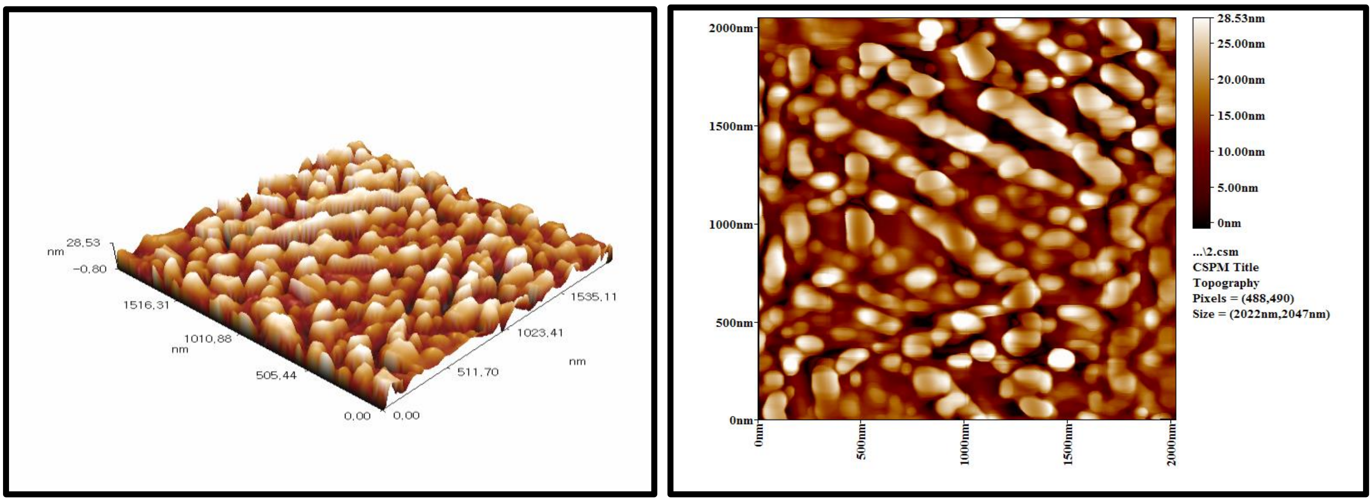

A B

Figure (4.6): Images of AFM for kaolin

Figure (4.7) explains AFM images for metakaolin with (size =2017 , 2009nm) and ability analytical (pixel=484,484) . Figures (4.7-A) is AFM images in three dimensions (3D), it explain structure shape for grain, and Figure (4.7-B) is AFM images in two dimensions (2D), it is found that average roughness is (1.03) nm and the root mean square (RMS) is (1.19) nm .

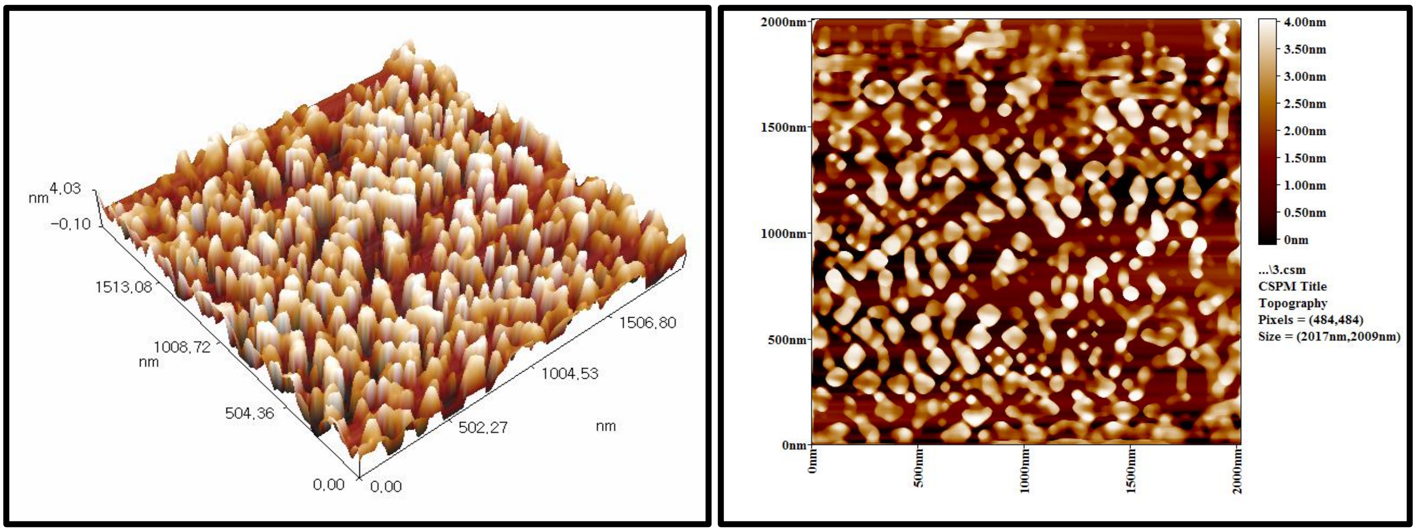

A B

Figure (4.7): Images of AFM for metakaolin

Figure (4.8) explains AFM images for alumina with (size =2063 , 2059 nm) and ability analytical (pixel=496,492) . Figures (4.8-A) is AFM images in three dimensions (3D), it explain structure shape for grain, and Figure (4.8-B) is AFM images in two dimensions (2D), it is found that average roughness is (1.87) nm and the root mean square (RMS) is (2.15) nm .

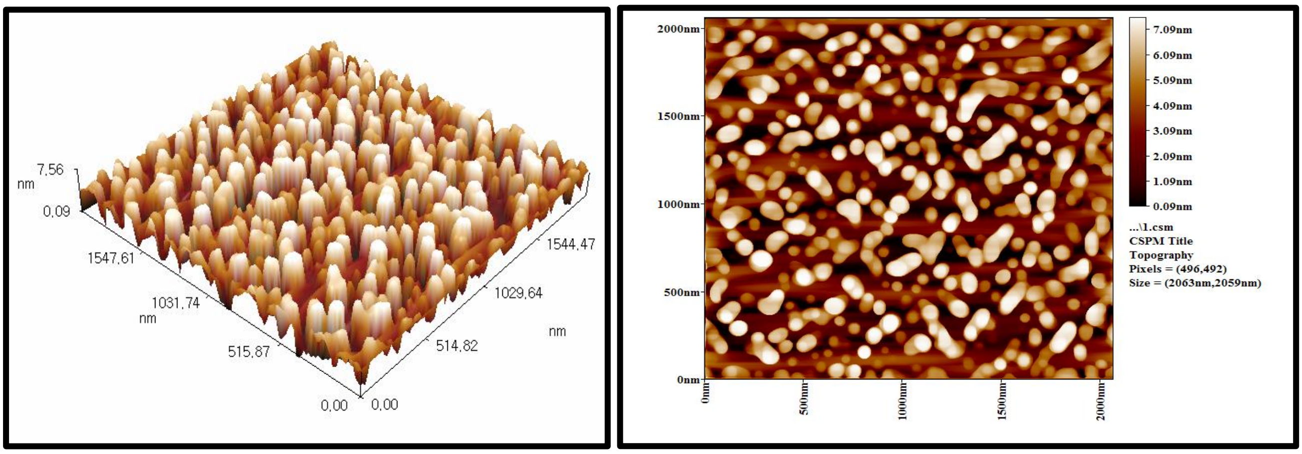

A B

Figure (4.8): Images of AFM for alumina

Figure (4.9) explains AFM images for Silica with (size =1533 , 1533 nm) and ability analytical (pixel=428,432) . Figures (4.9-A) is AFM images in three dimensions (3D), it explain structure shape for grain, and Figure (4.9-B) is AFM images in two dimensions (2D), it is found that average roughness is (9.51) nm and the root mean square (RMS) is (11) nm .

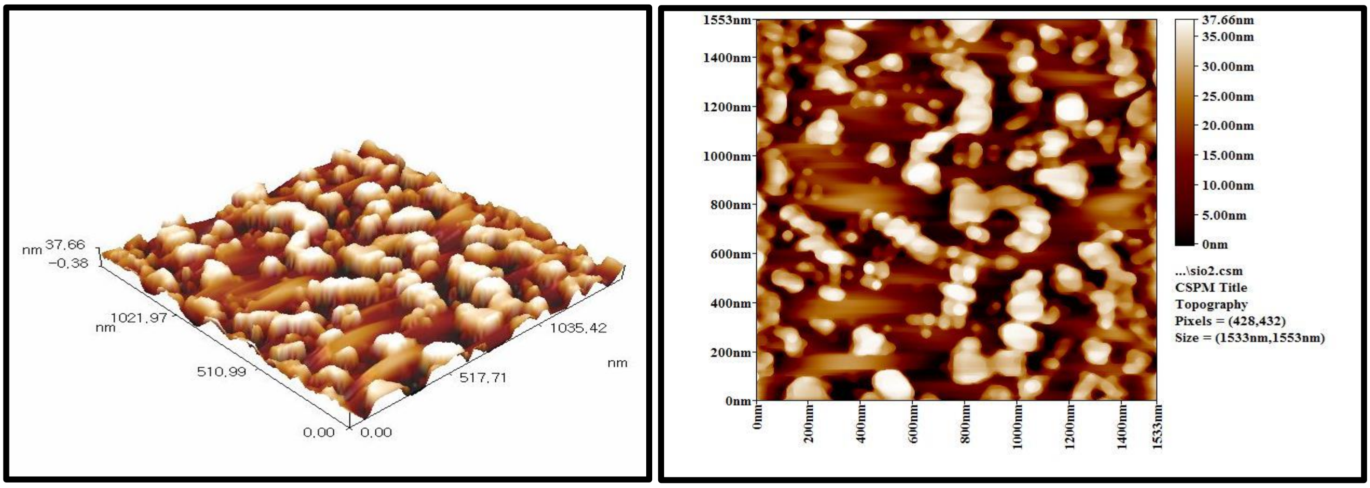

A B

Figure (4.9): Images of AFM for silica

Figure (4.10) explains AFM images for zeolite with (size =2051 , 2051nm) and ability analytical (pixel=492,492) . Figures (4.10-A) is AFM images in three dimensions (3D), it explain structure shape for grain, and Figure (4.10-B) is AFM images in two dimensions (2D), it is found that average roughness is (10) nm and the root mean square (RMS) is (11.8) nm .

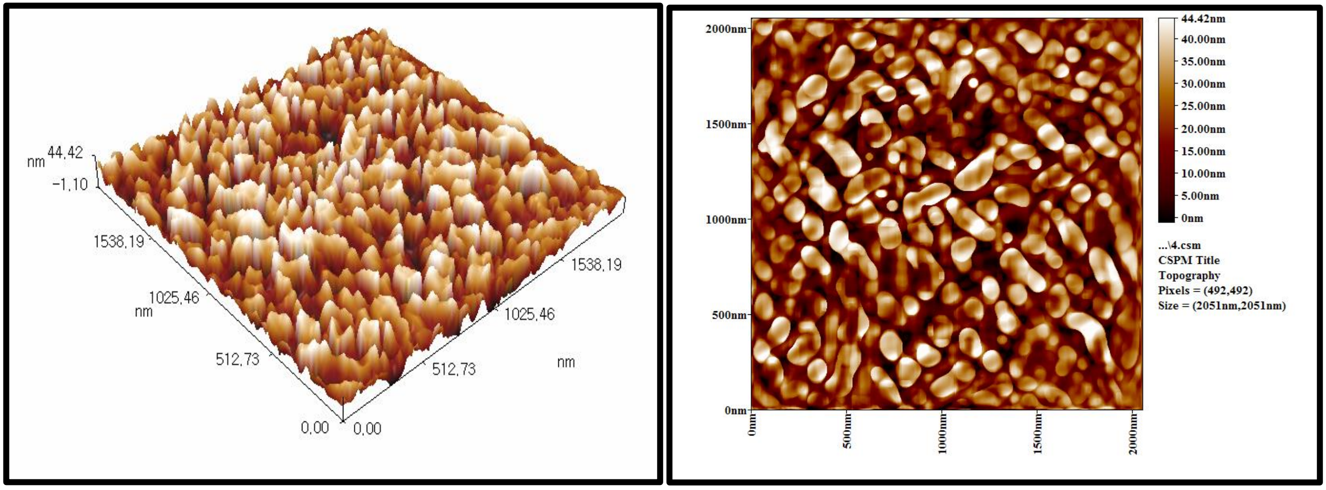

A B

Figure (4.10): Images of AFM for zeolite 4A◦

Tables (4.6),(4.7),(4.8),(4.9) and (4.10) and Figures (4.11) ,(4.12) ,(4.13),(4.14) and (4.15), show the granularity cumulating distribution and average diameter of the kaolin, metakaolin , alumina, silica and zeolite respectively.

The average diameter of kaolin is (98.41) nm , and the particle size of less than 10 % of the total particles is 0 nm, less than 50 % is 95 nm and less than 90% is 120 nm and the average diameter of metakaolin is (64.69) nm ,and the particle size of less than 10 % of the total particles is 40 nm, less than 50 % is 60 nm and less than 90% is 85 nm and the average diameter of alumina is (66.99) nm ,and the particle size of less than 10 % of the total particles is 40 nm, less than 50 % is 65 nm and less than 90% is 85 nm .and the average diameter of silica is (90.40) nm , and the particle size of less than 10 % of the total particles is 60 nm, less than 50 % is 80 nm and less than 90% is 125 nm and the average diameter of zeolite is (73) nm ,and the particle size of less than 10 % of the total particles is 50 nm, less than 50 % is 65 nm and less than 90% is 95 nm.

Table (4.6): Granularity cumulating distribution and average diameter of kaolin.

Avg. Diameter:98.41 nm								
Diameter (nm) <	**Volume (%)**	**Cumulation (%)**	**Diameter (nm)<**	**Volume (%)**	**Cumulation (%)**	**Diameter (nm)<**	**Volume (%)**	**Cumulation (%)**
80.00	10.48	10.48	100.00	12.90	60.48	120.00	5.65	85.48
85.00	13.71	24.19	105.00	6.45	66.94	125.00	8.87	94.35
90.00	11.29	35.48	110.00	11.29	78.23	130.00	5.65	100.00
95.00	12.10	47.58	115.00	1.61	79.84			

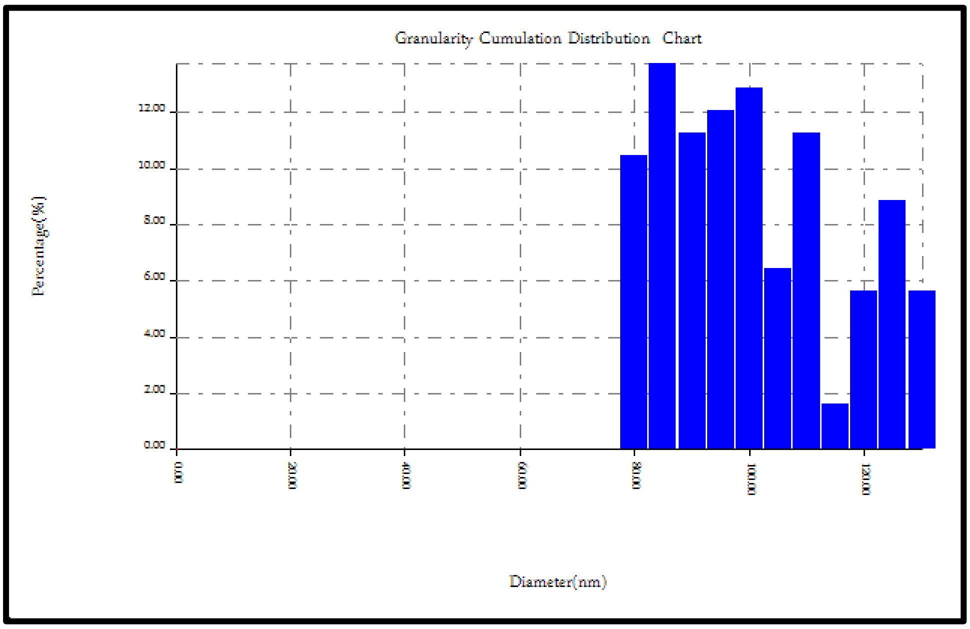

Figure (4.11): Granularity cumulating distribution of kaolin.

Table (4.7): Granularity cumulating distribution and average diameter of metakaolin.

Avg. Diameter: 64.69 nm								
Diameter (nm) <	**Volume (%)**	**Cumulation (%)**	**Diameter (nm)<**	**Volume (%)**	**Cumulation (%)**	**Diameter (nm)<**	**Volume (%)**	**Cumulation (%)**
35.00	1.75	1.75	65.00	9.02	53.38	95.00	3.51	94.24
40.00	5.01	6.77	70.00	9.02	62.41	100.00	2.01	96.24
45.00	7.77	14.54	75.00	9.02	71.43	105.00	2.01	98.25
50.00	8.27	22.81	80.00	8.27	79.70	110.00	1.00	99.25
55.00	9.02	31.83	85.00	7.77	87.47	115.00	0.75	100.00
60.00	12.53	44.36	90.00	3.26	90.73			

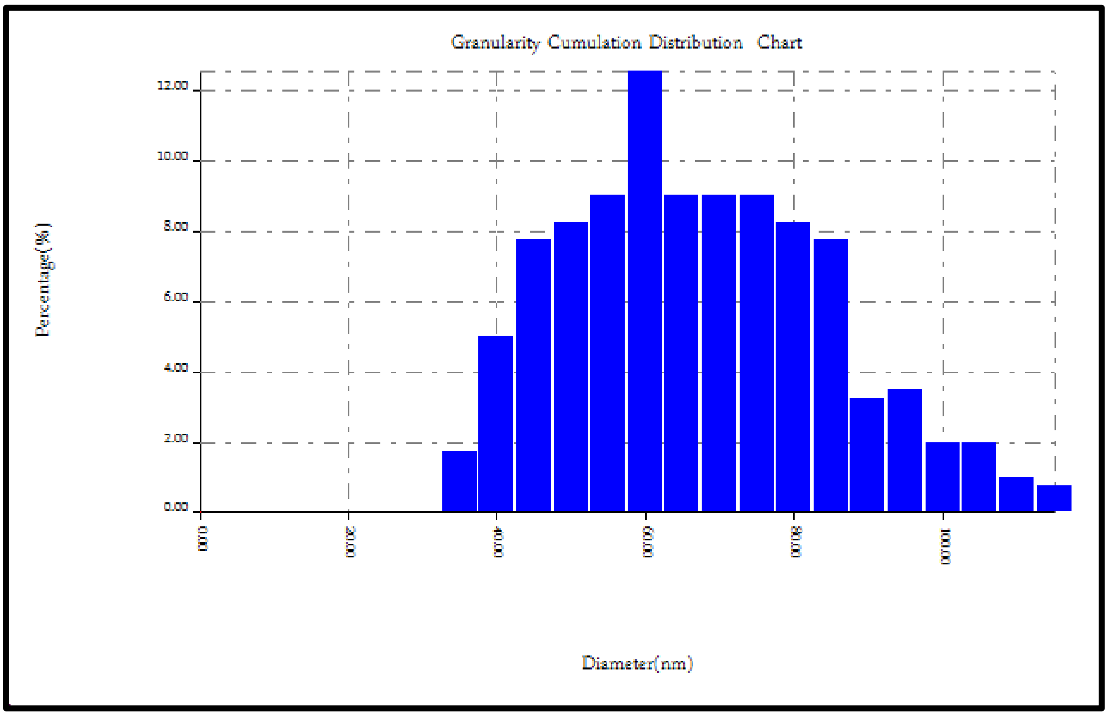

Figure (4.12): Granularity cumulating distribution of metakaolin.

Table (4.8): Granularity cumulating distribution and average diameter of alumain.

<table>
<tr><th colspan="9">Avg. Diameter: 66.99 nm</th></tr>
<tr><th>Diameter (nm) <</th><th>Volume (%)</th><th>Cumulation (%)</th><th>Diameter (nm)<</th><th>Volume (%)</th><th>Cumulation (%)</th><th>Diameter (nm)<</th><th>Volume (%)</th><th>Cumulation (%)</th></tr>
<tr><td>35.00</td><td>1.59</td><td>1.59</td><td>60.00</td><td>8.37</td><td>33.47</td><td>85.00</td><td>9.56</td><td>85.66</td></tr>
<tr><td>40.00</td><td>5.58</td><td>7.17</td><td>65.00</td><td>8.76</td><td>42.23</td><td>90.00</td><td>8.37</td><td>94.02</td></tr>
<tr><td>45.00</td><td>5.98</td><td>13.15</td><td>70.00</td><td>9.96</td><td>52.19</td><td>95.00</td><td>5.98</td><td>100.00</td></tr>
<tr><td>50.00</td><td>5.98</td><td>19.12</td><td>75.00</td><td>11.16</td><td>63.35</td><td></td><td></td><td></td></tr>
<tr><td>55.00</td><td>5.98</td><td>25.10</td><td>80.00</td><td>12.75</td><td>76.10</td><td></td><td></td><td></td></tr>
</table>

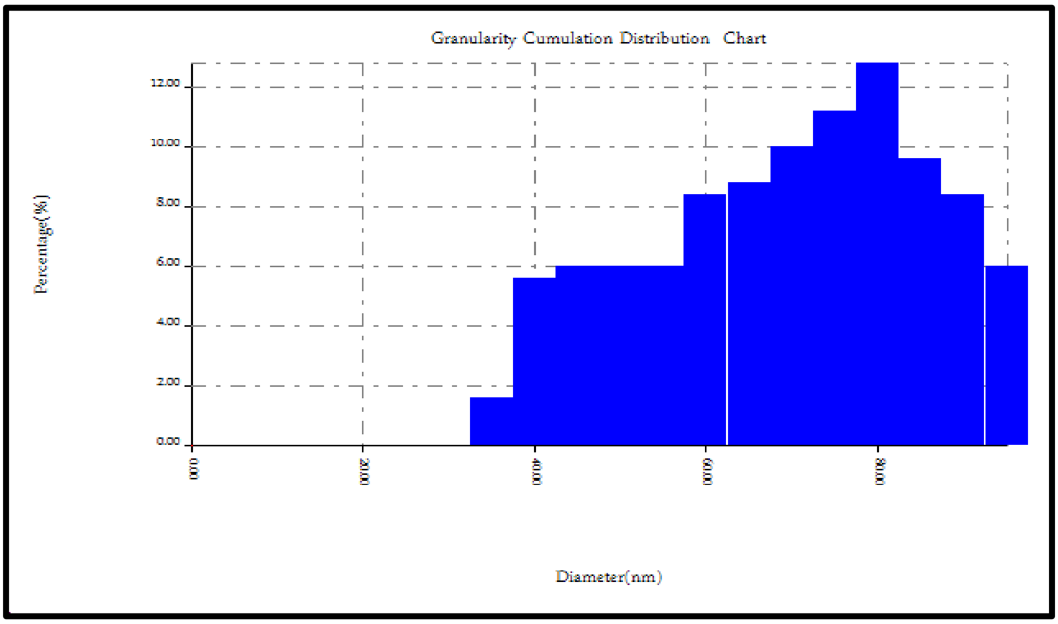

Figure (4.13): Granularity cumulating distribution of alumina.

Table (4.9): Granularity cumulating distribution and average diameter of silica.

Avg. Diameter: 90.40 nm								
Diameter (nm)<	**Volume(%)**	**Cumulation(%)**	**Diameter (nm)<**	**Volume(%)**	**Cumulation(%)**	**Diameter (nm)<**	**Volume (%)**	**Cumulation(%)**
60.00	0.78	0.78	95.00	8.53	65.12	130.00	2.33	92.25
65.00	9.30	10.08	100.00	6.98	72.09	135.00	2.33	94.57
70.00	10.85	20.93	105.00	5.43	77.52	140.00	0.78	95.35
75.00	11.63	32.56	110.00	3.88	81.40	145.00	1.55	96.90
80.00	11.63	44.19	115.00	4.65	86.05	160.00	1.55	98.45
85.00	6.20	50.39	120.00	2.33	88.37	180.00	0.78	99.22
90.00	6.20	56.59	125.00	1.55	89.92	185.00	0.78	100.00

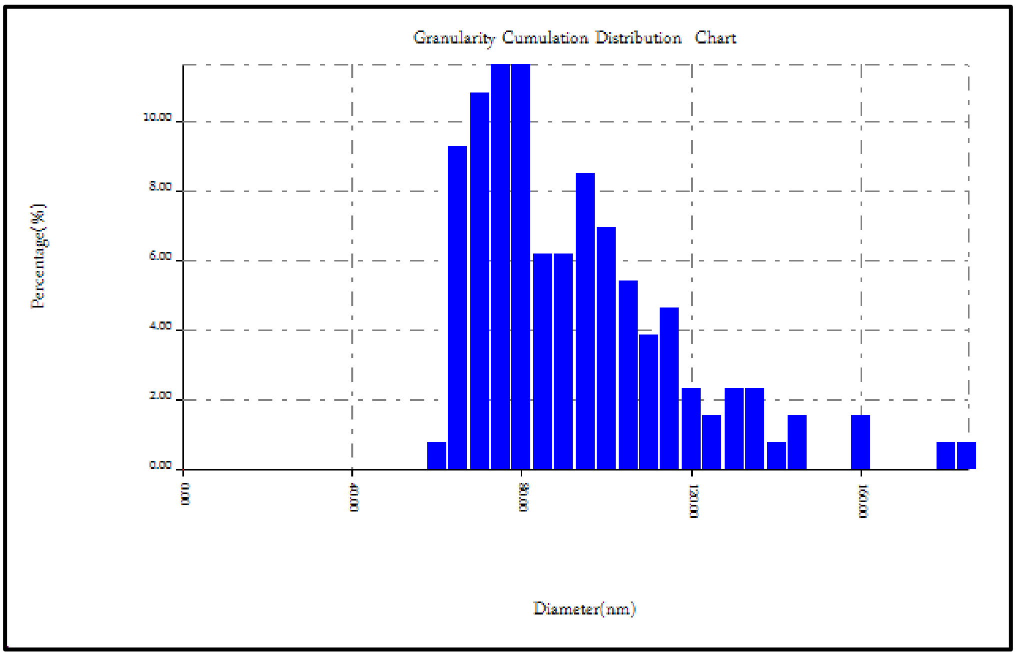

Figure (4.14): Granularity cumulating distribution of silica.

Table (4.10): Granularity cumulating distribution and average diameter of zeolite.

Avg. Diameter: 73.00 nm								
Diameter (nm)<	**Volume (%)**	**Cumulation (%)**	**Diameter (nm)<**	**Volume (%)**	**Cumulation (%)**	**Diameter (nm)<**	**Volume (%)**	**Cumulation (%)**
50.00	6.13	6.13	85.00	5.29	74.37	120.00	0.28	98.33
55.00	8.64	14.76	90.00	6.41	80.78	125.00	0.56	98.89
60.00	12.53	27.30	95.00	6.69	87.47	130.00	0.28	99.16
65.00	13.37	40.67	100.00	3.62	91.09	135.00	0.56	99.72
70.00	11.98	52.65	105.00	4.74	95.82	160.00	0.28	100.00
75.00	7.24	59.89	110.00	0.84	96.66			
80.00	9.19	69.08	115.00	1.39	98.05			

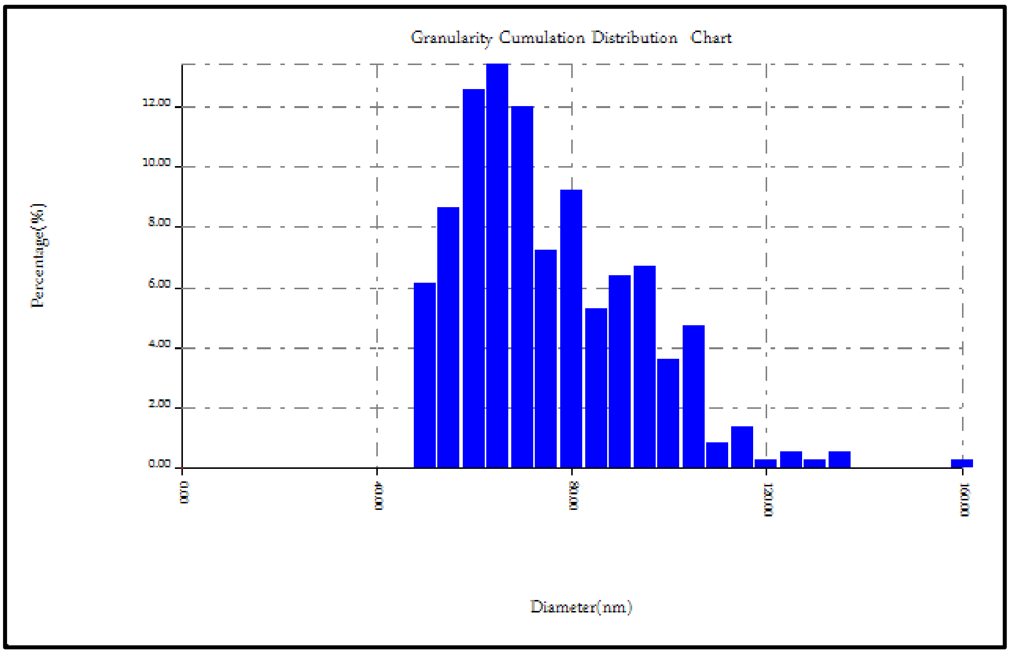

Figure (4.15): Granularity cumulating distribution of zeolite.

4.1.3. FTIR spectra analysis:

The FTIR spectra of the natural kaolin , metakaolin, alumina, silica and synthesis zeolite, in the lattice region of 400–4000 cm^{-1} was taken to identify the existence of some functional group which might be responsible for adsorption process. From Figure (4.16) as shown clearly, natural kaolin indicates a number of adsorption results which displays that the kaolin contains different groups. From the figure showed, the main bands observed were stretching the OH— group at 3699 cm^{-1} and 3465.7 cm-1. The broad band observed at 1822.3cm-1was assigned as the Si-O in the molecule of SiO4. The other vibration band was seen at 1638cm^{-1} attributed to the Al-OH group. The bands recorded at 911.72 cm^{-1} and 795.08 cm^{-1} were symmetrical stretching of Si-O. The band for absorption value at 753.7 cm^{-1} was assigned for Si-O-Al, in which the Al is found in octahedral coordination.

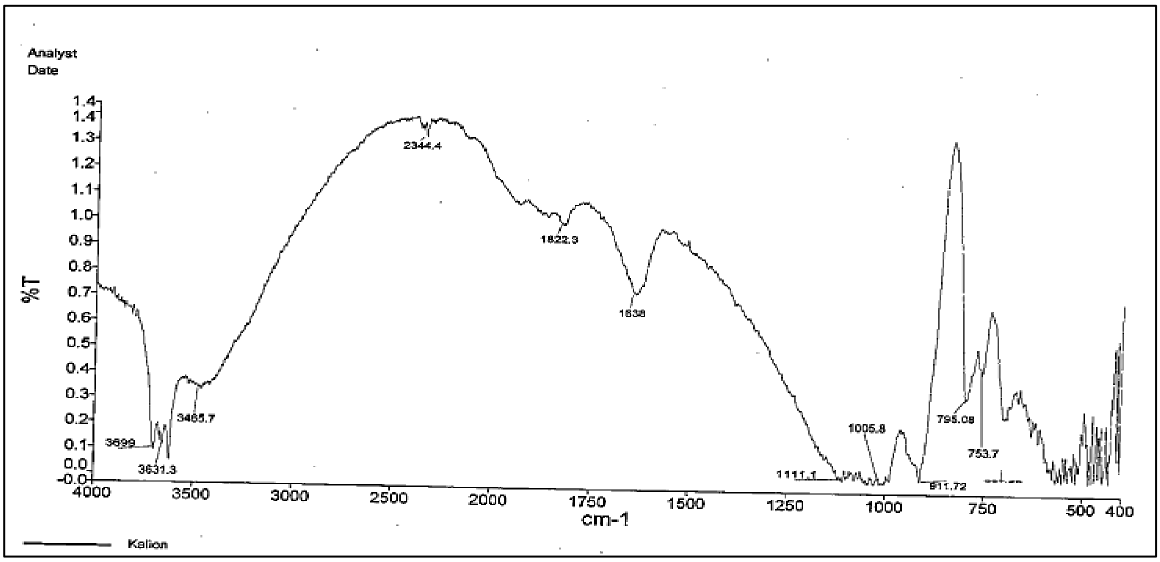

Figure (4.16) **FTIR pattern of prepared kaolin.**

In the same way, Figure (4.17) shows the metakaolin FTIR spectrum with peaks at approximately 3657.7 cm^{-1} and 1090.5 cm^{-1} reflect the stretching and bending vibration frequencies of the hydroxyl groups, respectively [99]. The absorption peaks at 3450 cm^{-1} and peak at 796.3 cm^{-1} characteristic stretching vibration. of Al-OH indicate that clay is dioctahedric [100]and The absorption peak at about 2344 cm^{-1} is due to adsorptive CO_2 vibration are formed. The peaks at 481.06 cm^{-1} are attributed to in-plane bending of Si-O and Al-O linkages [101] originating from reconstruction of AlO_4 and SiO_4 species characterizing the tetrahedral structure.

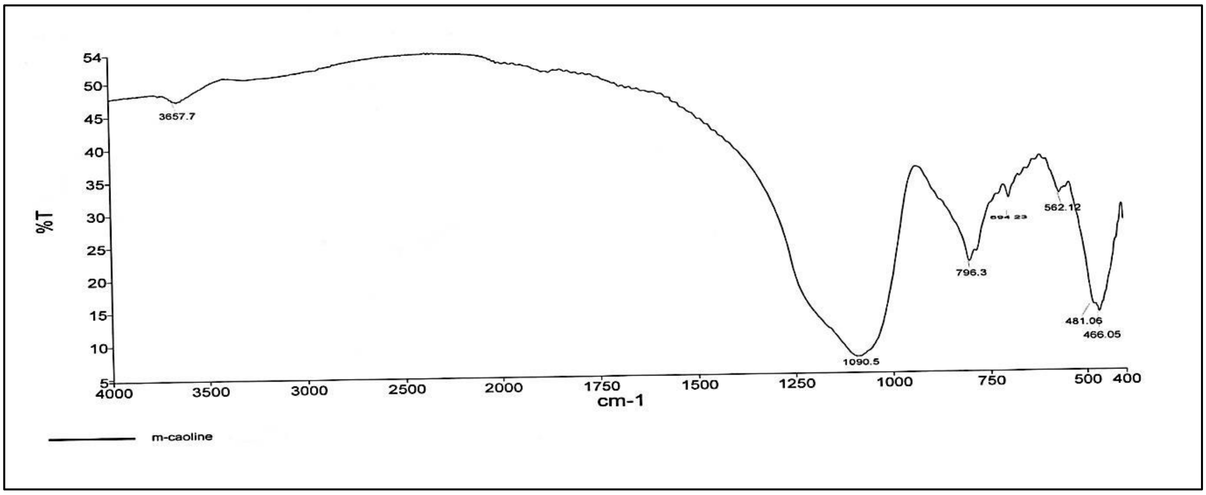

Figure (4.17) : **FTIR pattern of prepared metakaolin.**

FTIR spectra Figure (4.18) show aluminium trioxide broad peak in the spectral at (3351.5) cm–1 which is assigned to –OH stretching vibration due to hydrogen bonding formation of this group in the aluminium the intensity and the width of the peak, are related to the amount of –OH group, because of the number of H2O molecules and consequently hydrogen bond generation[102]. The peak at 1667 cm–1 is assigned to the bending mode of water molecules[103].

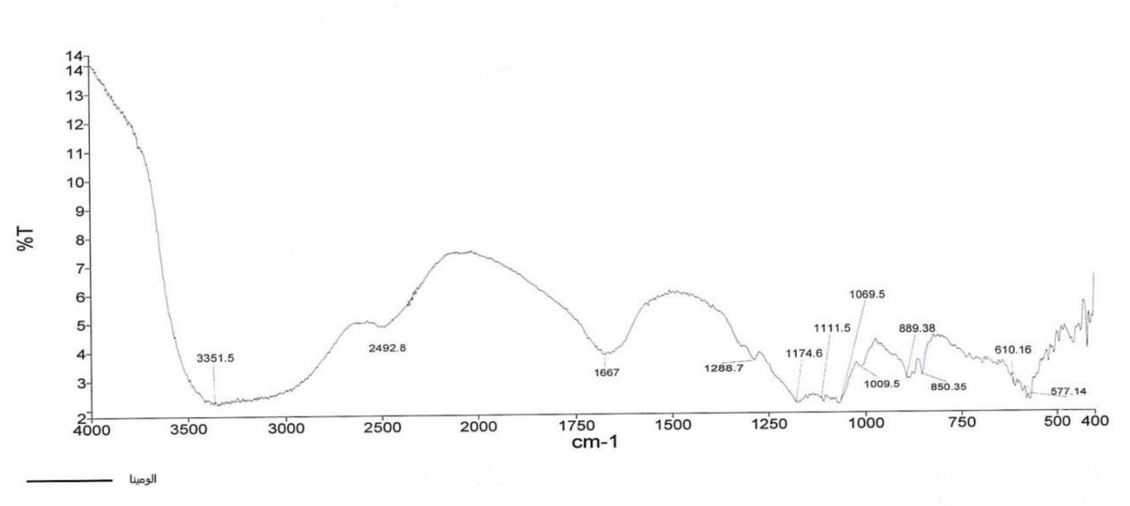

Figure (4.18) : FTIR pattern of prepared alumina

In the IR spectra of Figure (4.19) SiO_2; rocking, bending, and stretching vibrational bands of Si-O can be observed at 3413 cm^{-1}, 2382 cm^{-1}, and 1863.7 cm-1, respectively Transmittance peaks at wavenumbers ranging between 400 and 4000 cm^{-1} often exhibit peak at 3413 $cm^{-1}$and 1640 cm^{-1} owing to absorbed moisture.

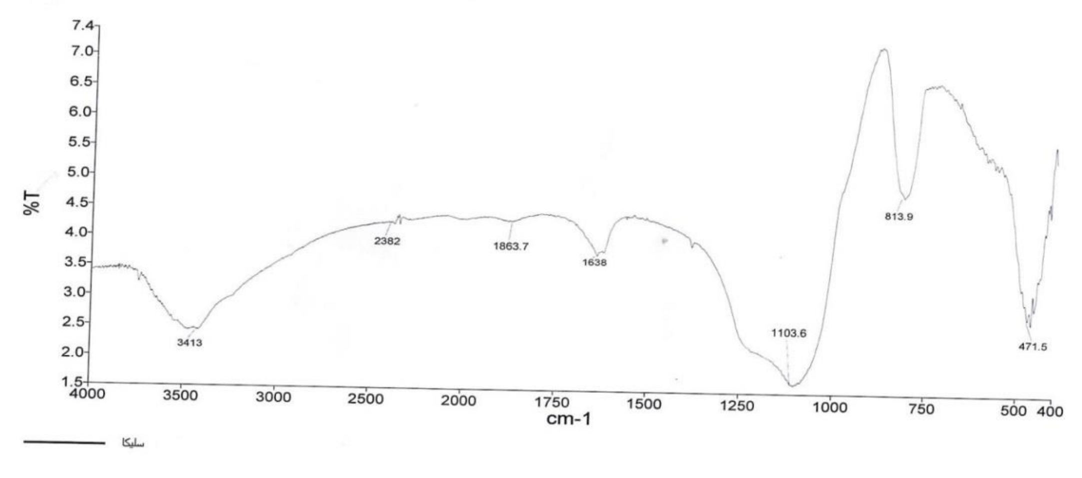

Figure (4.19) : FTIR pattern of prepared silica

Figure (4.20) shows the synthesis zeolite FTIR main adsorption results at 3465.6 cm^{-1} that is OH– stretching. The band that at 1066.5 cm^{-1} confirms the Si-O bond. The bands at 793.3cm^{-1} and 622.17cm^{-1} show from the Figure down that the synthesis zeolite high sharp peak, which has a higher absorbance value than the raw kaolin[104] and that the synthesized zeolite is free from any contaminates or trace elements. However, in natural kaolin, some other minerals and oxides may be present before treatment and the absorbance value of natural kaolin is lower than the synthesized zeolite. Synthesized zeolite is therefore preferred over natural kaolin for adsorption.

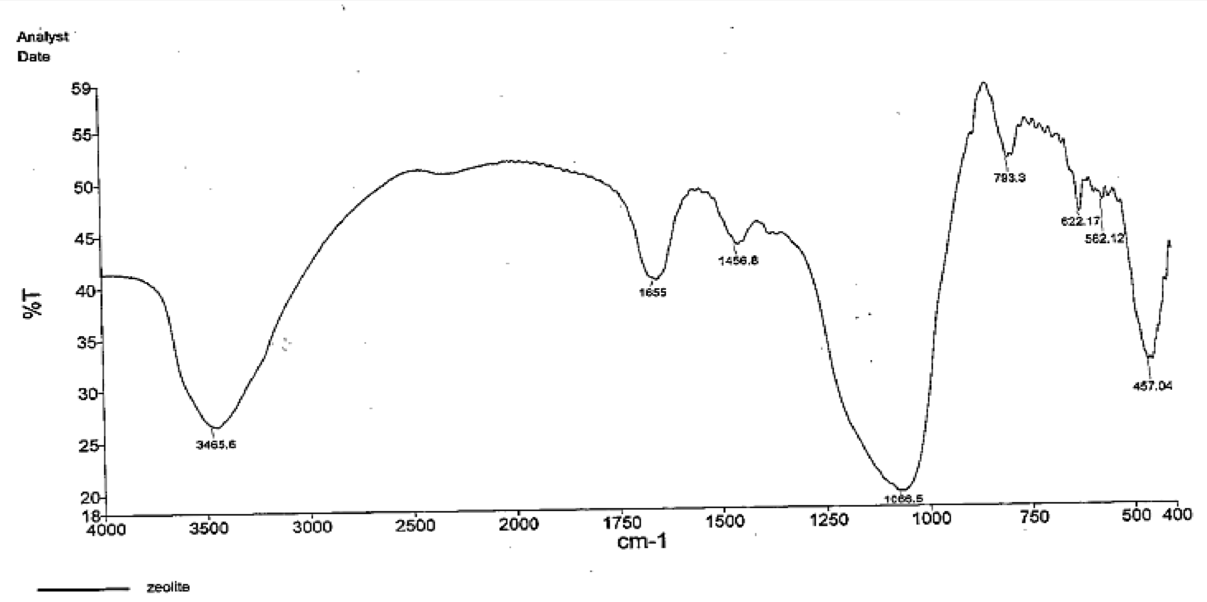

Figure (4.20) FTIR pattern of prepared zeolite

4.1.4. Scanning electron microscope

Scanning electron microscopy (SEM) is a convenient technique to study microstructure of materials . Scanning electron microscope (SEM) analysis was used to investigate the microstructural development of the tested samples , The tested samples were dried for SEM and small specimens of both untreated and treated samples were prepared and the fractured surfaces of the specimens were coated with gold before scanning.

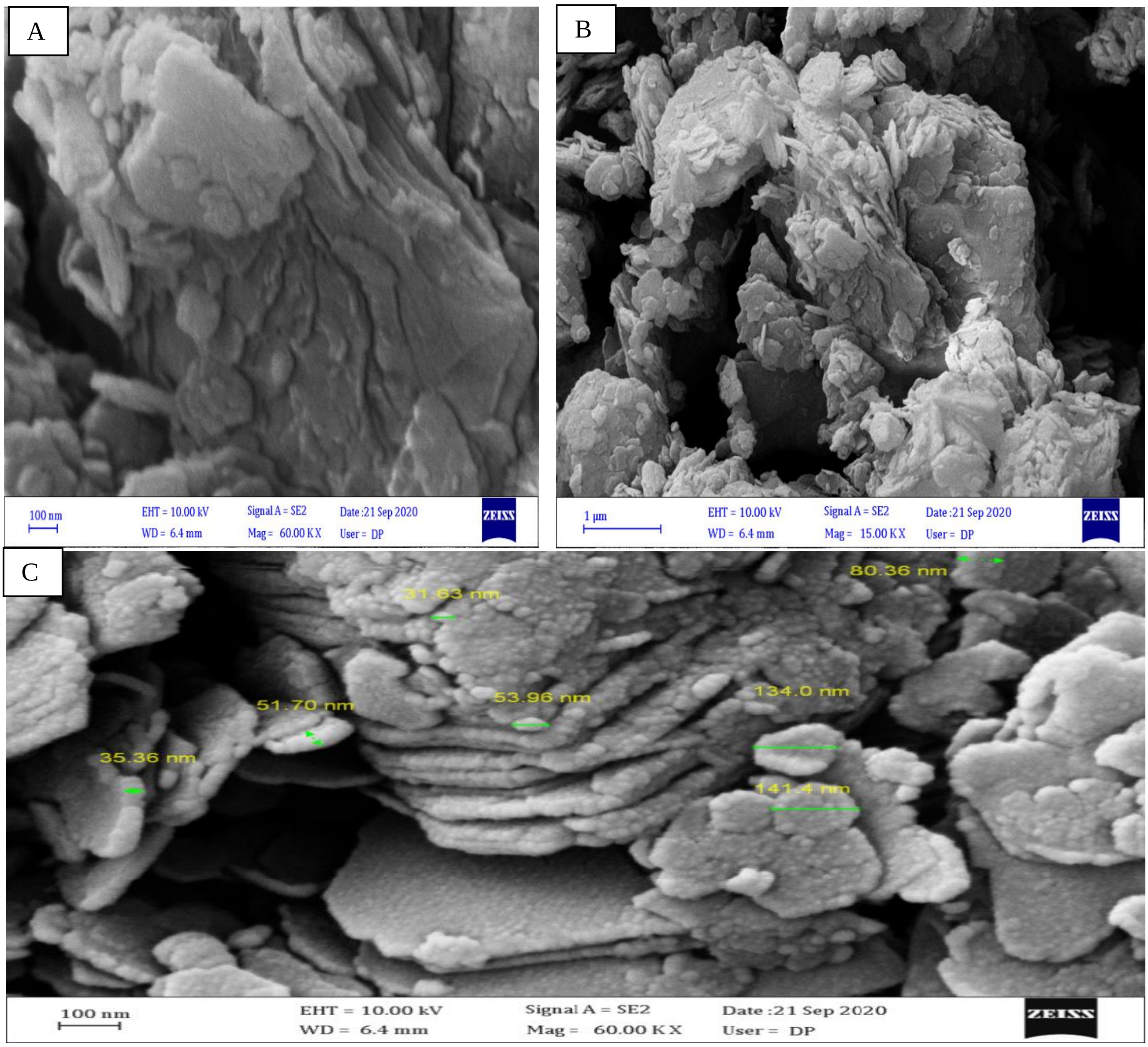

Figure (4.21): SEM images of Kaoline.

Figure (4.21), a SEM image of untreated kaolin clay, it was noticed that the clay showed a flaky tissue (peels), and that the image (4.21.A) was enlarged by 60.00KX and a thickness of 6.4 mm.Image (4.21.B)was enlarged by 15.00KX and a thickness of 6.4 mm, image higher magnification SEM (4.21.C) was enlarged by 60.00KX and a thickness of 6.4 mm .Its and molecular size ranges from 31.63 nm to 141.4 nm.

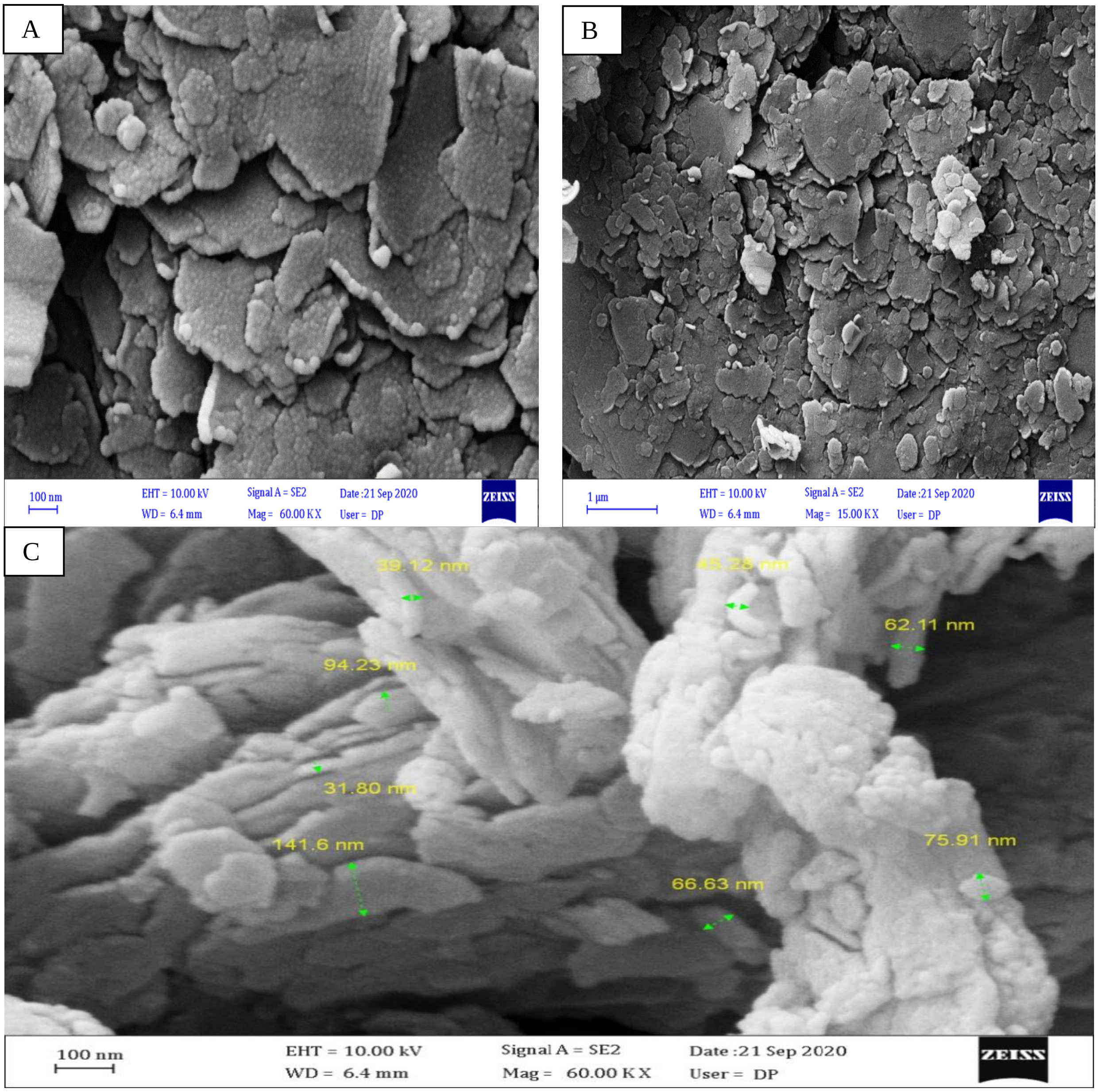

Figure (4.22): SEM images of metakaolin.

Figure (4.22), a SEM image of metakaolin calcined at 800 C°. They are bulk deposits of various shapes as a results of high temperture treatment which cause agglomeration of particles , and that a image (4.22.A) was enlarged by 60.00 KX and a thickness of 6.4 mm.and image (4.22.B) was enlarged by 15.00KX and a thickness of 6.4 mm,image higher magnification SEM (4.22.C) was enlarged by 60.00KX and a thickness of 6.4 mm .Its molecular size ranges from 31.80 nm to 141.6 nm.

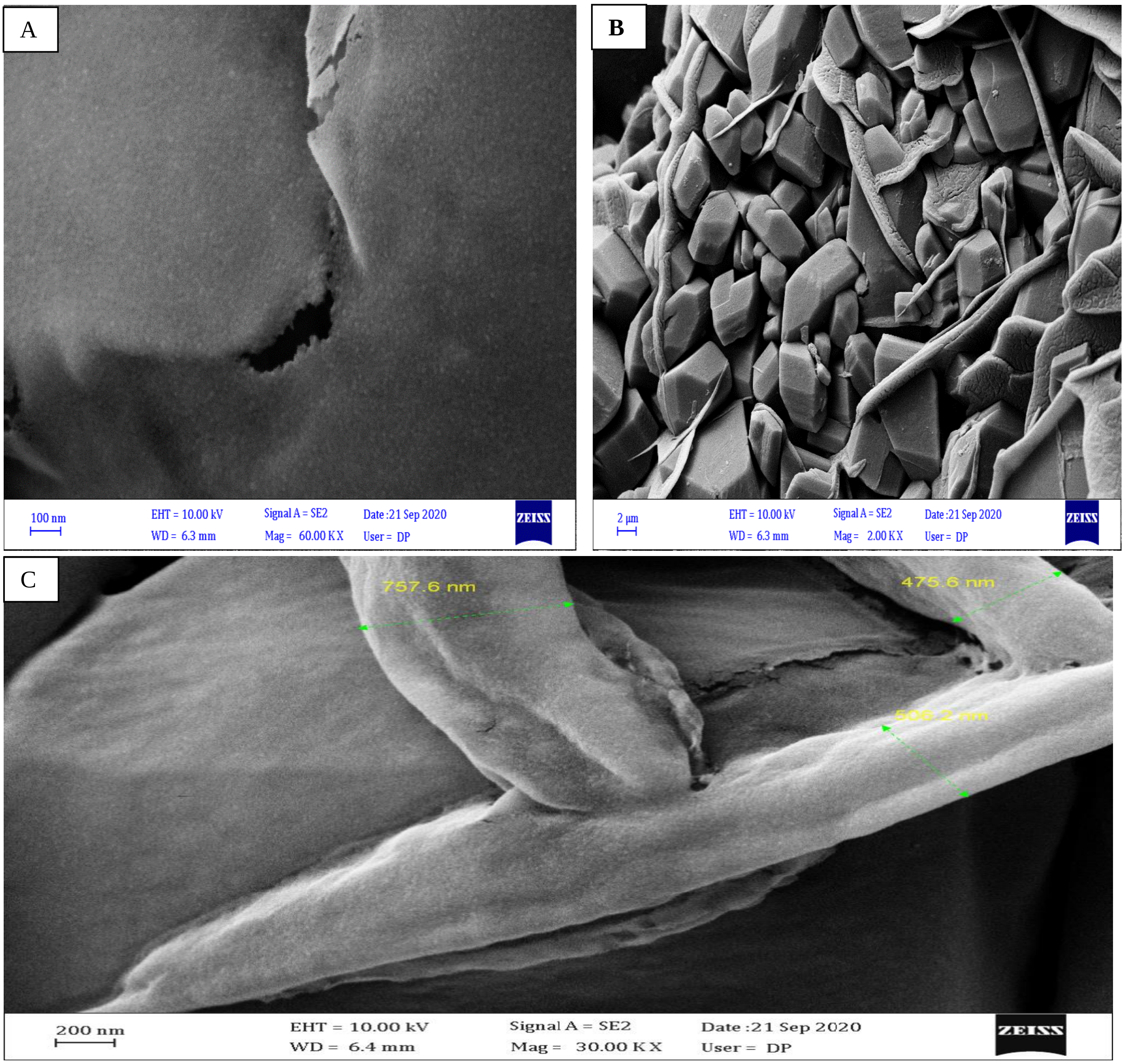

Figure.(4.23) SEM images of alumina.

Figure (4.23), a SEM image of alumina they are polygonal shapes , and that a image (4.23.A) was enlarged by 30.00 KX and a thickness of 6.3 mm.and image (4.23.B) was enlarged by 2.00KX and a thickness of 6.3 mm,image higher magnification SEM (4.23.C) was enlarged by 30.00KX and a thickness of 6.3 mm. Its and molecular size ranges from 475.6 nm to 757.6 nm.

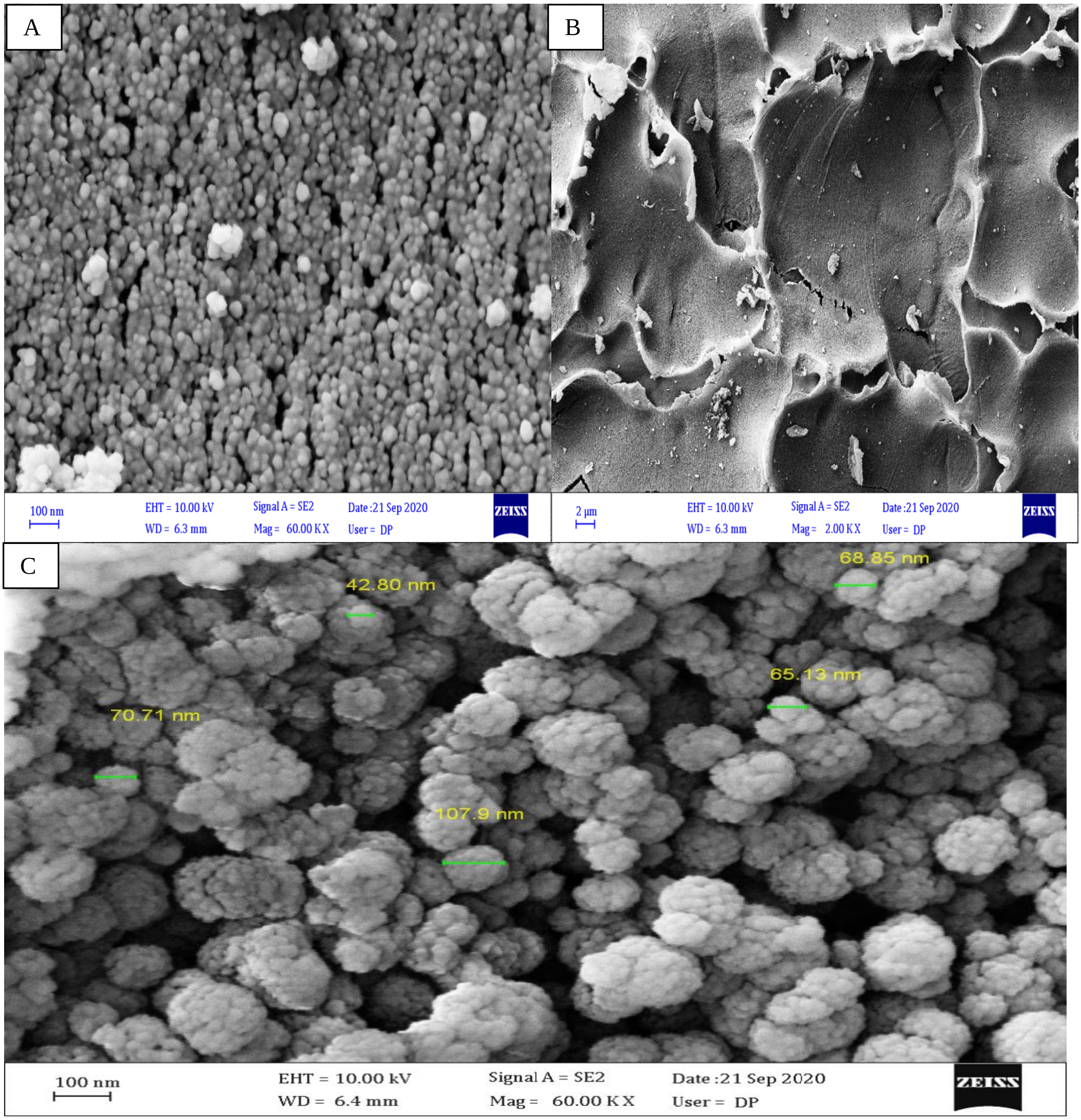

Figure.(4-24) SEM images of silica.

Figure (4.24), a SEM image of silica which is formed by sintering rice husk below 800C° , It seems that particles of silica rice husk are agglomerates of small nano¬range particles. Thus, it is very common to find aggregates of silica forming fine globules or platelets of varied sizes. and that a image (4.24.A) was enlarged by 30.00 KX and a thickness of 6.3 mm.and image (4.24.B) was enlarged by 200KX and a thickness of 6.3 mm,image higher magnification SEM (4.24.C) was enlarged by 6000KX and a thickness of 6.4 mm .Its molecular size ranges from 42.80 nm to 107.9 nm.

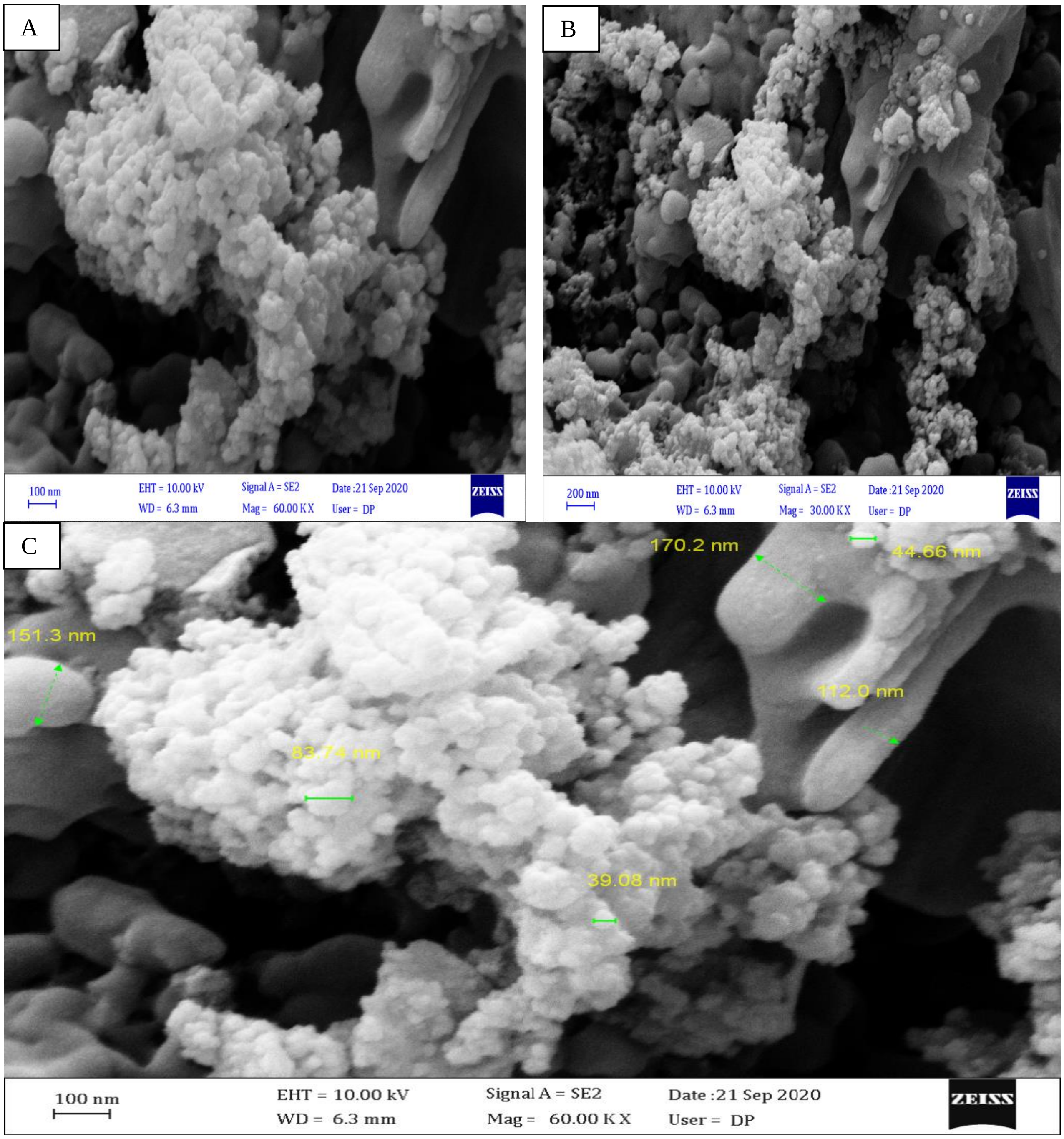

Figure.(4.25) SEM images of zeolite.

Figure (4.25), a SEM image of zeolite which is a prepared Zeolite 4Å was prepared from Iraqi kaolin and rice husk using the process of conversion of rice husk to silica and kaolin to sodium aluminate where zeolite was prepared from it.The shape is described as spherical, cylindrical, and clustered shapes . and that the image (4.25.A) was enlarged by 60.00 KX and a thickness of 6.3 mm. and image (4.25.B) was enlarged by 15.00 KX and a thickness of 6.3 mm, image higher magnification SEM (4.25.C) was enlarged by 60.00KX and a thickness of 6.3 mm . Its and molecular size ranges from 44.66 nm to 170.2 nm.

4.1.5. Energy dispersive spectroscopy (EDX)

The Energy Dispersive X-ray (EDX) microanalysis is a technique of elemental analysis associated to electron microscopy based on the generation of characteristic X- rays that reveals the presence of elements present in the specimens. The EDX microanalysis is used in different biomedical fields by many researchers and clinicians. Nevertheless, most of the scientific community is not fully aware of its possible applications. The spectrum of EDX microanalysis contains both semi-qualitative and semi-quantitative information. EDX technique is made useful in the study of drugs, such as in the study of drugs delivery in which the EDX is an important tool to detect nanoparticles (generally, used to improve the therapeutic performance of some chemotherapeutic agents). EDX is also used in the study of environmental pollution and in the characterization of mineral bio- accumulated in the tissues. In conclusion, the EDX can be considered as a useful tool in all works that require element determination[105]. Figuer (4.26), (4.27), (4.28),(4.29) and (4.30) demonstrate the EDX spectra of kaolin,metakaolin,alumina,silica and zeolite 4A° respectively .the summary of elemental compositions are given in table (4.11) with the main composition of aluminium and silicon .it is clear that there is a change in composition of kaolin and metakaolin.Also it confirm the formation of zeolite by the insertion of sodium in the structure .On the other hand it show that the prepared rice husk silica is very pure.

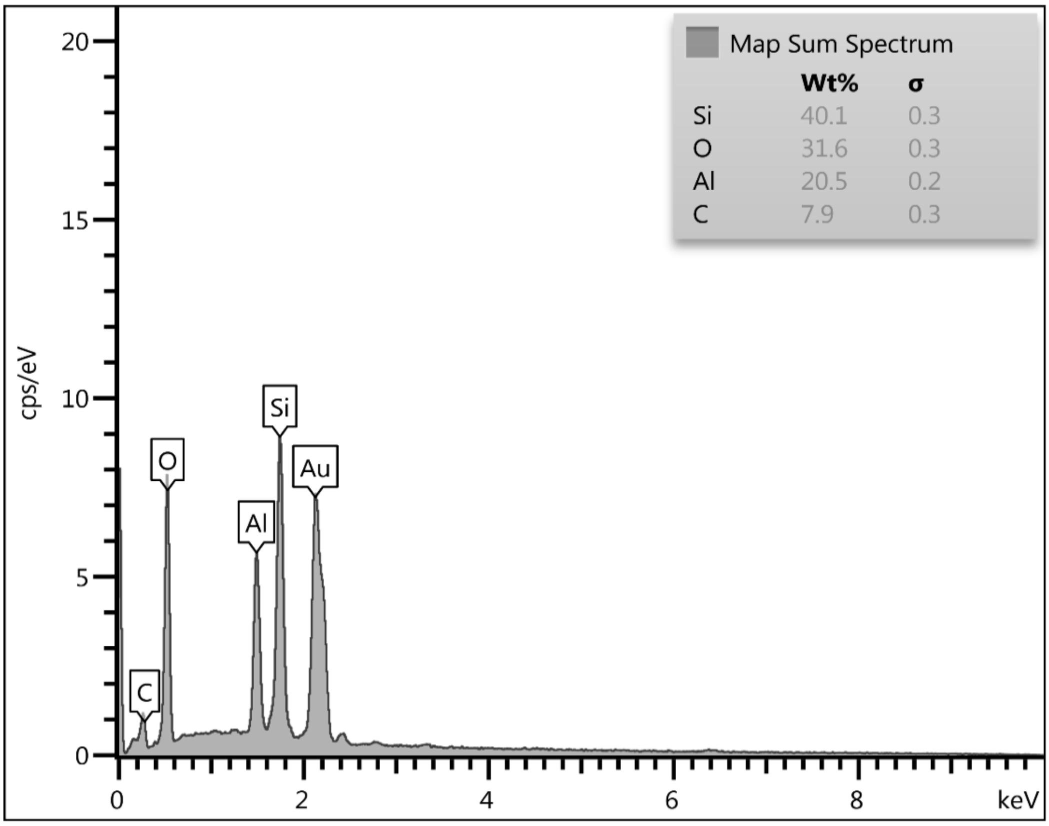

	Wt%	σ
Si	40.1	0.3
O	31.6	0.3
Al	20.5	0.2
C	7.9	0.3

Figure (4.26) :EDX of kaolin

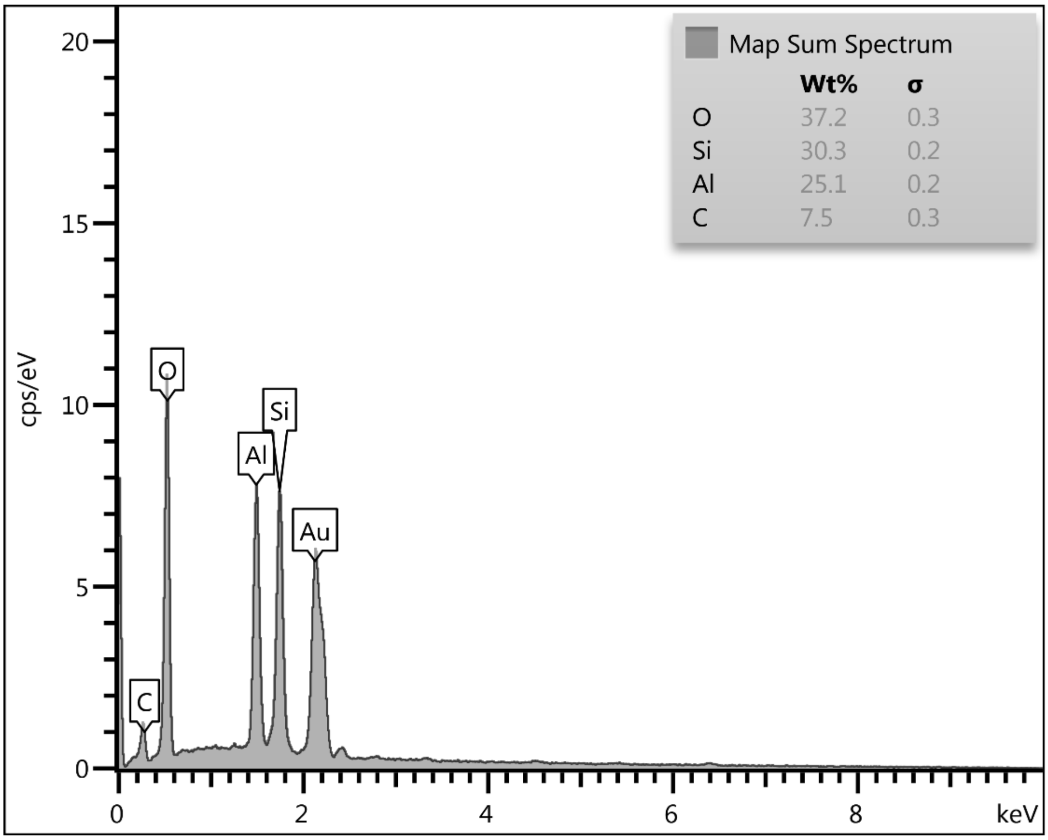

Figure (4.27) :EDX of metakaolin

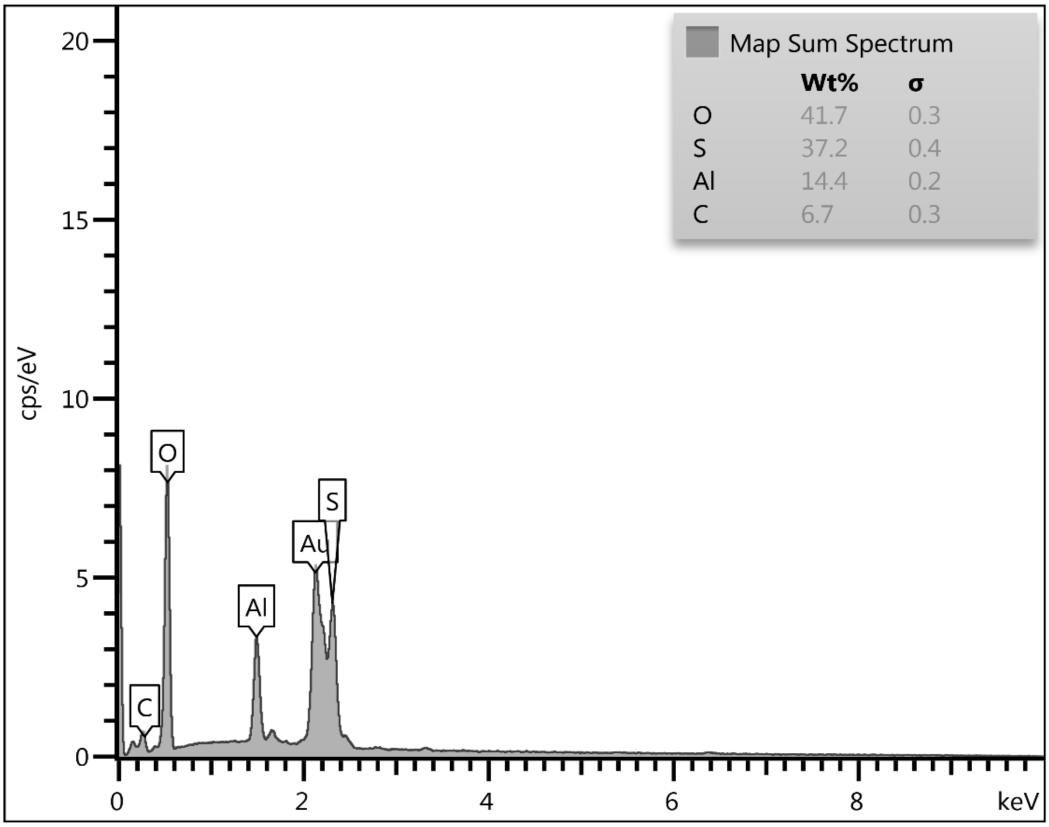

Figure (4.28) :EDX of alumina

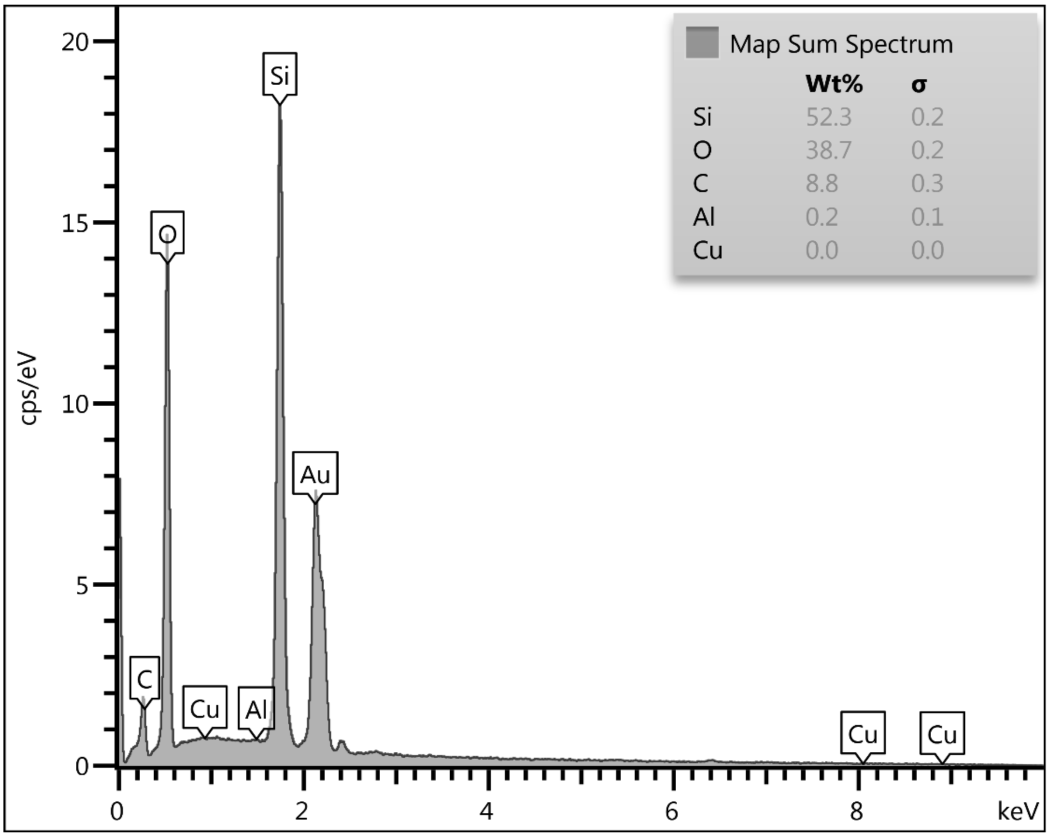

	Wt%	σ
Si	52.3	0.2
O	38.7	0.2
C	8.8	0.3
Al	0.2	0.1
Cu	0.0	0.0

Figure (4.29) :EDX of silica.

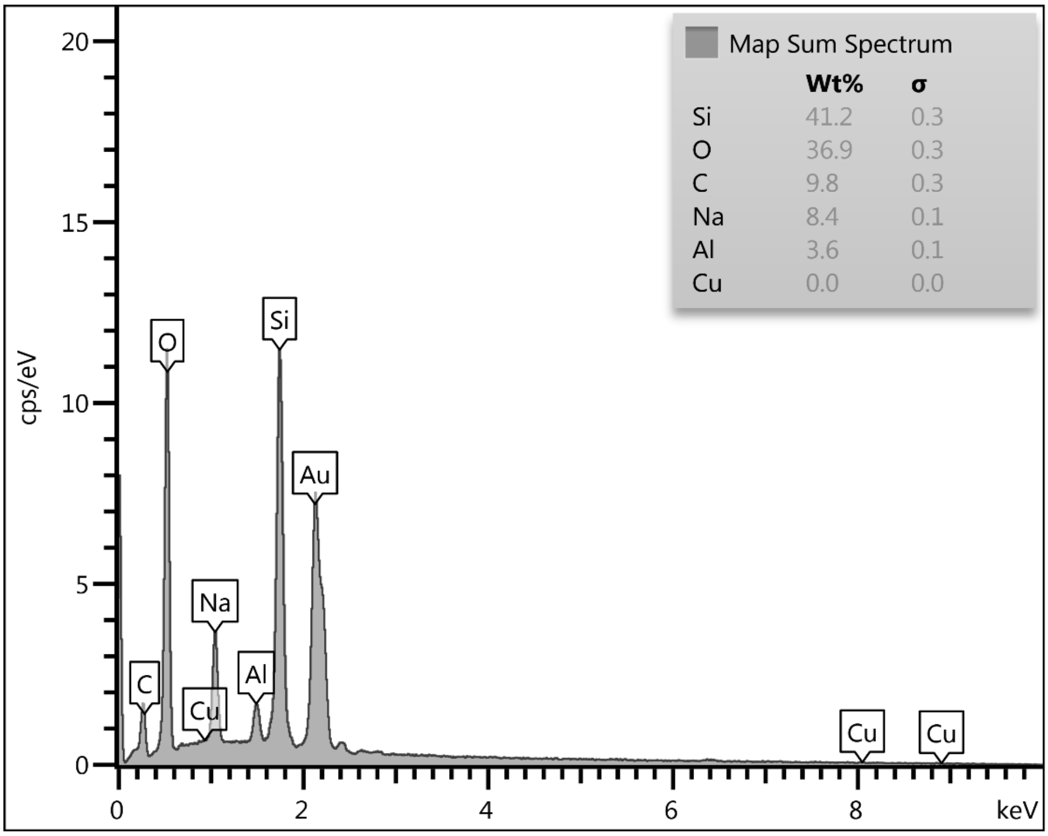

	Wt%	σ
Si	41.2	0.3
O	36.9	0.3
C	9.8	0.3
Na	8.4	0.1
Al	3.6	0.1
Cu	0.0	0.0

Figure (4.30) :EDX of 4A° zeolite.

Table:(4.11) Elements EDX composition of the materials.

Component	Elements					
	Si%	O%	Al%	C%	Na%	S%
Kaolin	40.1	31.6	20.5	7.9		
Metakaolin	30.3	37.2	25.1	7.5		
Alumina	37.2	41.7	14.4	6.7		37.2
Silica	52.3	38.7	0.2	8.8		
Zeolite	41.2	36.9	3.6	9.8	8.4	

We note that the proportions of the components of the samples are different, as the ratio of Al, Si, and O was different, as AL recorded the highest percentage in methacholine and choline, and that its low percentage in alumina was due to the presence of silica aluminate and not pure alumina, as it was found that silica was free from the element Al..the highest percentage of silicon was recorded in the silica sample followed by 4A° Zeolite ,kaolin, metakaolin.while the higest percentage of oxygen was recorded in alumina sample followed silica,metakaolin, 4A° zeolite,kaolin. and that the highest percentage of aluminum was recorded in the metakaolin sample,kaolin,alumina While there were small percentages of the sodium and carbon component in the zeolite sample,indicating the presence of 4A° in the preparation.

4.2 The adsorption of Ca (II) and Mg(II) ions on prepared 4A° zeolite.

4.2.1 Effect of contact time on adsorption

The effect of contact time on adsorption of Ca (II) and Mg(II) ions using 4A° zeolite was studied at (10, 20, 30, 40 and 50) min and temperature of (298) K, initial concentration of (100) mg/l of metal ions Tables (4.12) and (4.13) explain the change in percentage removal with contact time. As seen from them, that the time required to reach equilibrium for the adsorption of Ca+2 and Mg+2 ions on the 4A° zeolite are (50) min for both .It seems that the percentage removal of calcium and magnesium increased with increase in contact time .This increase is clear from the beginning and up to 50 minute and after that there is no significant change in percentage removal of their ions as shown in Figure (4.31) and (4.32). This explains the fact that all adsorbent sites were free and the solute concentration was high at the beginning and then, the ions adsorption by 4A° zeolite was decreased compared with adsorption rate in the beginning due to the number of adsorption sites were decrease.

Table (4.12): Effect of contact time on the removal (%) of Ca(II) ion on 4°A zeolite at 298 K .

Time (min)	Ca (II)		
	Co(mg/L)	Ct(mg/L)	R%
10	100	6.0928	93.9072
20	100	4.3792	95.6208
30	100	4.7600	95.24
40	100	2.2848	97.7152
50	100	0.0904	99.9096

Table (4.13): Effect of contact time on the removal (%) of Mg(II) ion on 4A° Zeolite at 298 K.

Time (min)	Mg (II)		
	Co(mg/L)	Ct(mg/L)	R%
10	100	9.672	90.328
20	100	8.2212	91.7788
30	100	9.7526	90.2474
40	100	5.642	94.358
50	100	2.418	97.582

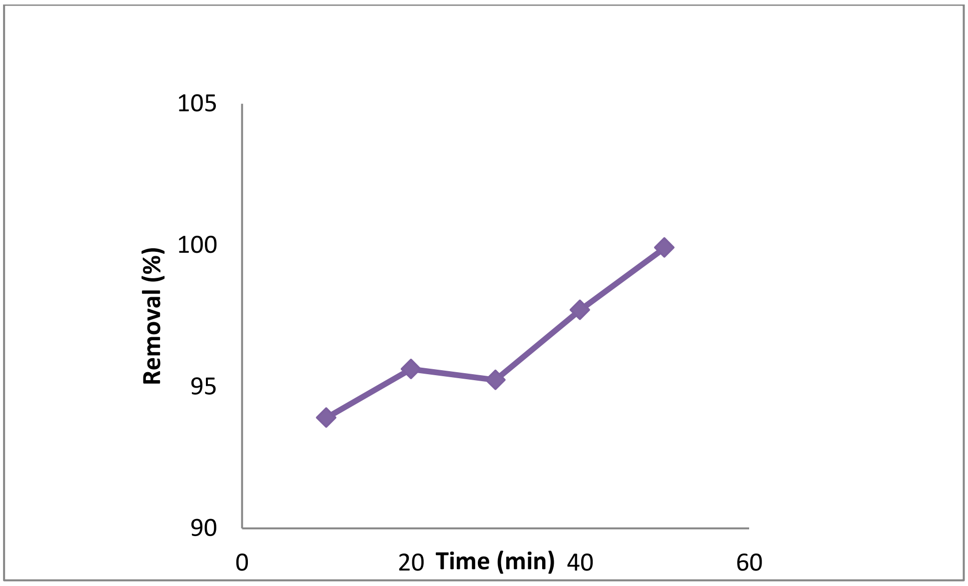

Figure (4.31): Effect of contact time on removal (%) of Ca (II) ion on prepared 4A° Zeolite at 298 K.

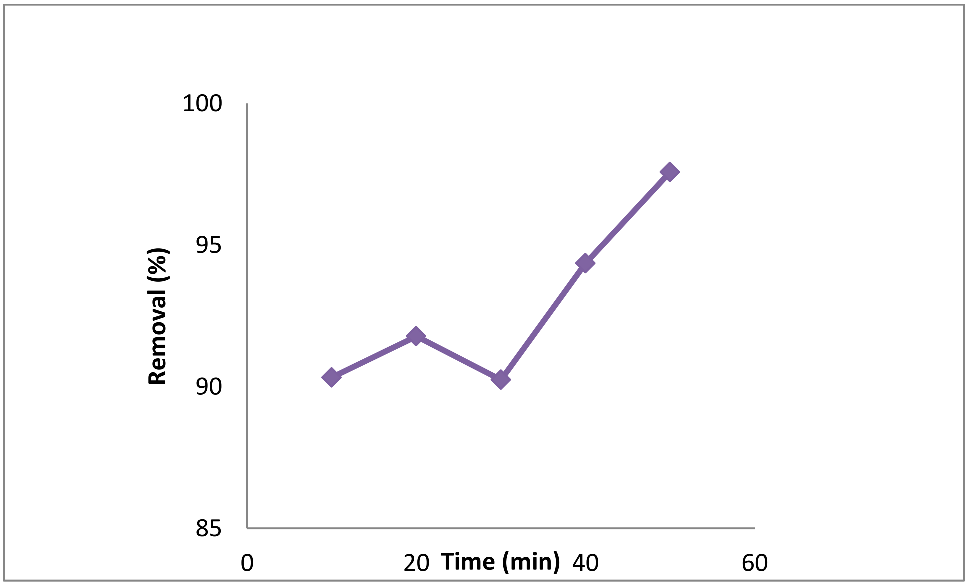

Figure (4.32): Effect of contact time on removal (%) of Mg (II) ion on prepared 4A° Zeolite at 298 K.

4.2.2 Effect of adsorbent quantity on adsorption.

The effect of the adsorbent quantity of 4A° zeolite on the adsorption of calcium and magnesium ions, was studied using different quantity of the adsorbent (0.06, 0.08, 0.10, 0.12 and 0.15) g of prepared 4A° zeolite , with a contact time being (50) min only.

The influence of adsorbent quantity on the uptake of Ca (II) and Mg (II) ions on to prepared 4A° Zeolite are shown in Tables (4.14), and (4.15), and in Figure (4.33) and (4.34) . On increasing the quantity of surface, the metals removal will increases too, this means that increasing the amount of surface increases the percentage removal for Ca+2 and Mg+2. This can be explained by the increasing surface area where the adsorption take place and this increasing of percentage removal should be due to the presence of a large number of adsorbent sites at increased weight [106,107]

Table (4.14): Effect of adsorbent quantity on the removal (%) of Ca(II) ion on prepared 4A° zeolite at 298 K.

Adsorbent quantity (g)	Ca (II) ions		
	Co (mg/L)	Ct (mg/L)	R%
0.06	100	6.9695	93.0305
0.08	100	5.7334	94.2666
0.10	100	5.1942	94.8058
0.12	100	5.523	94.477
0.15	100	4.734	95.266

Table (4.15): Effect of adsorbent quantity on the removal (%) of Mg (II) ion on prepared 4A° zeolite at 298 K.

Adsorbent quantity (g)	Mg (II) ions		
	Co (mg/L)	Ct (mg/L)	R%
0.06	100	9.402	90.598
0.08	100	9.0102	90.9898
0.10	100	8.0230	91.977
0.12	100	8.7752	91.2248
0.15	100	7.8976	92.1024

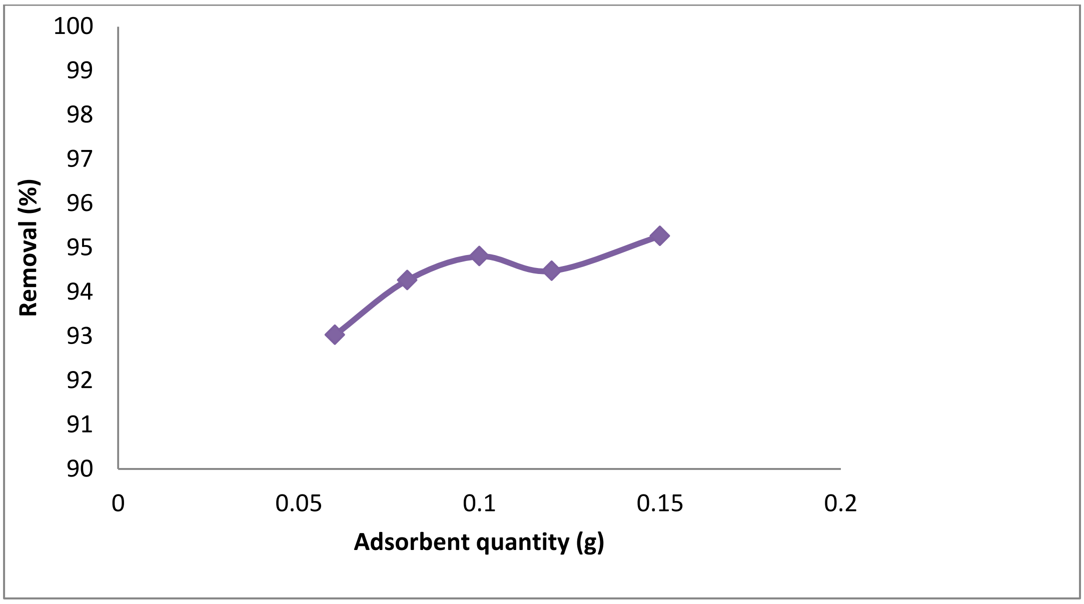

Figure (4.33): Effect of adsorbent quantity on the removal (%) of Ca (II) ion on prepared 4A° Zeolite at 298 K.

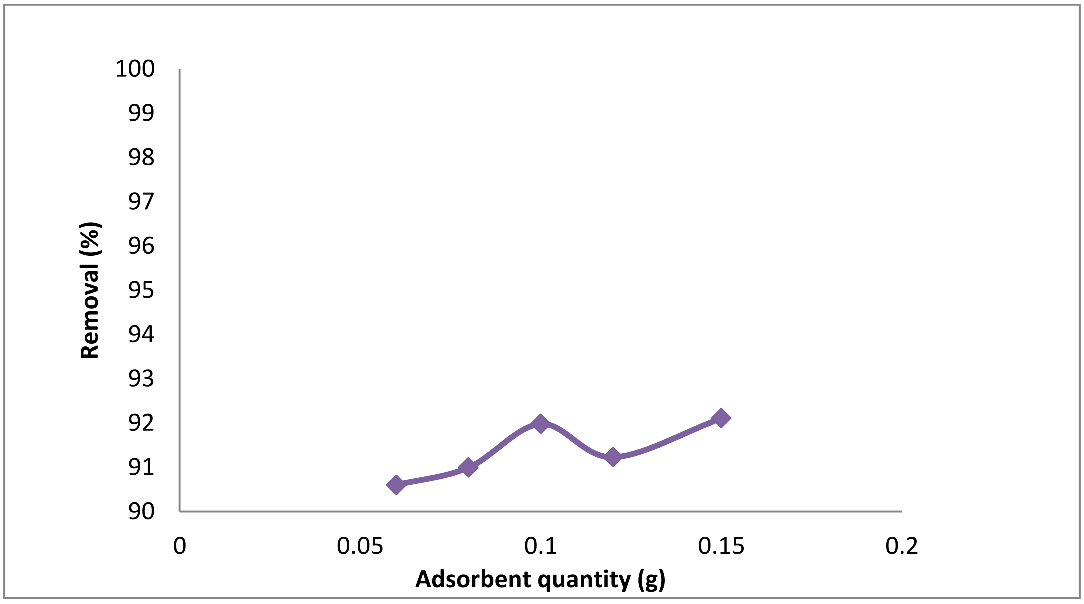

Figure (4.34): Effect of adsorbent quantity on the removal (%) of Mg (II) ion on prepared 4A° zeolite at 298 K.

4.2.3 Effect of temperature on adsorption.

The effect of temperature on the adsorption of calcium and magnesium ions with prepared 4A°zeolite has been studied at five different temperatures (293, 303, 313,323 and 333) K , initial concentration of (100) mg/l of Ca (II) and Mg(II) quantity of adsorbent is (0.1) g for prepared sample , contact time was maintain at (50) min.

The data shows that the percentage removal decreases with increasing in temperature. These observations means that adsorption of Ca +2 and Mg+2 ions on prepared 4A° zeolite surface are of exothermic nature in all cases, the reduction in the rate of adsorption with increasing in the temperature, may be due to back weakening of interaction force between the active sites of the adsorption surface and the Ca (II) and Mg (II) ion (53). All these are shown in the Tables(4.16) and (4.17) and Figures (4.35) and (4.36).

Table (4.16): Effect of temperature on the removal (%) of Ca(II) ion with 4A° zeolite.

Temperature (K)	Ca(II) ions		
	Co (mg/L)	Ct (mg/L)	R%
293	100	5.4145	94.5855
303	100	5.8976	94.1024
313	100	6.9972	93.0028
323	100	6.6973	93.3027
333	100	9.3296	90.6704

Table (4.17): Effect of temperature on the removal (%) of Mg (II) ion with 4A° zeolite.

Temperature (K)	Mg (II) ions		
	Co (mg/L)	Ct (mg/L)	R%
293	100	5.5216	94.4784
303	100	5.9024	94.0976
313	100	6.7592	93,2408
323	100	7.4065	92.5935
333	100	8.0729	91.9271

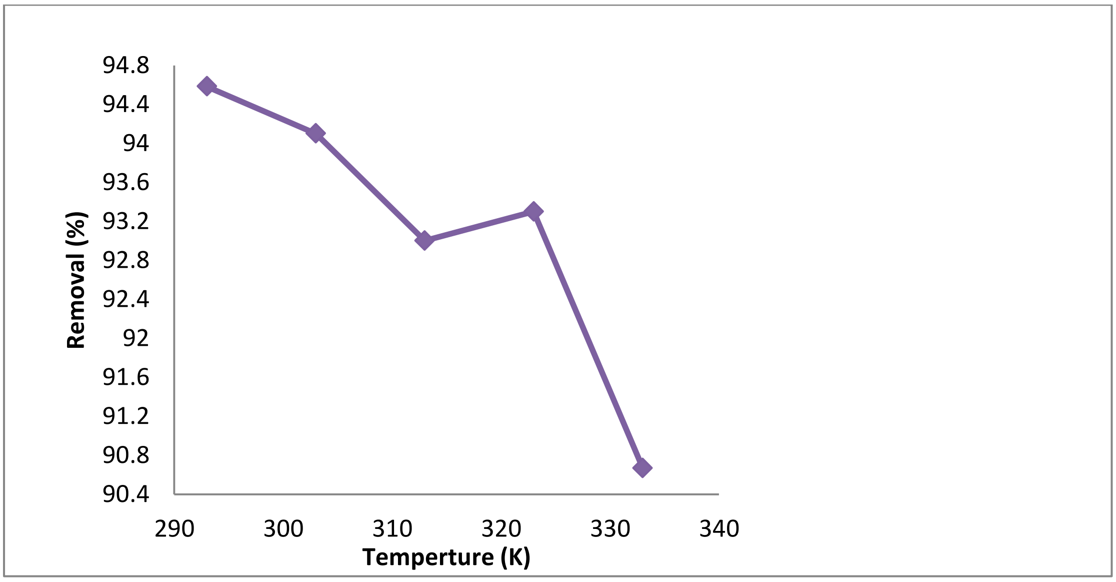

Figure (4.35): Effect of temperature on the removal (%) of Ca (II) ion with prepared Zeolite.

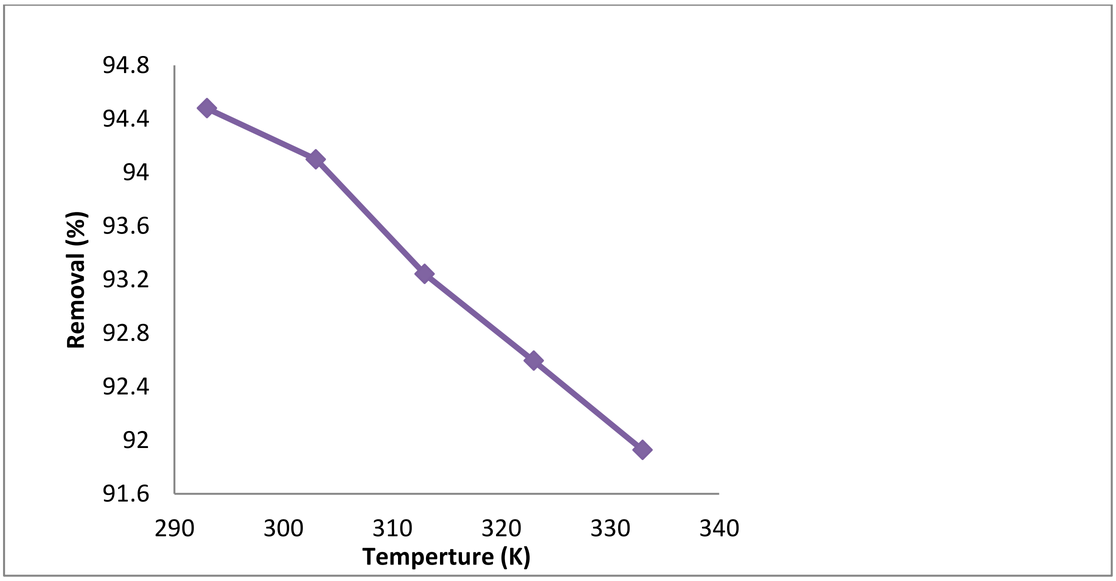

Figure (4.36): Effect of temperature on the removal (%) of Mg (II) ion with prepared4A° zeolite.

4.2.4 Effect of initial concentration of Ca (II), Mg(II) on adsorption

Adsorption of calcium and magnesium (II) ions from an aqueous solution on the prepared 4A° Zeolite was studied using different initial concentration of aqueous solution of (50,100,150,200, and 250) mg/L at (298K) the results are shown in Tables (4.18) , (4.19) and Figures (4.37) and (4.38) respectirely . The impact of the initial concentration indicates decrease in the percentage removal with increasing of initial concentration of Ca(II) and Mg(II) ions with prepared

4A° Zeolite. The effect of initial concentration on the Ca+2, Mg+2 ions percentage removal plays an important role in the adsorption process. The percentage removal decreases with the increasing of initial ions concentration is due to increase in the driving force of the concentration gradient. Also if the concentrations decreased, the percentages removals were higher due to a larger surface area of the adsorbent being available for the adsorption of metal ions. When the concentration is high, the percentages removals are low because the available sites for the adsorption became occupied and when initial concentration increased more, it reached the saturation point with time where no more ions was further removed from solution [94] **.**

Table (4.18): Effect of initial concentration on the removal (%) of Ca(II) ions on 4A° zeolite at 298 K.

Initial concentration C0 (mg/L)	Ca (II) ions	
	Ct (mg/L)	R%
50	1.9856	96.0288
100	1.5122	98.4878
150	6.312	95.792
200	13.5444	93.2278
250	22.0262	91.1895

Table (4.19): Effect of initial concentration on the removal (%) of Mg(II) ions on 4A° zeolite at 298 K.

Initial concentration (mg/L)	Mg (II) ions	
	Ct (mg/L)	R%
50	1.0577	97.8846
100	5.5471	94.4529
150	15.2782	89.8145
200	26.0122	86.9939
250	58.7625	76.495

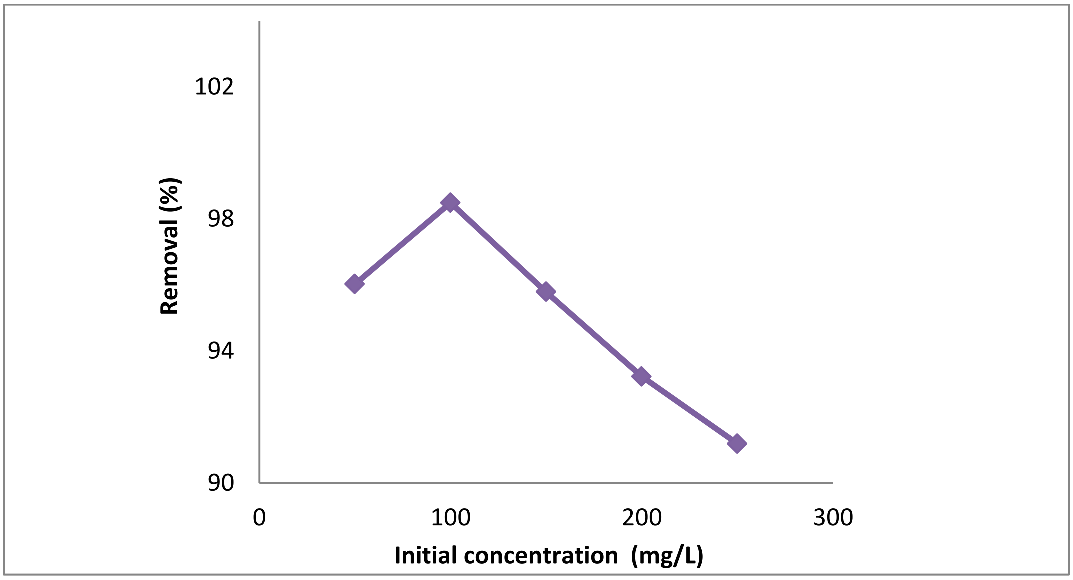

Figure (4.37): Effect of initial concentration on the removal (%) of Ca(II) ions on 4A° zeolite at 298 K.

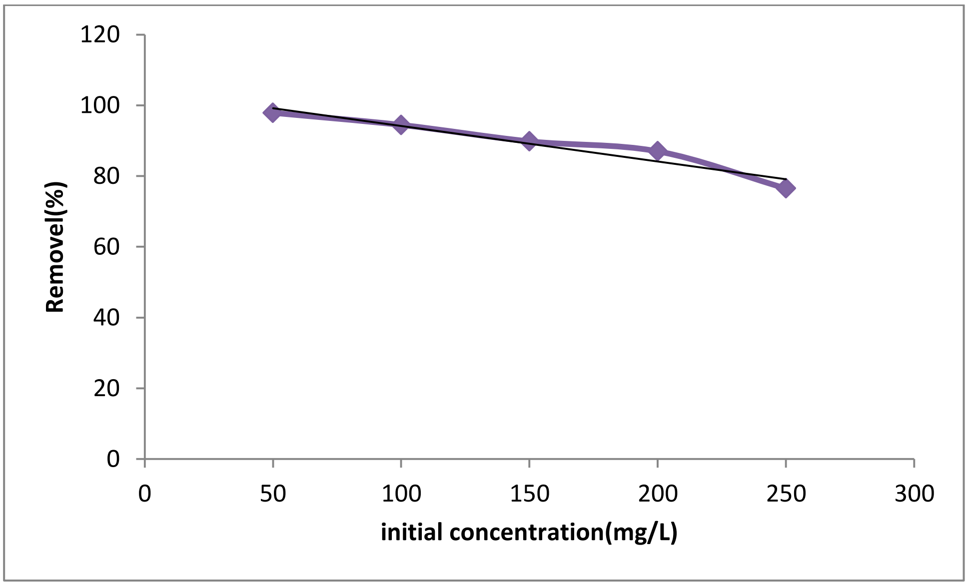

Figure (4.38): Effect of initial concentration on the removal (%) of Mg(II) ions on 4A° zeolite at 298 K.

4.3 Kinetics studies for adsorption process of Ca(II) and Mg(II) ions.

The kinetic study was carried out for adsorption of Ca (II) and Mg(II) ions on prepard 4A° zeolite by using experimental conditions of initial concentration of (100 mg/l), different temperatures (308, 313, 318, and 323) K , with constant stirring speed 150 rpm and intervals times (5, 15, 25 ,35 and 45) minutes . The value of Ce is the concentration of metal ion after adsorption at any time (mg /l), qt is the amount adsorbed at any time (mg/g), qe which is the amount adsorbed at equilibrium (mg/g) in Tables(4.20) and (4.21) are the absorption data using 4A° zeolite .

These data were applied for pseudo first order model expressed by equation (2.11) by plotting ln(qe-qt) against a time (t) to calculate the value of k1 as shown in Figures (4.39) and (4.43) for the adsorption of Ca (II) and Mg(II) ions on 4A° zeolite . The data was then applied for pseudo second model given by equation (2.13) by plotting t/qe against a time to calculate the value k2 as shown in Figures (4.40) and (4.44) for the adsorption of Ca (II) and Mg (II) ions on 4A° Zeolite. The data was applied for intraparticle diffusion model given by equation (2.15) by plotting qt against a t1/2 to calculate the value of kD as shown in figures (4.41) and (4.45) for the adsorption of Ca (II) and Mg (II) ions on 4A° Zeolite, Finally the data was applied for elovich model given by equation (2.17) by plotting qt against a ln t to calculate the value of k as shown in Figures (4.42) and (4.46) for the adsorption of Ca (II) and Mg (II) ions on 4A° Zeolite In tables (4.22)and (4.23) the adsorption kinetic constants for Ca (ll) and Mg(II) ions removal on 4A° zeolite are presented>

Table (4.20) the adsorption data of qt and qe for Ca (II) ions removal with 4A° zeolite.

Ca								
T(K)	**Time (t)**	**√*t***	**Ce**	**qt**	**qe-qt**	**ln(qe-qt)**	**t/qt**	**lnT**
308	5	2.2360	14.68	42.66	5.43	1.6919	0.1172	1.6094
	15	3.8729	11.35	44.325	3.765	1.3257	0.3384	2.7080
	25	5	9.94	45.03	3.06	1.1184	0.5551	3.2188
	35	5.9160	5.01	47.495	0.695	-0.3638	0.7369	3.5553
	45	6.7082	3.82	48.09			0.9357	3.8066
T(K)	**Time (t)**	**√*t***	**Ce**	**qt**	**qe-qt**	**ln(qe-qt)**	**t/qt**	**lnT**
313	5	2.2360	16.22	41.89	5.73	1.7457	0.1193	1.6094
	15	3.8729	13.12	43.44	4.18	1.4303	0.3454	2.7080
	25	5	11.99	44	3.62	1.2864	0.5681	3.2188
	35	5.9160	8.34	45.83	1.79	0.5822	0.7636	3.5553
	45	6.7082	4.76	47.62			0.9449	3.8066
T(K)	**Time(t)**	**√*t***	**Ce**	**qt**	**qe-qt**	**ln(qe-qt)**	**t/qt**	**lnT**
318	5	2.2360	19.01	40.49	6.78	1.9139	0.1234	1.6094
	15	3.8729	15.45	42.27	5	1.6094	0.3548	2.7080
	25	5	14.684	42.66	4.61	1.5282	0.5860	3.2188
	35	5.9160	9.52	45.24	2.03	0.7080	0.7736	3.5553
	45	6.7082	5.46	47.27			0.9519	3.8066
T(K)	Time(t)	**√*t***	Ce	**qt**	**qe-qt**	**ln(qe-qt)**	**t/qt**	**lnT**
323 323	5	2.2360	24.94	37.53	8.195	2.1035	0.13322	1.6094
	15	3.8729	19.44	40.28	5.44	1.6946	0.3723	2.7080
	25	5	15.65	42.175	3.55	1.2669	0.5927	3.2188
	35	5.9160	10.31	44.845	0.8	-0.1278	0.7804	3.5553
	45	6.7082	8.55	45.725			0.9841	3.8066

Table (4.21) the adsorption data of qt and qe for Mg (II) ions removal with 4A° zeolite

Mg								
T(K)	**Time (t)**	**√*t***	**Ce**	**qt**	**qe-qt**	**ln(qe-qt)**	**t/qt**	**lnT**
308	5	2.2360	10.65	44.67	5.08	1.6253	0.1119	1.6094
	15	3.8729	9.27	45.36	4.39	1.4793	0.3306	2.7080
	25	5	6.93	46.53	3.22	1.1693	0.5372	3.2188
	35	5.9160	4.35	47.82	1.93	0.6575	0.7319	3.5553
	45	6.7082	0.5	49.75			0.9045	3.8066
T(K)	**Time (t)**	**√*t***	**Ce**	**qt**	**qe-qt**	**ln(qe-qt)**	**t/qt**	**lnT**
313	5	2.2360	11.95	44.025	4.475	1.4985	0.1135	1.6094
	15	3.8729	9.92	45.04	3.46	1.2412	0.3330	2.7080
	25	5	7.99	46.005	2.495	0.9142	0.5434	3.2188
	35	5.9160	5.95	47.025	1.475	0.3886	0.7442	3.5553
	45	6.7082	3	48.5			0.9278	3.8066
T(K)	**Time(t)**	**√*t***	**Ce**	**qt**	**qe-qt**	**ln(qe-qt)**	**t/qt**	**lnT**
318	5	2.2360	14.06	42.97	3.565	1.2711	0.1163	1.6094
	15	3.8729	12.93	43.535	3	1.0986	0.3445	2.7080
	25	5	10.24	44.88	1.655	0.5038	0.5570	3.2188
	35	5.9160	9.65	45.175	1.36	0.3074	0.7747	3.5553
	45	6.7082	6.93	45.535			0.9670	3.8066
T(K)	Time(t)	**√*t***	Ce	**qt**	**qe-qt**	**ln(qe-qt)**	**t/qt**	**lnT**
323	5	2.2360	22.91	38.545	6.505	1.8725	0.1297	1.6094
	15	3.8729	20.01	39.995	5.055	1.6203	0.3750	2.7080
	25	5	14.46	42.77	2.28	0.8241	0.5845	3.2188
	35	5.9160	10.22	44.89	0.16	-1.8325	0.7817	3.5553
	45	6.7082	9.90	45.05			0.9988	3.8066

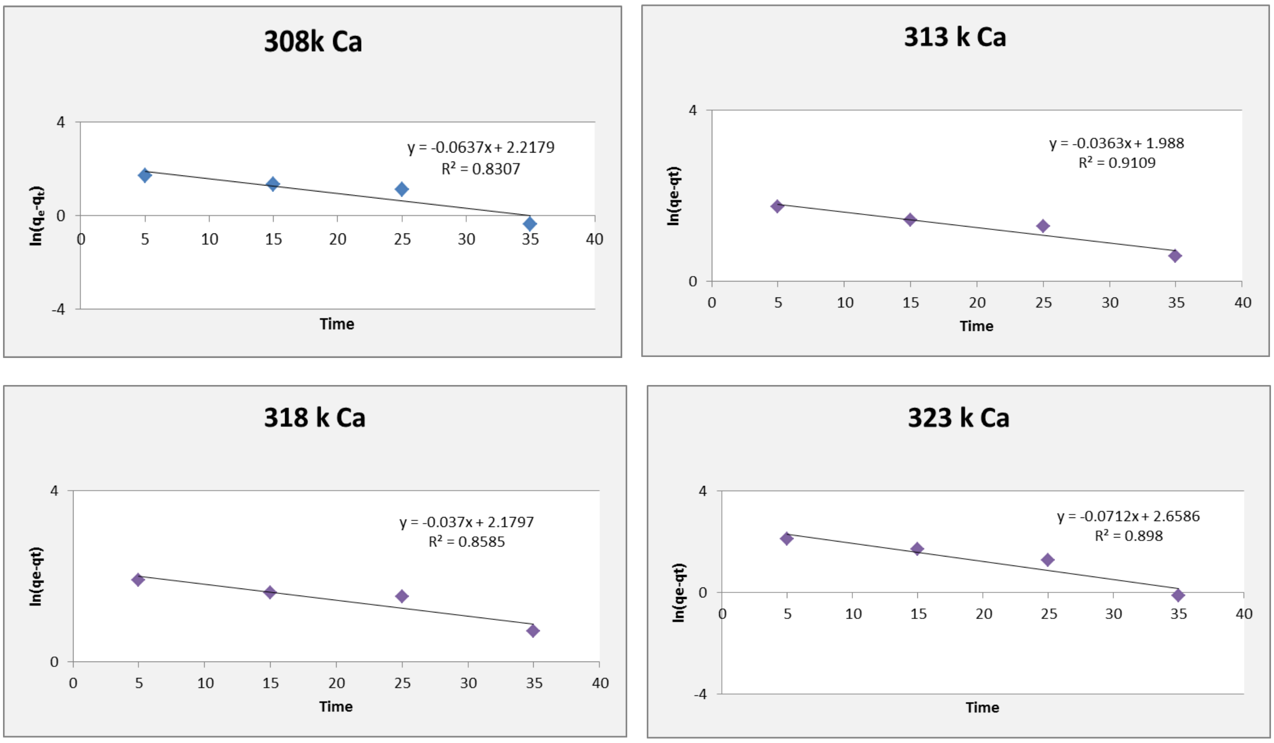

Figure (4.39): The Pseudo first – order kinetic model for Ca ions adsorption on 4A° zeolite.

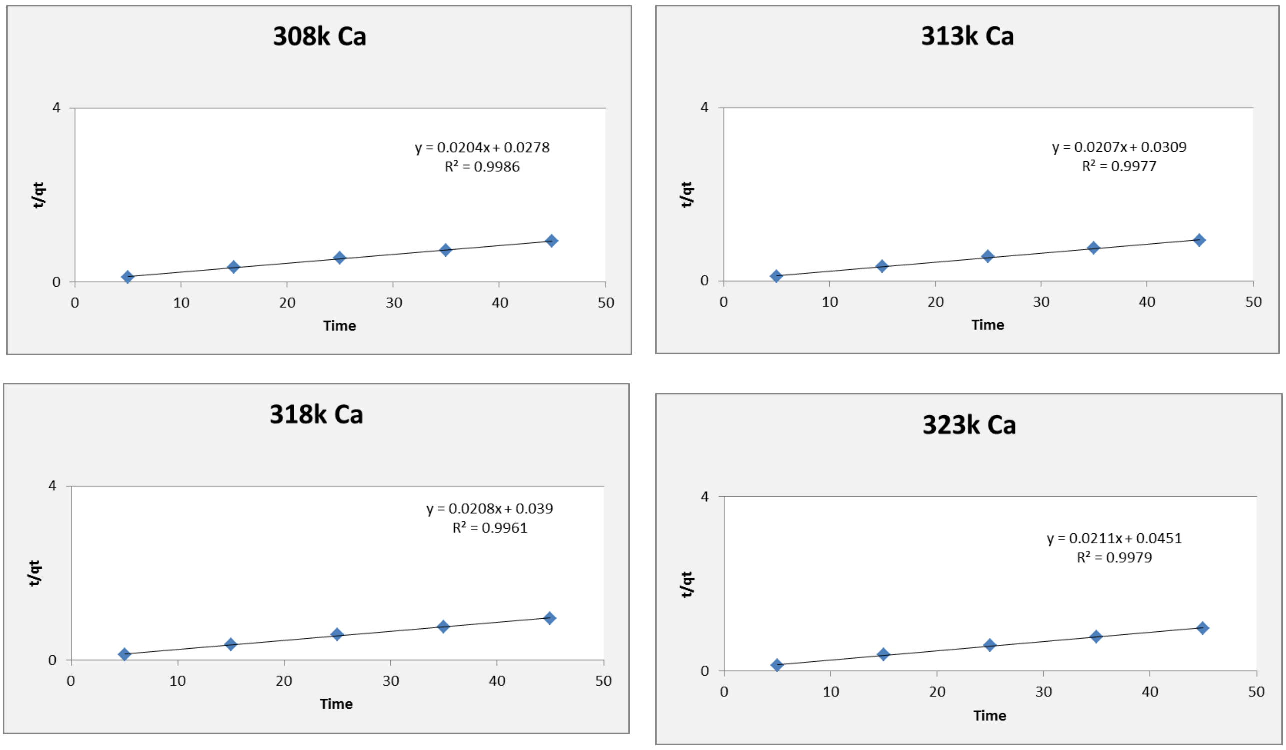

Figure (4.40) The pseudo second – order kinetic model for Ca ions adsorption on 4A° zeolite .

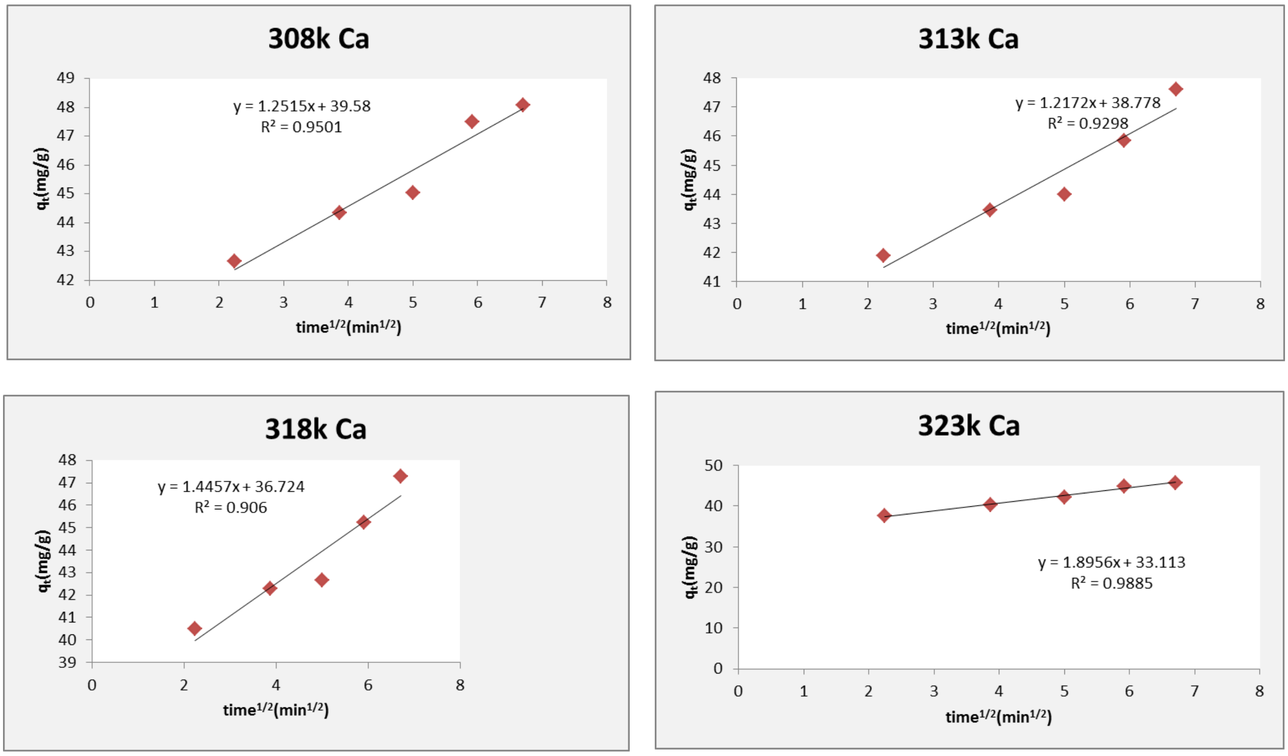

Figure (4.41) The intraparticle diffusion model for Ca ions adsorption on 4A° zeolite .

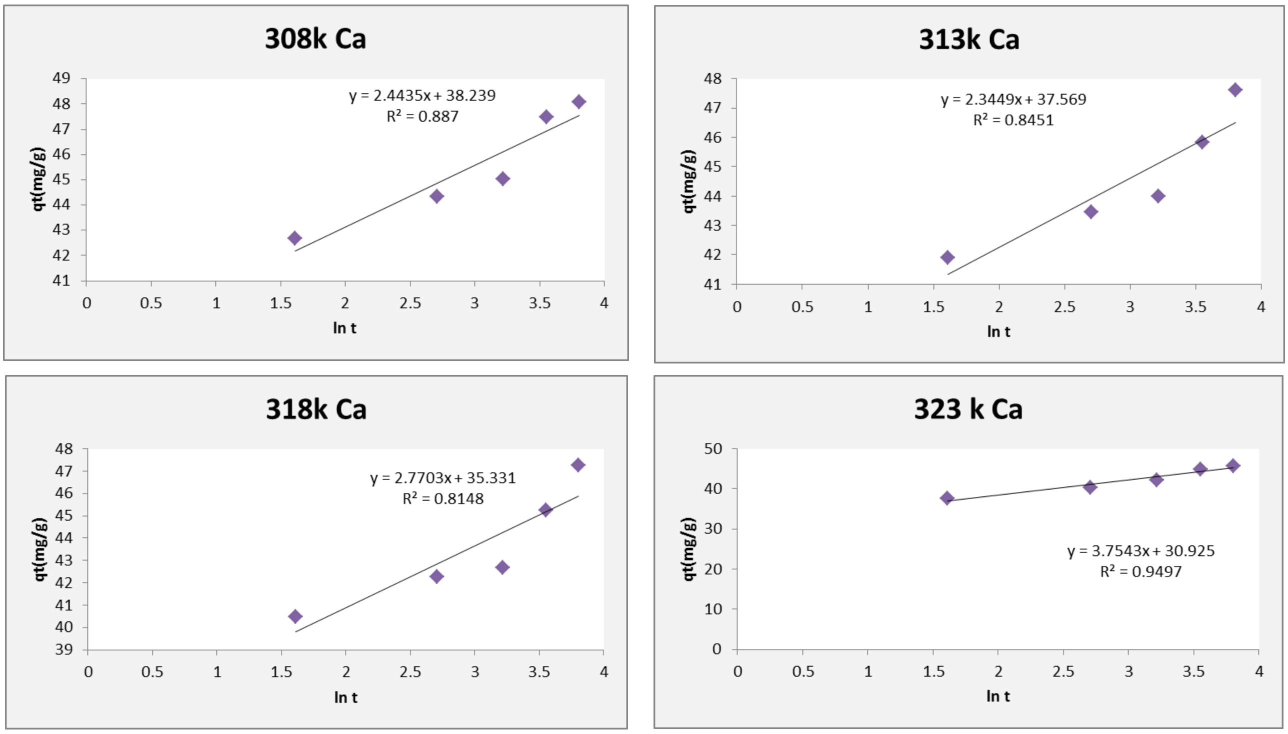

Figure (4.42) The elovich model for Ca ions adsorption on 4A° zeolite

Table (4.22): Adsorption kinetics constants for Ca(II) ions adsorption on 4A°zeolite.

T(K)	qe (mg/g)	Pseudo-first order		Pseudo-second order		Intrapartical diffusion		Elovich Model	
		K1 min-1	R2	K2 g/mg.min	R2	KD mg/g.min-1	R2	Kelovich mg/g.s	R2
308	48.09	0.0637	0.8307	0.0149	0.9986	1.2515	0.9501	9008	0.887
313	47.62	0.0363	0.9109	0.0138	0.9977	1.2171	0.9298	1303	0.8451
318	47.27	0.0369	0.8585	0.011	0.9961	1.4457	0.906	4983	0.8148
323	45.725	0.0712	0.898	9.8941	0.9979	1.8956	0.9885	5364	0.9497

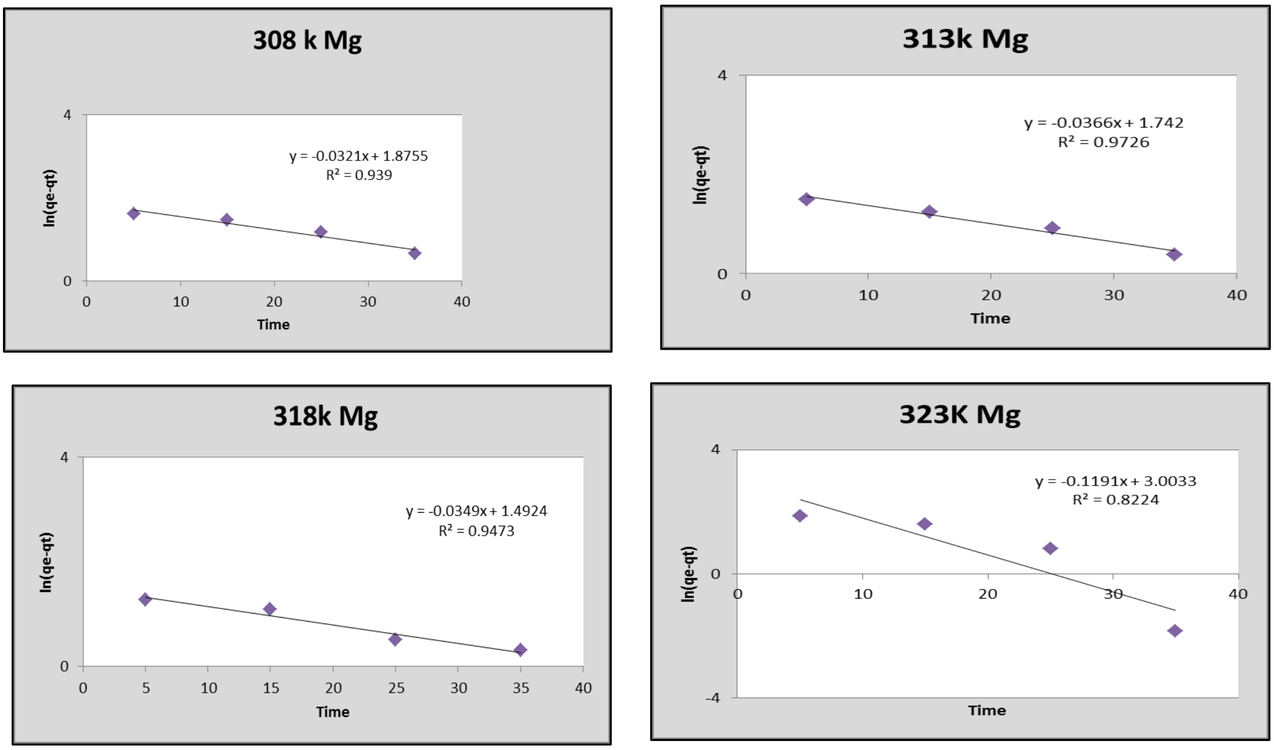

Figure (4.43) The pseudo first – order kinetic model for Mg ions adsorption on 4A° zeolite

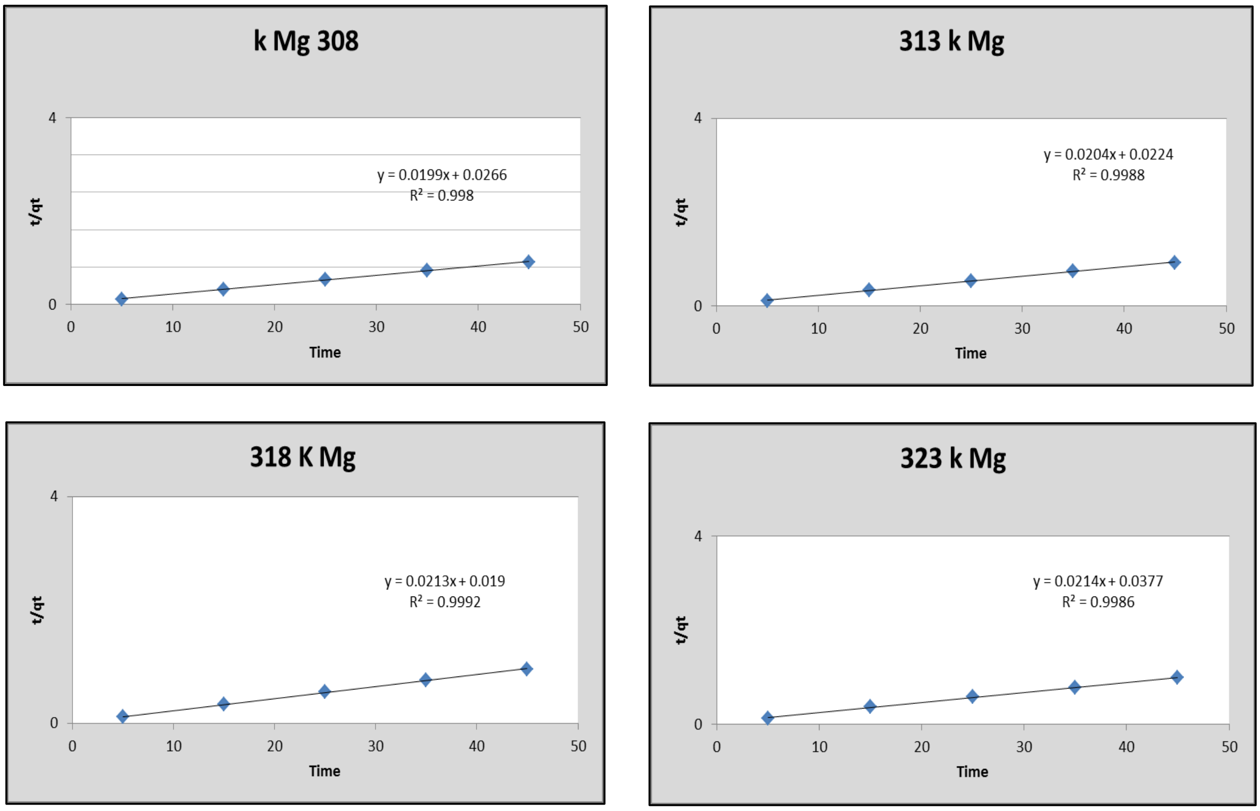

Figure (4.44) The pseudo second – order kinetic model for Mg ions adsorption on 4A° zeolite .

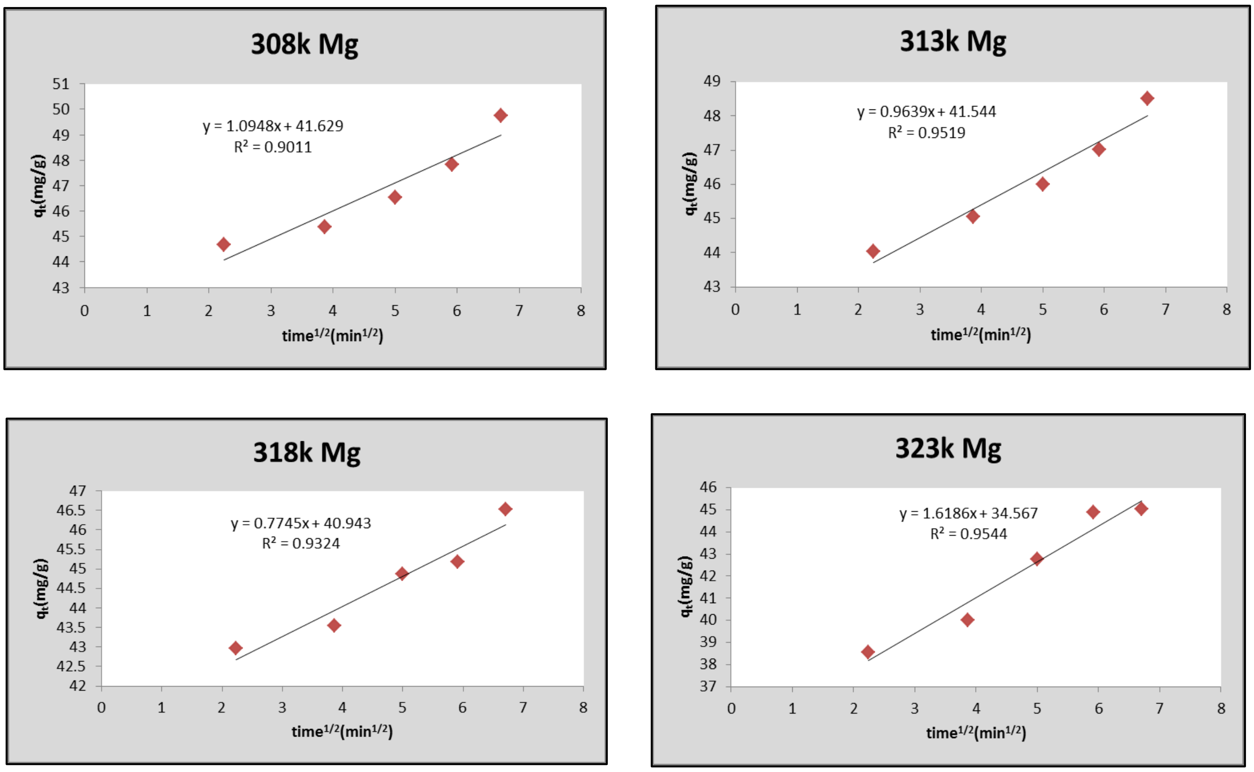

Figure (4.45) The intraparticle diffusion model for Mg ions adsorption on 4A° zeolite .

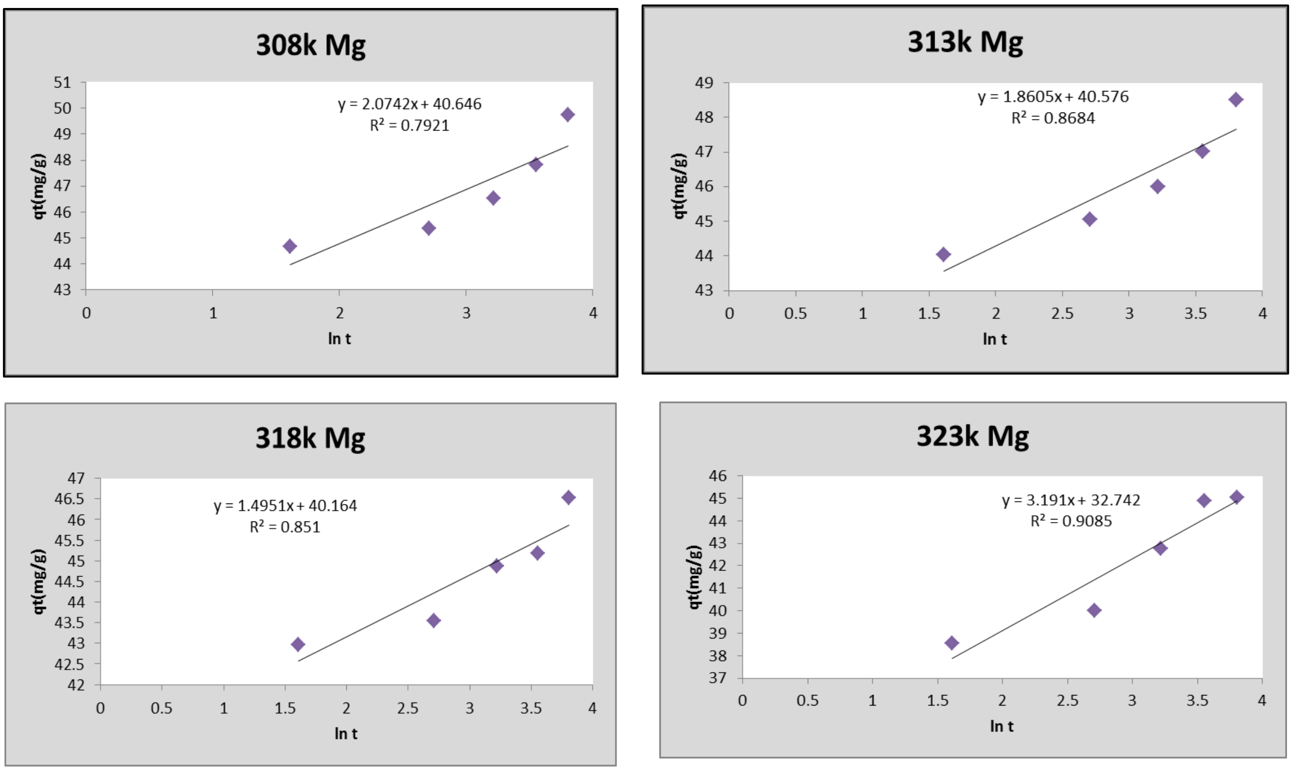

Figure (4.46) The elovich model for Mg ions adsorption on 4A° zeolite

Table (4.23): Adsorption kinetics constants for Mg(II) ions adsorption on 4A° zeolite.

T(K)	qe (mg/g)	Pseudo-first order		Pseudo-second order		Intrapartical diffusion		Elovich model	
		K1 min-1	R2	K2 g/mg.min	R2	KD mg/g.min-1	R2	Kelovich mg/g.s	R2
308	49.75	0.0321	0.939	0.0147	0.998	1.0948	0.9011	4603	0.7921
313	48.5	0.0365	0.9726	0.0184	0.9988	0.9639	0.9519	4138	0.8684
318	46.535	0.0348	0.9473	0.0238	0.9992	0.7744	0.9324	6.0651	0.851
323	45.05	0.0119	0.8224	0.0121	0.9986	1.6186	0.9544	4101	0.9085

The calculated values of k1, k2, KD and kelovich constant with their correlation coefficient for adsorption of Ca (II) and Mg(II) ions on prepared 4A° zeolite are given in Tables (4.22), and (4.23) respectively. The results showed in Tables (4.22) and (4.23) show the correlation coefficient of pseudo-second order is higher than the pseudo-first-order and intrapartical diffusion models and even elovich model and the kinetic data fits well with for adsorption Ca(II) and Mg (II) on 4A° zeolite [106,107]

4.4 The adsorption isotherm

The adsorption of Ca(II) and Mg (II) ions on 4A° Zeolite in aqueous solution at ideal condition, are shown in Table (4.24):

Table (4.24): Ideal condition for adsorption

No.	Conditions on two adsorbent	Value	
		Ca (II) ion	Mg(II) ion
1	Temperature	293 K	293 K
3	Volume of metals Solution	50 mL	50 mL
4	Contact time on 4A° Zeolite	50 min	50 min
5	Quantity of adsorbents	0.1 (g)	0.1(g)
6	Stirring speed	180 (rpm)	180 (rpm)

Three adsorption isotherm models Langmuir,Freundlich and Temkin were used to study the adsorption process of Ca (II) and Mg (II) ions using the data given in Table(4.25).

Table (4.25) present the adsorption data of Ca (II) and Mg(II) removal on (4A° Zeolite) .

Ca							Mg					
C0 mg/L	Ce mg/L	Qe mg/g	Log Ce	Log Qe	Ln Ce	Ce/Qe	Ce mg/L	Qe mg/g	Log Ce	Log Qe	Ln Ce	Ce/Qe
50	1.9856	24.0072	0.2978	1.3803	0.6859	0.0827	1.0577	24.4711	0.0243	1.3886	0.0560	0.0432
100	1.5122	49.2439	0.1796	1.6923	0.4135	0.0307	5.5471	47.2264	0.744	1.6741	1.7132	0.1174
150	6.312	71.844	0.8001	1.8563	1.8424	0.0878	15.2782	67.3609	1.1840	1.8284	2.7264	0.2268
200	13.5444	93.2278	1.1317	1.9695	2.6059	0.1452	26.0122	86.9939	1.4151	1.9394	3.2585	0.2990
250	22.0262	113.9869	1.3429	2.0568	3.0922	0.1932	58.7625	95.6187	1.7691	1.9805	4.0735	0.6145

4.4.1 Langmuir isotherm

Langmuir isotherm equation (2.3) was applied for adsorption of Ca(II) and Mg(II) on 4A° zeolite at various initial concentrations. Adsorption isotherm data for Ca and Mg solution removals are presented in Table (4.25) and plotted in Figures (4.47) and (4.48). The values of the Langmuir isotherm constant (a) which is the monolayer adsorption capacity and (b) which is a constant related to the energy of adsorption are calculated from the slope and intercept of the plots (Ce/Qe) versus (Ce) and are shown in Table (4.26)

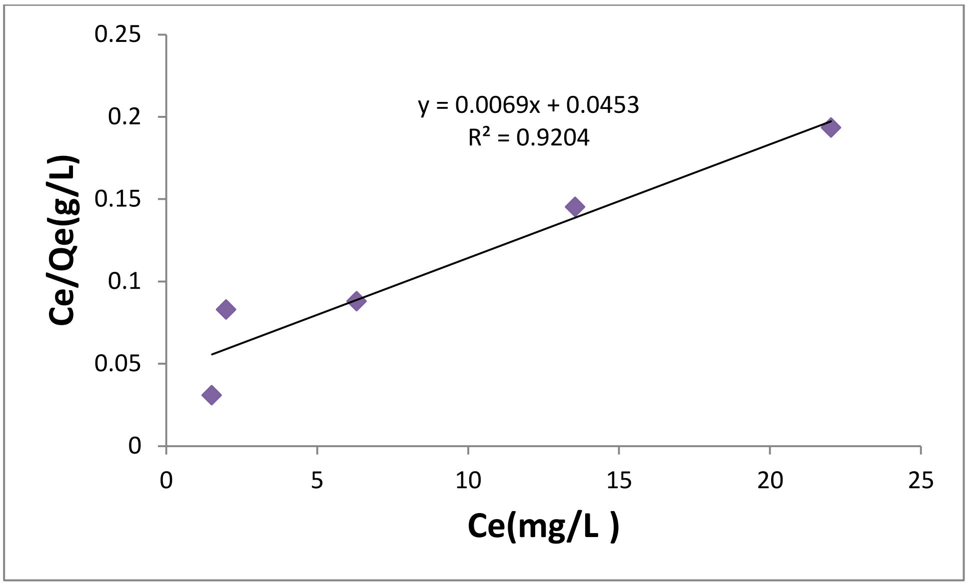

Figure (4.47): Linear Langmuir isotherm of Ca (II) ions adsorption on 4A°zeolite surface.

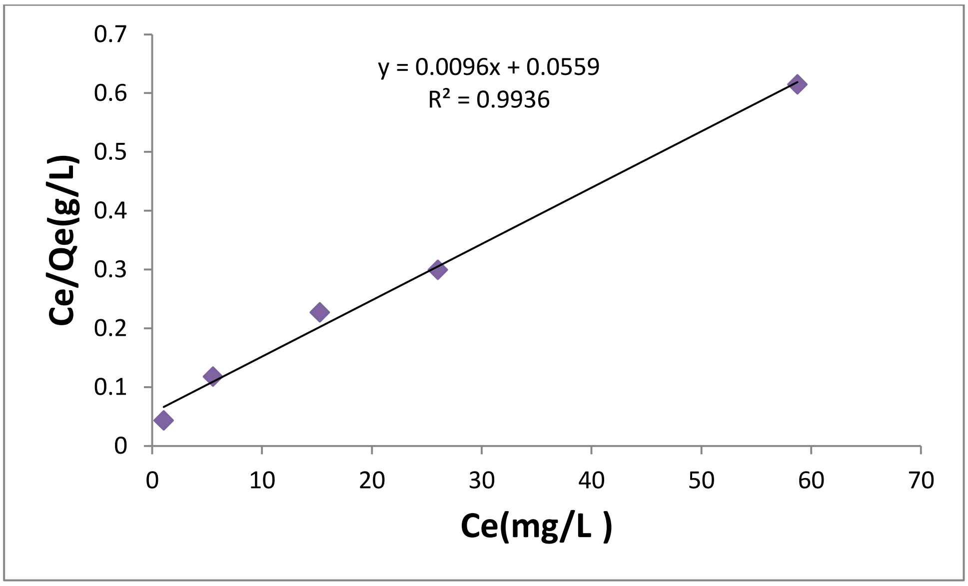

Figure (4.48): Linear Langmuir isotherm of Mg (II) ions adsorption on 4A°zeolite surface .

4.4.2 Freundlich isotherm

Freundlich isotherm equation (2.5) was applied on adsorption of Ca and Mg ions on 4A° zeolite. Adsorption isotherm data for Ca and Mg ions were plotted and shown in Table (4.26) and Figures (4.49) and (4.50). The Freundlich isotherm constant (KF) which is the adsorption capacity of the adsorbent, and (n) is the adsorption intensity being calculated from the slope and intercept of the plot of (log Qe) versus (log Ce), with the results are shown in Table (4.26).

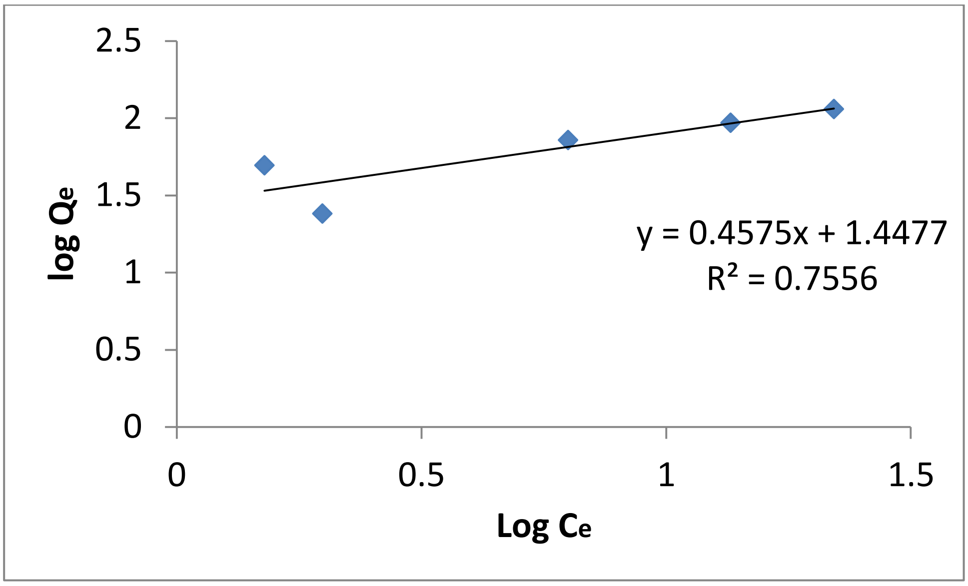

Figure (4.49): Linear Freundlich isotherm of Ca(II) ions adsorption on 4A° Zeolite surface at various initial concentrations

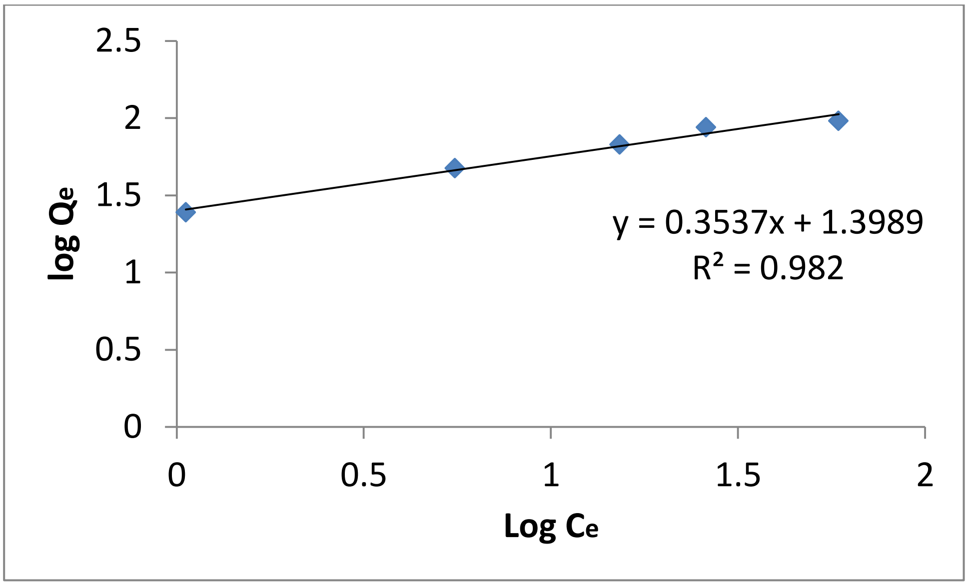

Figure (4.50): Linear Freundlich isotherm of Mg(II) ions adsorption on 4A° zeolite surface at various initial concentrations

4.4.3 Temkin isotherm

Temkin isotherm equation (2.6) model was applied for the adsorption of Ca (II) and Mg (II) ions on the 4A° Zeolite . Adsorption isotherm data for Ca+2 and Mg+2 ions were plotted and presented in Table (4.26) and Figures (4.51) and (4.52).

The Temkin isotherm constant (AT), which is the equilibrium binding constant (L/g) corresponding to the maximum binding energy, and (BT) is related the adsorption heat, being calculated from the slope and intercept of the plots of (Qe) versus (ln Ce) and the results are shown in Tables (4.26).

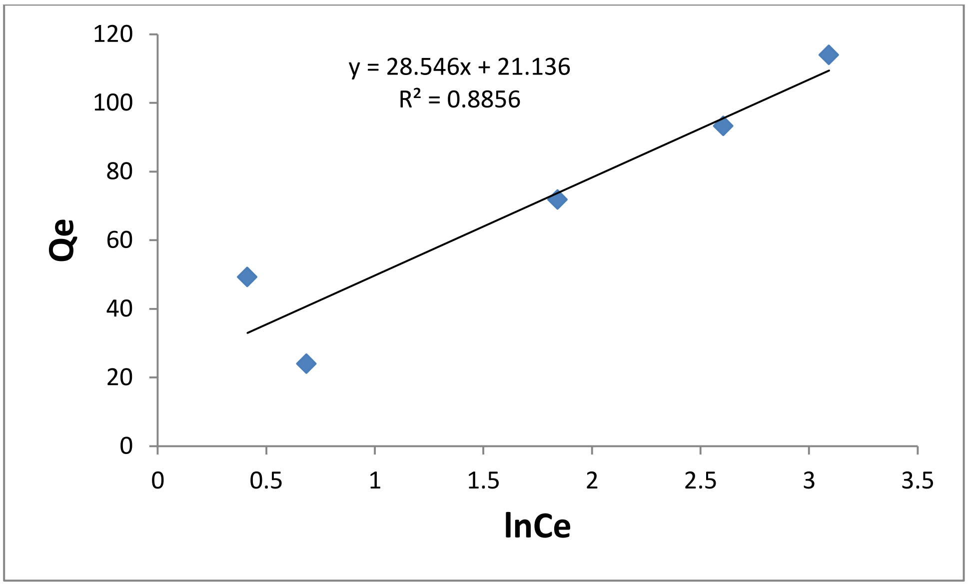

Figure (4.51): Temkin isotherm of Ca (II) ions adsorption on (4A° Zeolite) surface at various initial concentrations

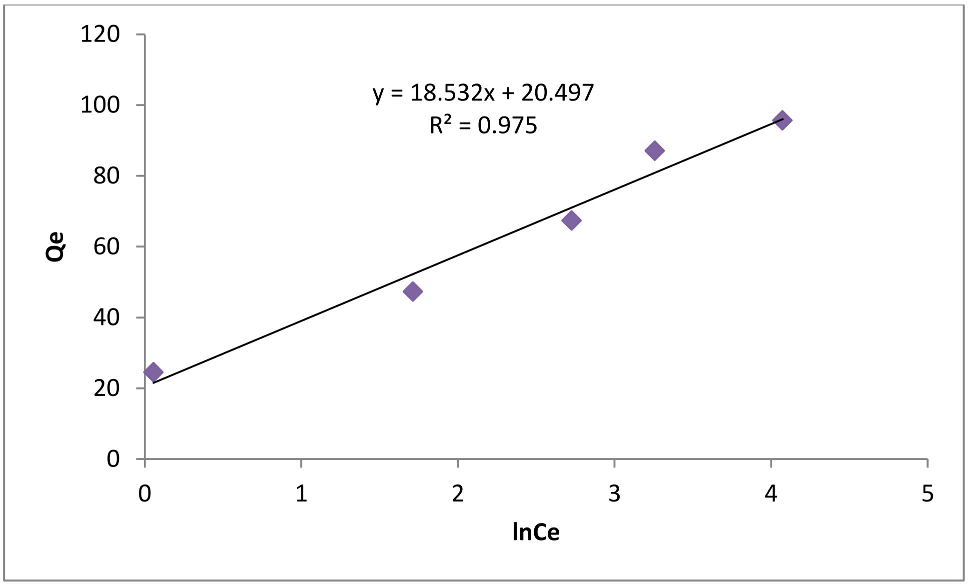

Figure (4.52): Temkin isotherm of Mg (II) ions adsorption on 4A° zeolite surface at various initial concentration

Table (4.26): Langmuir, Freundlich and Temkin constants for the adsorption of Ca(II) and Mg (II) ions with 4A° zeolite

Metals	**a (mg/g)**	**b (L/mg)**	**R2**
Langmuir			
Ca (II)	144.9065	0.1523	0.9204
Mg(II)	104.4277	0.1712	0.9936
Freundlich	N	Kf (mg/g)	R2
Ca (II)	2.1858	4.2534	0.7556
Mg (II)	2.8273	4.0505	0.982
Temkin	A_T (L/g)	B_T (J/mole)	R2
Ca (II)	-0.3005	28.5456	0.8856
Mg (II)	0.1007	18.5318	0.975

4.5 Thermodynamic study adsorption of Ca (II) and Mg (II) on 4A° zeolite.

The effect of temperature on removal of Ca+2and Mg+2 ions using 4A°zeolite at different temperature (293, 303, 313,323 and 333) K was investigated .This study is used for evaluation of the basic thermodynamic change of free energy ΔG, enthalpy ΔH, and entropy ΔS of adsorption processes .

Equilibrium of adsorption constant. K is explained thermodynamically by Van ’t Hoff equation below:

$$\ln K=\frac{-\Delta H}{R}.\left(\frac{1}{T}\right)+\frac{\Delta S}{R} \quad \text{.........(4.2)}$$

The equilibrium constant, K were calculated at any different temperature by equation below

$k=(Qe \times m)/(Ce \times V)$ …………. (4.3)

Where:

Qe: The adsorption capacity of metals ion, (mg/g) .

m: The quantity of zeolite surface (g).

Ce: The concentration at equilibrium after removal of Ca (II) and Mg (II)(mg/L).

V: Volume of aqueous solution containing Ca (II) and Mg ions, (L).

Table (4.27) and (4.28) illustrate values of (k) for adsorption of Ca (II) and Mg(II) ions with prpared 4A° Zeolite at different temperatures.

The ΔG° Gibes free energy change can be calculated from relationship:

$\Delta G^\circ = -RT \ln k$ ……. (4.4)

Where:

ΔG° is the standard free energy change, (kJ/mole), R is the gas constant, (8.314J/mol.K), T is the absolute temperature (K), and k is the equilibrium constant.

Finally, the values of (ΔH) and (ΔS) can be calculated from the slope and intercept of plot (lnk) versus (1/T) as explained by equations:

$\text{Slope} = -\Delta H/R$ **…..** (4.5)

$\text{Intercept} = \Delta S/R$ …… (4.6)

Figures (4.53) and (4.54) shows the Van ’t Hoff Plot for , prepared 4A°zeolite and for the two ions Ca+2 and Mg+2 respectively, and Table (4.29) display the thermodynamic value of metals ion removal on adsorbent surface.

Table (4.27): Effect of temperature on equilibrium constant for the adsorption of Ca (II) ions on prepared 4A° Zeolite.

Ca(II)						
Surfaces	**Temperature (K)**	**1/T,K-1**	**Ce (mg/L)**	**Qe (mg/g)**	**K**	**ln K**
4A° Zeolite	293	0.00341	5.4145	47.2927	17.4705	2.8605
	303	0.00330	5.8976	47.0512	15.9603	2.7701
	313	0.00319	6.9972	46.5014	13.2914	2.5871
	323	0.00309	6.6973	46.6513	13.9340	2.6343
	333	0.00300	9.3296	45.3352	9.7202	2.2742

Table (4.28): Effect of temperature on equilibrium constant for the adsorption of Mg (II) ions on prepared 4A° Zeolite.

Mg (II)						
surfaces	**Temperature (K)**	**1/T,K-1**	**Ce (mg/L)**	**Qe (mg/g)**	**K**	**ln K**
4A° Zeolite	293	0.00341	5.5216	47.2392	17.1156	2.8399
	303	0.00330	5.9024	47.0488	15.9433	2.7690
	313	0.00319	6.7592	46.6204	13.7970	2.6244
	323	0.00309	7.4065	46.2967	12.5024	2.5259
	333	0.00300	8.0729	45.9635	11.3883	2.4325

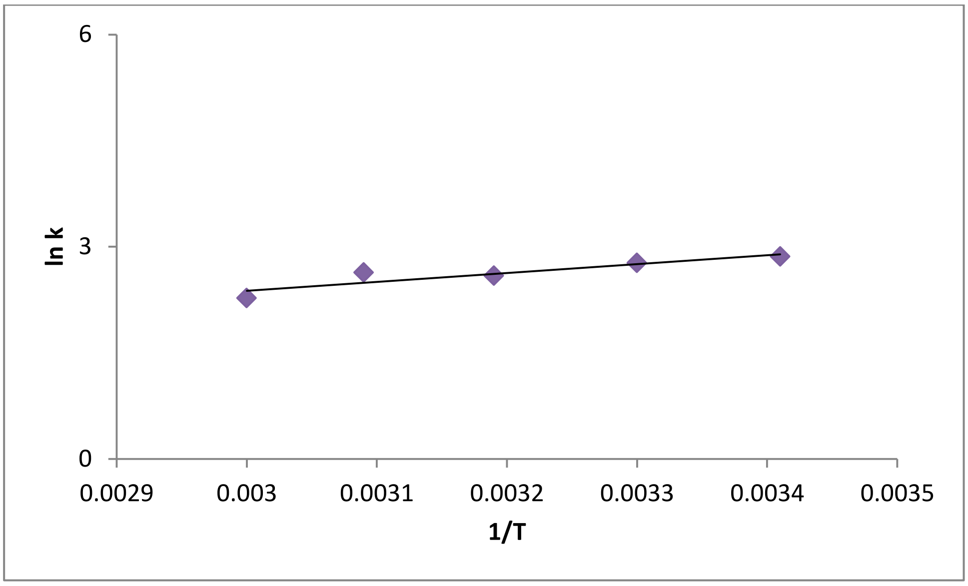

Figure (4.53): Van ʾt Hoff plot for adsorption of Ca (II) ions on 4A° zeolite.

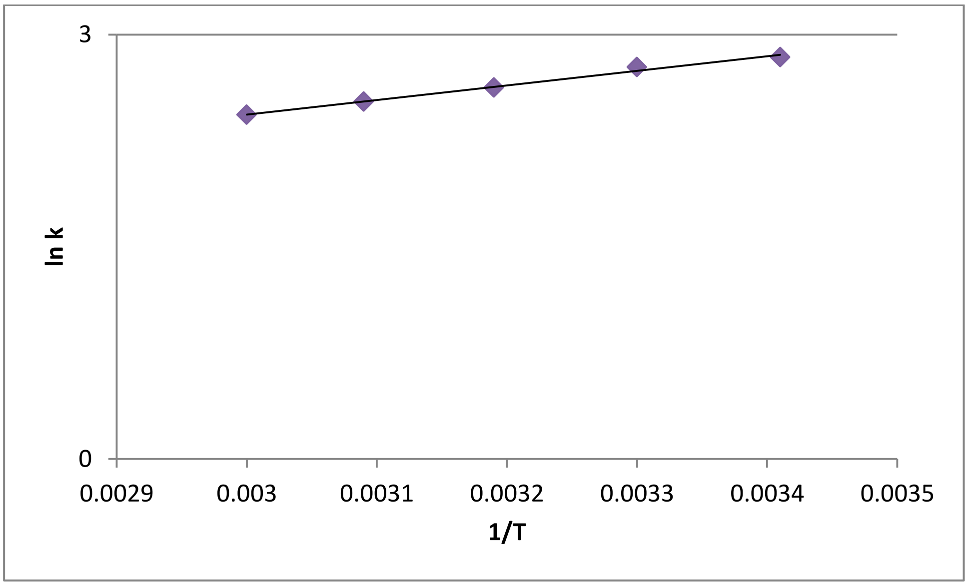

Figure (4.54): Van ʾt Hoff plot for adsorption of Mg (II) ions on 4A° zeolite

The free energy (ΔG), enthalpy (ΔH), and entropy (ΔS) changes were recorded in table (4.29) at different temperatures (293,303,313,323 and 333) K, as it was found from the obtained values that the negative G values are evidence of the spontaneity of the adsorption process of Ca and Mg ions on the 4A° zeolite surface and the decrease in its value . The negative entropy with an increase in the temperature of the same concentration is an indication that the adsorption process is of a spontaneous nature in the adsorption of positive ions inversely proportional to the temperature. As for the negative entropy values, it indicates an increase in the irregularity on the surface, which is an indication that the ions that suffer adsorption are restricted because they are affected by surface atoms.

Table (4.29): Values of thermodynamic function for the adsorption of Ca (II) and Mg(II)ions on prepared 4A° zeolite at different temperatures.

Surfaces	Temperature (K)	Ca(II)			Mg(II)		
		ΔG (KJ/mol)	**ΔH (KJ/mol)**	**ΔS (J/mol.K)**	**ΔG (KJ/mol)**	**ΔH (KJ/mol**	**ΔS (J/mol.K)**
4A°zeolite	293	-6968	-10442	-11.5674	-6918	-8532	-5.3508
	303	-6978			-6975		
	313	-6732			-6829		
	323	-7074			-6783		
	333	-6296			-6734		

4.6. Conclusions

1. Zeolite 4Å was prepared from Iraqi kaolin and rice husk using the process of conversion of rice husk to silica and kaolin to sodium aluminate where zeolite was prepared from. It was then characterized by X-ray diffraction, FTIR spectroscopy which prove the formation of zeolite and also indicate that this kaolin/rice husk can be used as a raw material for zeolite production.

2. X-ray diffraction revealed that the particle size obtained for kaolin, metakaolin, alumina, silica and zeolite are (50.88) nm, (50.88)nm,(34.36)nm,(33.88)nm and (43.37)nm respectively ,which agree fairly well with results of SEM. From AFM the average particle size observed in the nano scale less (100) nm .

3. The 4A° zeolite catalysts have the ability to remove calcium and magnesium ions.

4. The percentage removal of Ca+2 and Mg+2 reaches equilibrium in contact time (50) min on 4°A zeolite.

5. The percentage removal (R%) of calcium and magnesium by 4A° zeolite increases with increasing in adsorbent quantity and decrease with increasing Temperature initial concentration of Ca(II) and Mg(II) ions.

6. The kinetics results confirms the best correlation of the experimental data of adsorption of 4A° zeolite by pseudo – second order equation .

7. The negative values of the thermodynamic Functions ΔG, ΔH and ΔS for the adsorption of Ca+2 and Mg+2 ions on 4A° zeolite on adsorbents indicates that the adsorption processes is spontaneous, exothermic and less randomness at solid– solution interface.

8. Equilibrium data obtained for the adsorption of 4A°zeolite were fitted to the Langmuir model more than freundlich and Temkin isotherms.

9. EDX analysis of the kaolin, metakaolin,alumina,silica and zeolite proved the difference ratio of Al,Si, and O for each sample, as well as the analysis data for zeolite shown presence of Na ion, this mean the formation of zeolite.

4.7. Future works

1. Studying other types of zeolite such as 3°A Zeolite , 5°A Zeolite , 13X Zeolite.
2. Mathematical modeling of adsorption process and the factors and parameters effect it.
3. Intensifying studies on mechanism and chemistry of adsorption.
4. Using industrial waste water to study its purifications instead of synthetically prepared aqueous solutions.
5. Calculating the removal percentage of Calcium and Magnesium ions at different pH.
6. Using initial concentration of Calcium and Magnesium ions less than 100 mg/L.
7. Using synthesis 4A°zeeolite for removal toxic heavy metals from industrial wast water and prepared solution.

References

References

[1] LLC, A.M. *Introduction to Zeolites*. 2018 [cited 2021 Feb]; Available from: https://www.acsmaterial.com/blog-detail/introduction-to-zeolites.html.

[2] Askari, S., S.M. Alipour, R. Halladj, and M.H.D.A. Farahani, *Effects of ultrasound on the synthesis of zeolites: a review.* Journal of Porous Materials, 2013. **20**(1): p. 285-302.

[3] Moshoeshoe, M., M.S. Nadiye-Tabbiruka, and V. Obuseng, *A review of the chemistry, structure, properties and applications of zeolites.* Am. J. Mater. Sci, 2017. **7**(5): p. 196-221.

[4] Vegere, K., R. Kravcevica, A.E. Krauklis, and T. Juhna, *Comparative study of hydrothermal synthesis routes of zeolite A.* Materials Today: Proceedings, 2020. **33**: p. 1984-1987.

[5] Vickers, N.J., *Animal communication: when i'm calling you, will you answer too?* Current biology, 2017. **27**(14): p. R713-R715.

[6] Ghasemi Mobtaker, H., H. Kazemian, M.A. Namdar, A. Malekinejad, and M.R. Pakzad, *Ion Exchange Behavior of Zeolites A and P Synthesized Using Natural Clinoptilolite.* Iranian Journal of Chemistry and Chemical Engineering (IJCCE), 2008. **27**(2): p. 111-117.

[7] Wang, Y. and F. Lin, *Synthesis of high capacity cation exchangers from a low-grade Chinese natural zeolite.* Journal of hazardous materials, 2009. **166**(2-3): p. 1014-1019.

[8] Chandrasekhar, S. and P. Pramada, *Investigation on the synthesis of zeolite NaX from Kerala kaolin.* Journal of Porous Materials, 1999. **6**(4): p. 283-297.

[9] Ahmed, N., *Preparation of zeolite 3A and 5A from locally available raw materials and their extrusion with different binders*. 2000, M. Sc. thesis, University of Baghdad.

[10] Keka, O., N.C. Pradhan, and A.N. Samanta, *Zeolite from fly ash: synthesis and characterization.* Bulletin of Materials Science, 2001. **27**(6): p. 555-564.

[11] Yaşyerli, S., İ. Ar, G. Doğu, and T. Doğu, *Removal of hydrogen sulfide by clinoptilolite in a fixed bed adsorber.* Chemical Engineering and Processing: Process Intensification, 2002. **41**(9): p. 785-792.

[12] Al-Khattaf, S., *The influence of Y-zeolite unit cell size on the performance of FCC catalysts during gas oil catalytic cracking.* Applied Catalysis A: General, 2002. **231**(1-2): p. 293-306.

[13] Chantawong, V. and N. Harvey. *Synthesis of zeolite from Thai Kaolin for wastewater treatment*. in *Proceeding of the 2 nd Regional Conference on Energy Technology towards a Clean Environmental*. 2003.

[14] Shams, K. and S. Mirmohammadi, *Preparation of 5A zeolite monolith granular extrudates using kaolin: Investigation of the effect of binder on sieving/adsorption properties using a mixture of linear and branched paraffin hydrocarbons.* Microporous and Mesoporous Materials, 2007. **106**(1-3): p. 268-277.

[15] Wu, A.-h. and C.A. Drake, *Hydrocarbon conversion process employing promoted zeolite catalyst*. 2000, Google Patents.

[16] Dalai, A.K., N.C. Pradhan, M.S. Rao, and K. Gokhale, *Synthesis and characterization of NaX and Cu-exchanged NaX zeolites from silica obtained from rice husk ash*. 2005.

[17] Shawabkeh, R. and A. Harahsheh, *H~ 2S removal from sour liquefied petroleum gas using Jordanian oil shale ash.* Oil shale, 2007. **24**(2): p. 109.

[18] Atta, A., O. Ajayi, and S. Adefila, *Synthesis of faujasite zeolites from Kankara kaolin clay*. Journal of Applied Sciences Research, 2007. **3**(10): p. 1017-1021.

[19] Christidis, G.E. and H. Papantoni, *Synthesis of FAU type zeolite Y from natural raw materials: hydrothermal SiO2-Sinter and Perlite glass.* The open mineralogy journal, 2008. **2**(1).

[20] Htay, M.M. and M.M. Oo, *Preparation of Zeolite Y catalyst for petroleum cracking.* World Academy of Science, Engineering and Technology, 2008. **48**: p. 114-120.

[21] Kovo, A., O. Hernandez, and S. Holmes, *Synthesis and characterization of zeolite Y and ZSM-5 from Nigerian Ahoko Kaolin using a novel, lower temperature, metakaolinization technique.* Journal of Materials Chemistry, 2009. **19**(34): p. 6207-6212.

[22] Rahman, M., N. Hasnida, and W.W. Nik, *Preparation of zeolite Y using local raw material rice husk as a silica source.* Journal of Scientific Research, 2009. **1**(2): p. 285-291.

[23] Reyes, C.A.R., C.D. Williams, O. Mauricio, and C. Alarcón, *Synthesis of zeolite LTA from thermally treated kaolinite Síntesis de zeolita LTA a partir de caolinita tratada térmicamente.*

[24] Ugal, J.R., K.H. Hassan, and I.H. Ali, *Preparation of type* The 4A° *zeolite from Iraqi kaolin: Characterization and properties measurements.* Journal of the Association of Arab Universities for Basic and Applied Sciences, 2010. **9**(1): p. 2-5.

[25] Yousif, R., *Catalytic cracking of cumene in fluidized bed reactor with zeolite*. 2010, MSC. Thesis, Baghdad University.

[26] Mostafa, A., H. Youssef, M. Sorour, S. Tewfik, and H. Shalaan. *Utilization of Egyptian kaolin for zeolite-A preparation and performance evaluation*. in *2nd International Conference on Environmental Science and Technology IPCBEE*. 2011.

[27] Mezni, M., A. Hamzaoui, N. Hamdi, and E. Srasra, *Synthesis of zeolites from the low-grade Tunisian natural illite by two different methods.* Applied Clay Science, 2011. **52**(3): p. 209-218.

[28] Farag, I.H. and J. Zhang, *Simulation of synthetic zeolites*- The 4A° *and 5A manufacturing for green processing.* Simulation, 2012. **2**(2): p. 188-195.

[29] Saceda J., Rintramee K., Khabuanchalad S., Prayoonpokarach S., D. R.L., and W. J., *Properties of Zeolites as Promising Materials for Value*

Upgradation of Jatropha Oil. Journal of Material Science, 2012. **4**(8): p. 7949-7959.

[30] Georgiev, D., B. Bogdanov, I. Markovska, and Y. Hristov, *A study on the synthesis and structure of zeolite NaX.* Journal of Chemical Technology and Metallurgy, 2013. **48**(2): p. 168-173.

[31] Ma, Y., C. Yan, A. Alshameri, X. Qiu, and C. Zhou, *Synthesis and characterization of 13X zeolite from low-grade natural kaolin.* Advanced Powder Technology, 2014. **25**(2): p. 495-499.

[32] Cheng, Q., H. Li, Y. Xu, S. Chen, Y. Liao, F. Deng, and J. Li, *Study on the adsorption of nitrogen and phosphorus from biogas slurry by NaCl-modified zeolite.* PloS one, 2017. **12**(5): p. e0176109.

[33] Chai, Y., W. Shang, W. Li, G. Wu, W. Dai, N. Guan, and L. Li, *Noble metal particles confined in zeolites: synthesis, characterization, and applications.* Advanced Science, 2019. **6**(16): p. 1900299.

[34] Ramamurthy, V., *Achiral Zeolites as Reaction Media for Chiral Photochemistry.* Molecules, 2019. **24**(19): p. 3570.

[35] Schulman, E., W. Wu, and D. Liu, *Two-Dimensional Zeolite Materials: Structural and Acidity Properties.* Materials, 2020. **13**(8): p. 1822.

[36] Gackowski, M. and J. Datka, *Acid properties of hierarchical zeolites Y.* Molecules, 2020. **25**(5): p. 1044.

[37] Derakhshankhah, H., S. Jafari, S. Sarvari, E. Barzegari, F. Moakedi, M. Ghorbani, B.S. Varnamkhasti, M. Jaymand, Z. Izadi, and L. Tayebi, *Biomedical applications of zeolitic nanoparticles, with an emphasis on medical interventions.* International journal of nanomedicine, 2020. **15**: p. 363.

[38] Christie, T., B. Thompson, and B. Brathwaite, *Mineral commodity report 22–aggregate.* New Zealand mining, 2001. **30**: p. 6-26.

[39] Bell, R.G., R.A. Jackson, and C.R.A. Catlow, *Löwenstein's rule in zeolite A: A computational study.* Zeolites, 1992. **12**(7): p. 870-871.

[40] M, D. *Zeolites*. 1996 [cited 2021 Feb]; Available from: https://cool.culturalheritage.org/byorg/abbey/an/an20/an20-7/an20-702.html.

[41] Hriljac, J., M. Eddy, A. Cheetham, J. Donohue, and G. Ray, *Powder neutron diffraction and 29Si studies of siliceous zeolite-Y.* Journal of Solid State Chemistry, 1993. **106**(1): p. 66-72.

[42] Flanigen, E.M., *Zeolites and molecular sieves: An historical perspective*, in *Studies in Surface Science and Catalysis*. 2001, Elsevier. p. 11-35.

[43] Kunkeler, P., R. Downing, and H. Van Bekkum, *The use of bulky molecules as probes for investigating the contributions of the external and internal pore-wall activities of zeolite catalysts*, in *Studies in Surface Science and Catalysis*. 2001, Elsevier. p. 987-1001.

[44] Puppe, L. and J. Weitkamp, *Catalysis and zeolites: fundamentals and applications*. 1999: Springer.

[45] Mgbemere, H.E., I.C. Ekpe, and G.I. Lawal, *Zeolite Synthesis, Characterization.*

[46] Lee, E. and F.R. Groves Jr, *Mathematical model of the fluidized bed catalytic cracking plant.* Transactions of the Society for Computer Simulation International, 1985. **2**(3): p. 219-236.

[47] D3906-19, A., *Standard Test Method for Determination of Relative X-ray Diffraction Intensities of Faujasite-Type Zeolite-Containing Materials*, in *ASTM International, West Conshohocken, PA,*. 2019.

[48] Hey, M., *XII.-The nature and relations of the zeolites: a review.* Trans. Brit. Ceram. Soc, 1937. **36**: p. 84-97.

[49] Williams, D.J., B.E. Huck, and A.P. Wilkinson, *First-year undergraduate laboratory experiments with zeolites.* The Chemical Educator, 2002. **7**(1): p. 33-36.

[50] Mastinu, A., A. Kumar, G. Maccarinelli, S.A. Bonini, M. Premoli, F. Aria, A. Gianoncelli, and M. Memo, *Zeolite clinoptilolite: Therapeutic virtues of an ancient mineral.* Molecules, 2019. **24**(8): p. 1517.

[51] Cejka, J., *Introduction to zeolite science and practice*. 2007: Elsevier.

[52] Association, I.Z. *Zeolite Framework Types.* 2010 [cited 2021 Feb]; Available from: http://izasc.ethz.ch/fmi/xsl/IZASC/ft.xsl.

[53] Xu, R., J. Chen, Z. Gao, and W. Yan, *From Zeolites to Porous MOF Materials-the 40th Anniversary of International Zeolite Conference, 2 Vol Set: Proceedings of the 15th International Zeolite Conference, Beijing, PR China, 12-17th August 2007*. 2007: Elsevier.

[54] Büchel, K.H., H.-H. Moretto, and D. Werner, *Industrial inorganic chemistry*. 2008: John Wiley & Sons.

[55] Auerbach, S.M., K.A. Carrado, and P.K. Dutta, *Handbook of zeolite science and technology*. 2003: CRC press.

[56] Zorpas, A. and V.J. Inglezakis, *Natural zeolites: Industrial and environmental applications*, in *Handbook of Zeolites: Structure, Properties and Applications*. 2009, Nova Science Publishers, Inc. p. 23-49.

[57] Stephenson, D.J., C.I. Fairchild, R.M. Buchan, and M.E. Dakins, *A fiber characterization of the natural zeolite, mordenite: A potential inhalation health hazard.* Aerosol Science & Technology, 1999. **30**(5): p. 467-476.

[58] Tsitsishvili, G., T. Andronikashvili, E. Thaddens, M. Carmen, and E. Wagener, *Natural Zeolites Ellis Horwood.* New York, USA, 1992.

[59] Heinze, G., M. Mengel, and G. Reiss, *Zeolite A with improved properties*. 1977, Google Patents.

[60] Sakuth, M., J. Meyer, and J. Gmehling, *Measurement and prediction of binary adsorption equilibria of vapors on dealuminated Y-zeolites (DAY).* Chemical Engineering and Processing: Process Intensification, 1998. **37**(4): p. 267-277.

[61] Breck, D.W., *Zeolite molecular sieves: structure, chemistry and use*. 1984: Krieger.

[62] Martins, L., R.T. Boldo, and D. Cardoso, *Ion exchange and catalytic properties of methylammonium FAU zeolite.* Microporous and mesoporous materials, 2007. **98**(1-3): p. 166-173.

[63] Cejka, J., A. Corma, and S. Zones, *Zeolites and catalysis: synthesis, reactions and applications*. 2010: John Wiley & Sons

[64] Barrer, R.M., *Hydrothermal chemistry of zeolites*. 1982: Academic press.

[65] Chandrasekhar, S., *Influence of metakaolinization temperature on the formation of zeolite* 4A° *from kaolin.* Clay Minerals, 1996. **31**(2): p. 253-261.

[66] Schweiker, G., *Sodium silicates and sodium aluminosilicates.* Journal of the American Oil Chemists' Society, 1978. **55**(1): p. 36-40.

[67] Basaldella, E. and J. Tara, *Synthesis of LSX zeolite in the NaK system: Influence of the NaK ratio.* Zeolites, 1995. **15**(3): p. 243-246.

[68] Organization, W.H., *WHO/UNICEF Joint Monitoring Programme (JMP) for Water Supply and Sanitation. 2015*. 2019.

[69] Vörösmarty, C.J., P.B. McIntyre, M.O. Gessner, D. Dudgeon, A. Prusevich, P. Green, S. Glidden, S.E. Bunn, C.A. Sullivan, and C.R. Liermann, *Global threats to human water security and river biodiversity.* nature, 2010. **467**(7315): p. 555-561.

[70] Organization, W.H., *Guidelines for drinking-water quality*. 1993: World Health Organization.

[71] Wang, C.-F., J.-S. Li, L.-J. Wang, and X.-Y. Sun, *Influence of NaOH concentrations on synthesis of pure-form zeolite A from fly ash using two-stage method.* Journal of Hazardous Materials, 2008. **155**(1-2): p. 58-64.

[72] Taqe, R.M.M., *Removal of some water pollutants using newly synthesised organoclays*, in *College of Science,*. 2015, University of Al-Mustansiriyah.

[73] Abdeen, Z. and S.G. Mohammad, *Study of the adsorption efficiency of an eco-friendly carbohydrate polymer for contaminated aqueous solution by organophosphorus pesticide.* Open Journal of Organic Polymer Materials, 2013. **2014**.

[74] Meisslamawy, H., *Sorption capacity measurement of sulphuric acid in the active mass of the Iraq lead acid storage battery*. 2006, M. Sc. thesis, College of Science for Women-University of Baghdad, Iraq.

[75] Abdulla, F.H., *Removal of Chromium (III) Ions from its Aqueous Solution on Adsorbent Surfaces: Charcoal, Attapulgite and Date Palm Leaflet Powder.* Iraqi Journal of Science, 2014. **55**(4A°): p. 1415-1430.

[76] Senthilkumar, R., K. Vijayaraghavan, M. Thilakavathi, P. Iyer, and M. Velan, *Application of seaweeds for the removal of lead from aqueous solution.* Biochemical Engineering Journal, 2007. **33**(3): p. 211-216.

[77] Yuh-Shan, H., *Citation review of Lagergren kinetic rate equation on adsorption reactions.* Scientometrics, 2004. **59**(1): p. 171-177.

[78] Robati, D., *Pseudo-second-order kinetic equations for modeling adsorption systems for removal of lead ions using multi-walled carbon nanotube.* Journal of nanostructure in Chemistry, 2013. **3**(1): p. 1-6.

[79] Wawrzkiewicz, M., M. Wiśniewska, V.M. Gun'ko, and V.I. Zarko, *Adsorptive removal of acid, reactive and direct dyes from aqueous solutions and wastewater using mixed silica–alumina oxide.* Powder Technology, 2015. **278**: p. 306-315.

[80] Low, M., *Kinetics of chemisorption of gases on solids.* Chemical Reviews, 1960. **60**(3): p. 267-312.

[81] Chien, S. and W. Clayton, *Application of Elovich equation to the kinetics of phosphate release and sorption in soils.* Soil Science Society of America Journal, 1980. **44**(2): p. 265-268.

[82] Spark, K., J. Wells, and B. Johnson, *The interaction of a humic acid with heavy metals.* Soil Research, 1997. **35**(1): p. 89-102.

[83] Mohamed, R., I. Mkhalid, and M. Barakat, *Rice husk ash as a renewable source for the production of zeolite NaY and its characterization.* Arabian Journal of Chemistry, 2015. **8**(1): p. 48-53.

[84] Al-Sumaidaie, D.M.O., *Study of alumina prepared from Iraqi kaolin.* Iraqi Journal of Physics (IJP), 2017. **15**(34): p. 148-152.

[85] Ahamed, M., H.A. Alhadlaq, M. Khan, P. Karuppiah, and N.A. Al-Dhabi, *Synthesis, characterization, and antimicrobial activity of copper oxide nanoparticles.* Journal of Nanomaterials, 2014. **2014**.

[86] Alaba, P.A., Y.M. Sani, and W.M.A.W. Daud, *Kaolinite properties and advances for solid acid and basic catalyst synthesis.* RSC advances, 2015. **5**(122): p. 101127-101147.

[87] Moghny, T.A., A.M.G. Mohamed, S.S. Saleem, and M. Fathy, *Abu Zenima synthetic zeolite for removing iron and manganese from Assiut governorate groundwater, Egypt.* Applied Water Science, 2017. **7**(6): p. 3087-3094.

[88] Mustafa, Y.A. and M.J. Zaiter, *Treatment of radioactive liquid waste (Co-60) by sorption on Zeolite Na-A prepared from Iraqi kaolin.* Journal of hazardous materials, 2011. **196**: p. 228-233.

[89] Guo, X., L. Zeng, and X. Jin, *Advanced regeneration and fixed-bed study of ammonium and potassium removal from anaerobic digested wastewater by natural zeolite.* Journal of Environmental Sciences, 2013. **25**(5): p. 954-961.

[90] Luukkonen, T., H. Runtti, M. Niskanen, E.-T. Tolonen, M. Sarkkinen, K. Kemppainen, J. Rämö, and U. Lassi, *Simultaneous removal of Ni (II), As (III), and Sb (III) from spiked mine effluent with metakaolin and blast-furnace-slag geopolymers.* Journal of environmental management, 2016. **166**: p. 579-588.

[91] Hamdan, H., M.N.M. Muhid, S. Endud, E. Listiorini, and Z. Ramli,Si *studies of rice husk silica for the synthesis of zeolites.* Journal of Non-Crystalline Solids, 1997. **211**(1-2): p. 126-131.

[92] Kapur, P., *Production of reactive bio-silica from the combustion of rice husk in a tube-in-basket (TiB) burner.* Powder Technology, 1985. **44**(1): p. 63-67.

[93] Shinohara, Y. and N. Kohyama, *Quantitative analysis of tridymite and cristobalite crystallized in rice husk ash by heating.* Industrial health, 2004. **42**(2): p. 277-285.

[94] Han, R., L. Zou, X. Zhao, Y. Xu, F. Xu, Y. Li, and Y. Wang, *Characterization and properties of iron oxide-coated zeolite as adsorbent for removal of copper (II) from solution in fixed bed column.* Chemical Engineering Journal, 2009. **149**(1-3): p. 123-131.

[95] Chou, C.-M., H.-T. Cho, V.K. Hsiao, K.-T. Yong, and W.-C. Law, *Quantum dot-doped porous silicon metal–semiconductor metal photodetector.* Nanoscale research letters, 2012. **7**(1): p. 1-4.

[96] Umar, A.A., M.Y. Abd Rahman, R. Taslim, M.M. Salleh, and M. Oyama, *A simple route to vertical array of quasi-1D ZnO nanofilms on FTO surfaces: 1D-crystal growth of nanoseeds under ammonia-assisted hydrolysis process.* Nanoscale research letters, 2011. **6**(1): p. 1-12.

[97] Esharghawi, A., *Élaboration de matériaux poreux à base de mullite par procédé SHS*. 2009, Limoges.

[98] Davidovits, J. *Properties of geopolymer cements*. in *First international conference on alkaline cements and concretes*. 1994. Kiev State Technical University, Ukraine: Scientific Research Institute on ….

[99] Gao, K., K.-L. Lin, D. Wang, H.-S. Shiu, C.-L. Hwang, and T.-W. Cheng, *Effects of nano-SiO2 on setting time and compressive strength of alkaliactivated metakaolin-based geopolymer.* The Open Civil Engineering Journal, 2013. **7**(1).

[100] Ro, J.C. and J.C. In, *Structures and properties of silica gels prepared by the sol—gel method.* Journal of non-crystalline solids, 1991. **130**(1): p. 8-17.

[101] Dabbagh, H.A., M. Yalfani, and B.H. Davis, *An XRD and Fourier-transformed infrared spectroscopy investigation of single and mixed γ-alumina and thorium oxide.* Journal of Molecular Catalysis A: Chemical, 2005. **238**(1-2): p. 72-77.

[102] Aragaw, T.A. and A.A. Ayalew, *Removal of water hardness using zeolite synthesized from Ethiopian kaolin by hydrothermal method.* Water Practice and Technology, 2019. **14**(1): p. 145-159.

[103] . Scimeca, M., S. Bischetti, H.K. Lamsira, R. Bonfiglio, and E. Bonanno, *Energy Dispersive X-ray (EDX) microanalysis: A powerful tool in biomedical research and diagnosis.* European journal of histochemistry: EJH, 2018. **62**(1).

[104] Hu, C., P. Zhu, M. Cai, H. Hu, and Q. Fu, *Comparative adsorption of Pb (II), Cu (II) and Cd (II) on chitosan saturated montmorillonite: Kinetic, thermodynamic and equilibrium studies.* Applied Clay Science, 2017. **143**: p. 320-326.

الملخص

من المعروف أن المنخل الجزيئي عبارة عن مادة ذات مسام (ثقوب صغيرة جدًا) ذات حجم موحد. تتشابه أقطار المسام هذه في الحجم مع الجزيئات الصغيرة ، وبالتالي لا يمكن للجزيئات الكبيرة الدخول أو الامتصاص ، بينما يمكن للجزيئات الأصغر ، أن المناخل الجزيئية أو الزيوليت هي كضمادة صناعية واسعة الانتشار ذات بنية كيميائية فريدة ، والتي تستخدم في معظم المنشآت الصناعية مادة ماصة للغازات أو حتى كمحفزات. تم تحضير الزيوليت 4Å من الكاولين العراقي وقشر الأرز باستخدام عملية تحويل قشر الأرز إلى السيليكا والكاولين إلى ألومينات الصوديوم حيث تم تحضير الزيوليت. ثم تم تمييزه بحيود الأشعة السينية ، والتحليل الطيفي FTIR ومجهر القوة الذري (AFM) ،و المسح المجهري الإلكتروني (SEM) والتحليل المجهري للأشعة السينية المشتتة للطاقة (EDX) حيث تيم اخذ القياسات للعينات (الكاوولين و ميتا كولين والالومينا والسليكا والزيولايت) على التوالي .أثبت نتائج القياسات تكوين الزيوليت بالأضافة الى امكانية استخدام الكاوولين /قشر الارز كمواد خام لإنتاج الزيوليت .

يعد تلوث المياه مصدر قلق كبير لأن الماء هو ضرورة أساسية للحياة ولبقاء جميع الكائنات الحية. في جميع أنحاء العالم ، ولكن يتم تغيير جودته باستمرار من خلال الأنشطة البشرية المختلفة لهذا يتم إنفاق مبالغ من الاموال سنويًا لضمان تنقية المياه (تتم إزالة المعادن) لتجنب آثارها السلبية مثل الصابون المتدهور والترسب المتسارع على الصنابير يغير الخصائص الفيزيائية والكيميائية للماء . يتم تحديد عسر الماء عن طريق قياس التركيز الكلي للمغنيسيوم والكالسيوم في مصدر المياه. يؤثر عسر المياه على الثقافات البيئية وكذلك العديد من الأنواع الأخرى التي تعتمد على تركيز ثابت من كربونات الكالسيوم ان تلوث المياه بالعديد من المعادن يشكل ضررا كبيرا على البيئة لذلك استخدم الزيوليت 4Å لازالة ايونات الكالسيوم والمغنسيوم الثنائية من المحاليل المائية . وفي هذا المجال ، تم دراسة عدد من العوامل التي تؤثر على نسبة ازالة الكالسيوم وازالة المغنسيوم على المواد المازة (النانوية) .حيث وجد ان الزمن اللازم لازالة ايونات الكالسيوم والمغنسيوم والوصول الى حالة الاتزان هو ٥٠ دقيقة على الزيولايت وكذلك فان ازالة ايونات الكالسيوم وازالة ايونات المغنسيوم تقل بزيادة

تركيز المادة المتزة وتزداد بزيادة وزن السطح الماز، اما تاثير درجة الحرارة على امتزاز الكالسيوم والمغنسيوم فقد بينت ان نسبة الازالة تقل بزيادة درجة الحرارة مما يدل ان العملية هي باعثة للحرارة .

وعند حساب قيم الدوال الثرموديناميكية لعملية الامتزاز($\Delta S,\Delta H,\Delta G$) تبين ان عملية الامتزاز تكون تلقائية ،باعثة للحرارة واقل عشوائية عند تداخل ايونات الكالسيوم والمغنسيوم وقد تم مطابقة النتائج باستخدام اربعة من الحركية للمعادلات والتي هي :المعادلة الدرجة الاولى الكاذبة ومعادلة من الدرجة الثانية الكاذبة ومعادلة الانتشار الداخلي للجزيئات و معادلة Elovich من النتائج اعلاه تبين ان عملية الامتزاز تخضع لمعادلة الدرجة الثانية الكاذبة لان معامل الارتباط الذي هو($R2$) قد بين افضل نتيجة بالنماذج المتواجدة الاخرى قد وجد أيزوثيرم لانكماير هي الافضل لوصف سلوك عملية الأمتزاز مقارنة مع أيزوثيرمات فرندلش وتمكن .

وزارة التعليم العالي والبحث العلمي

جامعة ديالى

كلية العلوم

قسم الكيمياء

توصيف وتطبيقات الزيولايت المحضر من مواد متوفرة طبيعيا

(الكاؤلين العراقي وقشور الرز)

رسالة مقدمة إلى

مجلس كلية العلوم – جامعة ديالى

وهي جزء من متطلبات نيل شهادة الماجستير علوم في الكيمياء

من قبل

إيلاف حسين علي

بكالوريوس كيمياء – جامعة ديالى ٢٠٠٨

بإشراف

أ.د. كريم هنيكش حسن

أ.د. أحمد نجم عبد

١٤٤٢هجرية

٢٠٢١ميلادية